UNIVERSITY OF SALERNO

Department of Medicine, Surgery and Dentistry

PhD program in
Translational Medicine of Development and Active Aging

Cycle XXXV

Curriculum: Translation and Clinic Medicine

PhD thesis

IN VITRO MYOGENIC MODELS USING HUMAN BONE MARROW MESENCHYMAL STEM CELLS: FROM 2D STATIC TO BIOENGINEERED 3D DYNAMIC CO-CULTURES

Coordinator:

Prof. Palmiero Monteleone

Candidate:

Pasqualina Scala

Mat.no.: 8800900049

Tutors:

Prof. Nicola Maffulli

Prof. Giovanna Della Porta

Academic year 2021/2022

Abstract

Skeletal muscle injuries can spontaneously heal, because of an intrinsic regenerative potential of a resident stem cell pool, known as satellite cells. After injury, quiescent satellite cells start proliferating and differentiating toward mature muscle cells. Immune cells also play a central role in skeletal muscle regeneration process, by switching from a pro-inflammatory to an anti-inflammatory microenvironment, as healing process proceeds, and injured muscle is structurally and functionally recovered. However, skeletal muscle regenerative potential is limited, and severe injuries frequently result in incomplete recovery and chronic inflammation. Current therapies are restricted to conservative management, including RICE protocol (rest, ice, compression, and elevation) and nonsteroidal anti-inflammatory drugs or intramuscular corticosteroids for inflammatory symptom relief. These approaches do not provide a complete restoration to preinjury status, thus cell-based approach may represent a valid treatment option, even if these therapies show several technical issues, especially regarding cell collecting, harvesting and *in-vitro* expansion before transplantation. Therefore, peripheral blood mononuclear cell (PBMC) infusion can be an alternative and promising approach even though *in-vitro* and clinical studies are still few. Based on this evidence, the aim of this thesis work is to develop innovative *in vitro* models to study myogenic commitment of human bone marrow-derived mesenchymal stem cells (*h*BM-MSCs) by adopting two different approaches:

(i) two-dimensional (2D) co-culture of human stem cells and PBMCs under dynamic conditions, such as perfusion;

(ii) bioengineered three-dimensional (3D) co-culture of human stem cells and PBMCs.

First, appropriate culture conditions, including culture medium composition and cell seeding ratio between *h*BM-MSCs and human primary skeletal myoblasts (*h*SkMs), were investigated using standard monolayer culture approaches. Cells cultured using medium supplemented with 10 ng/mL of b-fibroblast growth factor (b-FGF) and co-cultured with *h*SkMs showed higher myogenesis-related gene expression (*Desmin*, 141-fold; *Myosin Heavy Chain II (MYH2*), 32-fold) after 21 days, and a prevalent expression of anti-inflammatory cytokines (*IL10*, 15-fold; and *IL4*, 11-fold) rather than pro-inflammatory ones (*IL1*, 1.4-fold). Subsequently, PBMCs collected using a commercial filtration system commonly used in clinical practice were added in an upper transwell chamber to investigate their potential paracrine effects on myogenic events. Myogenic commitment of *h*BM-MSCs in the presence and absence of PBMCs was investigated by gene expression profiling by qRT-PCR and protein expression using immunofluorescence (IF) assay and flow cytometry. In the presence of PBMCs, *h*BM-MSCs significantly upregulated myogenic genes, such as *Desmin* and *MYH2* starting at day 7 of culture, as confirmed by both qRT-PCR and IF, while pro-inflammatory cytokines (*IL12A* at day 14) were downregulated.

Subsequently, myogenic commitment of *h*BM-MSCs was further implemented using a 3D approach employing fibrin-based scaffolds embedded with *h*BM-MSCs plus *h*SkMs with and without PBMCs, cultured in dynamic conditions using a perfusion bioreactor. This culture system appeared as a valid biomimetic environment for myogenic commitment of stem cells. Indeed, all myogenic-related genes tended to be upregulated in the presence of PBMCs, and Desmin and Myosin Heavy Chain were also detected at protein level. Moreover, the presence of PBMCs in 3D culture

induced a significant downregulation of pro-inflammatory cytokine genes, such as *IL6*.

This blood filtration system was structurally investigated by optical and electron microscopy, Fourier-transform infrared spectroscopy (FTIR), Differential Scanning Calorimetry (DSC), and Thermogravimetric analysis (TGA). We investigated filter membrane structure and their polymer compositions showing a characteristic morphological structure composed by polyhydroxy butyrate (PHB) polymer. Filtered PBMCs were characterized by flow cytometry immunophenotyping to confirm the efficacy of this filtration system in concentrating PBMCs in smaller volumes by simultaneously preserving their composition.

In conclusion, our works confirm that *h*BM-MSCs represent a valid source of stem cells for skeletal muscle tissue engineering, as *h*BM-MSCs have a versatile myogenic potential, enhanced and modulated by blood filtered PBMC fraction co-culture. Moreover, our 3D biomimetic *in vitro* model better resembles physiological tissue architecture, improving stem cell survival and proliferation, and promoting complex biological *in vivo* cross-talks.

Table of contents

Abstract 1

List of figures 9

Abbreviations 13

Publications 17

Oral and poster presentations at conferences 19

Acknowledgments 21

CHAPTER 1. **Skeletal muscle tissue engineering** 23

1.1 Skeletal muscle: structure and function 25
1.2 Skeletal muscle injuries 28
1.3 Skeletal muscle regeneration 29
1.4 Satellite cells 31
1.5 Conventional therapies 32
1.6 Pharmacological therapies 34
1.7 Alternative therapies 35
1.8 Skeletal muscle tissue engineering 37
1.9 Thesis objective 41

CHAPTER 2. **Myogenesis in 2D monolayer co-cultures: static and dynamic approach** 43

2.1 Introduction 45
2.2 Aim 46
2.3 Materials and Methods 46
2.3.1 *h*MSC isolation and harvesting 46
2.3.2 MSC flow cytometry characterization 47
2.3.3 *h*BM-MSC-*h*SkM static co-culture 48
2.3.4 Dynamic culture condition 48
2.3.5 Brightfield images 49
2.3.6 RNA isolation and gene expression profiling 49
2.3.7 Immunofluorescence assay 50
2.3.8 Western blotting 50
2.3.9 Statistical analysis 51
2.4 Results 52

2.4.1 *h*BM-MSC and *h*SkM characterization 52
2.4.2 Myogenic commitment strategies of *h*BM-MSCs 53
2.4.3 Dynamic culture system 57
2.5 Discussion 61
2.6 Conclusion 64

CHAPTER 3. Peripheral Blood Mononuclear Cell contribution in 2D myogenic co-culture system 67
3.1 Introduction 69
3.2 Aim 70
3.3 Materials and methods 70
3.3.1 Filter characterization 70
3.3.2 PBMC concentration with filtration system and harvesting 71
3.3.3 BM-MSC isolation, harvesting and characterization 71
3.3.4 Flow cytometry 72
3.3.5 BM-MSC-SkM-PBMC static co-culture 73
3.3.6 RNA isolation and gene expression profiling 74
3.3.7 Cytokine detection 74
3.3.8 Immunofluorescence assay 75
3.3.9 Statistical analysis 75
3.4 Results 76
3.4.1 Filter characterization 76
3.4.2 Filtrate composition 79
3.4.3 Effective myogenic commitment of BM-MSCs: flow cytometry evidence 81
3.4.4 Effective myogenic commitment of BM-MSCs: gene expression profiling 85
3.4.5 Pro-inflammatory activities of T effector memory lymphocytes and Natural Killer cells could negatively influence myogenic commitment 89
3.5 Discussion 93
3.6 Conclusion 96

CHAPTER 4. Peripheral Blood Mononuclear Cell contribution in 3D bioengineered myogenic co-culture system 99

4.1 Introduction 101
4.2 Aim 102
4.3 Materials and methods 103
4.3.1 PBMC harvesting 103
4.3.2 *h*BM-MSC isolation, harvesting and characterization 103
4.3.3 *h*SkM characterization 104
4.3.4 Flow cytometry 104
4.3.5 3D fibrin scaffold preparation and characterization 105
4.3.6 Dynamic culture 106
4.3.7 Live&Dead assay 106
4.3.8 RNA isolation and gene expression profile 107
4.3.9 Immunofluorescence assay 109
4.3.10 Cytokine detection 109
4.3.11 Hematoxylin&Eosin staining 109
4.3.12 Statistical analysis 110
4.4 Results 110
4.4.1 3D scaffold characterization 110
4.4.2 Dynamic culture by perfusion bioreactor 113
4.4.3 *h*BM-MSC and PBMC characterization 116
4.4.4 Myogenic commitment in co-culture system gene expression profile and immunofluorescence evidence 119
4.4.5 Cytokine expression 123
4.5 Discussion 125
4.6 Conclusion 128

CHAPTER 5. Conclusions 131

References 135

- **List of figures**

Figure 1	Schematic illustration of skeletal muscle architecture	25
Figure 2	Sarcomere structure representation	26
Figure 3	Scheme of skeletal muscle contraction	27
Figure 4	Schematic illustration of skeletal muscle regeneration progression	30
Figure 5	Satellite cell differentiation progression	32
Figure 6	Skeletal muscle tissue engineering tools	39
Figure 7	Flow cytometry and gating strategy of *h*BM-MSCs	52
Figure 8	Brightfield images and immunofluorescence assay of *h*SkMs	53
Figure 9	Gene expression profiling for myogenic markers by quantitative RT-PCR obtained from *h*BM-MSCs and *h*SkMs co-seeding culture in static condition with myogenic medium (10 ng/mL of bFGF)	54
Figure 10	Brightfield and immunofluorescence images of *h*BM-MSCs and *h*SkMs co-seeded with ratio 2:1 in static condition with myogenic medium (10 ng/mL of bFGF)	55
Figure 11	Gene expression profiling for pro- and anti-inflammatory cytokines by quantitative RT-PCR obtained from *h*BM-MSCs and *h*SkMs co-seeding culture in static condition with myogenic medium (10 ng/mL of bFGF)	56
Figure 12	Schematic representation and image of perfused bioreactor system used for the dynamic co-culture of *h*BM-MSCs with *h*SkMs (2:1)	58
Figure 13	Gene expression profiling of myogenic markers and cytokines expressed by *h*BM-MSCs within perfusion bioreactor culture	59
Figure 14	Immunofluorescence images of *h*BM-MSCs with myogenic medium and under co-culture within perfusion bioreactor	60
Figure 15	Western blot assay for Desmin and MYH2 proteins	61
Figure 16	Filtration system membranes	76

Figure 17	Filtration system characterization: physical and chemical properties	77
Figure 18	Filtration system characterization: morphology	78
Figure 19	Commercial filtration system	79
Figure 20	Flow cytometry immunophenotyping of peripheral blood mononuclear cells	80
Figure 21	Flow cytometry and gating strategy of *h*BM-MSCs	82
Figure 22	Myogenic commitment of bone marrow-derived mesenchymal stem cells (BM-MSCs) by flow cytometry analysis	83
Figure 23	Myogenic commitment of mesenchymal subsets during co-culture	85
Figure 24	Gene expression profiling for myogenic markers by quantitative RT-PCR of BM-MSCs-SkMs-PBMCs in static culture	87
Figure 25	Brightfield and Immunofluorescence images of BM-MSCs:SkMs 2:1 co-seeded with PBMNCs in upper chamber of transwell insert	88
Figure 26	Flow cytometry immunophenotyping of peripheral blood mononuclear cells (PBMCs) in transwell	90
Figure 27	Pro- and anti- inflammatory cytokine expression by quantitative RT-PCR and immunoassay in static BM-MSC-SkM-PBMC co-culture	92
Figure 28	Fibrin scaffold, plant layout for drying and perfusion bioreactor images	111
Figure 29	FE-SEM aerogel images and pore size measurement plots	112
Figure 30	Live & Dead of *h*BM-MSC-*h*SkM-PBMC viability in a 3D fibrin scaffold cultured in perfusion system	114
Figure 31	Hematoxylin & Eosin staining	115
Figure 32	Immunophenotype of *h*BM-MSCs-*h*SkMs co-culture at day 0	116
Figure 33	Flow cytometry immunophenotyping of peripheral blood mononuclear cells (PBMCs) obtained by a HemaTrate® Blood Filtration system	118

Figure 34 Gene expression profiling for myogenic markers by quantitative RT-PCR of *h*SkMs (a) and of *h*BM-MSCs-*h*SkMs-PBMCs (b), both within 3D fibrin scaffold 120
Figure 35 Immunofluorescence images of 3D fibrin scaffold for Desmin and MYH2 121
Figure 36 Immunofluorescence images of 3D fibrin scaffold for stemness markers 122
Figure 37 Gene expression profiling for pro- and anti-inflammatory cytokines by quantitative RT-PCR of *h*SkMs (a) and of *h*BM-MSCs-*h*SkMs-PBMCs (b), both within 3D fibrin scaffold 124

Abbreviations

2D	Two- dimensional
3D	Three-dimensional
A-band	Anisotropic-band
ACS	Acute compartment syndromes
ADP	Adenosine diphosphate
APC	Allophycocyanin
ATP	Adenosine triphosphate
AZA	Azacytidine
BM	Bone marrow
BM-MSCs	Bone marrow derived Mesenchymal stem cells
Ca^{2+}	Calcium
CALCR	Calcitonin-Receptor
CCL2	CC-chemokine ligand 2
CLI	Critical limb ischemia
CO_2	Carbon dioxide
COX-2	Cyclooxygenase 2
CXCL1	CXC-chemokine ligand 1
CXCR4	C-X-C Chemokine Receptor type-4
DAPI	4′,6-diamidino-2-phenylindole
DC	Dendritic cell
DOMS	Delayed Onset Muscle Soreness
DMEM	Dulbecco's Modified Eagle Medium
DMSO	Dimethyl sulfoxide
DSC	Differential scanning calorimetry
ECL	Enhanced chemiluminescence
ECM	Extracellular matrix
EDTA	Ethylenediaminetetraacetic acid
EGF	Epidermal Growth Factor
EIMI	Exercise-induced muscle injury
ELISA	Enzyme linked immunosorbent assay
FBS	Fetal bovine serum
FE-SEM	Field emission electron scanning microscopy
FGF	Fibroblast growth factor
bFGF	Basic fibroblast growth factor

FITC	Fluorescein isothiocyanate
FSC-A	Forward scatter area
FTIR	Fourier transform infrared spectroscopy
GAPDH	Glyceraldehyde-3-phosphate dehydrogenase
GFs	Growth factors
G-CSF	Granulocyte Colony-Stimulating Factor
GM-CSF	Granulocyte-Macrophage Colony-Stimulating Factor
GRO	Growth-regulated oncogene
***h*BM-MSCs**	Human bone marrow derived Mesenchymal stem cells
***h*MSCs**	Human mesenchymal stem cells
***h*SkMs**	Human primary skeletal myoblasts
HGFA	Hepatocyte growth factor activator
HMGB1	High mobility group box-1 proteins
HO	Myositis ossificans
IF	Immunofluorescence
IFN-γ	Interferon- γ
Ig	Immunoglobulin
IGF1	Insulin-like growth factor 1
IL-10	Interleukin 10
IL-12A	Interleukin 12A
IL-1	Interleukin 1
IL-1α	Interleukin 1α
IL-1β	Interleukin 1β
IL-1RA	Interleukin-1 receptor antagonist
IL-2	Interleukin 2
IL-3	Interleukin 3
IL-4	Interleukin 4
IL-5	Interleukin 5
IL-6	Interleukin 6
IL-7	Interleukin 7
IL-8	Interleukin 8
IL-13	Interleukin 13
IL-33	Interleukin 33
I-band	Isotropic-band
LPS	Lipopolysaccharide
NSAIDs	Non-steroidal anti-inflammatory drugs

MCP-1	Monocyte Chemoattractant Protein-1
MFI	Median fluorescence intensity
MIP-1α	Macrophage inflammatory protein-1 α
MIP-1β	Macrophage inflammatory protein-1 β
MPs	Macrophages
M1-MPs	Pro-inflammatory phenotype macrophages
M2-MPs	Anti-inflammatory phenotype macrophages
MPCs	Myogenic progenitor cells
MRFs	Myogenic regulatory factor
MSCs	Mesenchymal stem cells
MyoD1	Myoblast determination protein-
Myf5	Myogenic factor 5
Myf6	Myogenic factor 6
Myog	Myogenin
MYH2	Myosin heavy Chain II
NK	Natural killer
Pax 3	Paired box gene 3
Pax 7	Paired box gene 7
PB	Peripheral blood
PBMCs	Peripheral blood mononuclear cells
PBS	Phosphate-buffered saline
PC5	Phycoerythrin cyanin 5
PC7	Phycoerythrin cyanin 7
PE	Phycoerythrin
Pen/Strep	Penicillin/Streptomycin
PFA	Paraformaldehyde
PHB	Polyhydroxy butyrate
Pi	Phosphate
PMMA	Polymethyl methacrylate
PRP	Platelet rich plasma
q-IF	Semiquantitative immunofluorescence
RICE	Rest, Ice, Compression and Elevation
RIPA	Radioimmunoprecipitation assay
RT	Room temperature
RT-qPCR	Reverse transcription quantitative polymerase chain reaction

SCs	Satellite cells
SD	Standard deviation
SDS-PAGE	Sodium Dodecyl Sulphate - PolyAcrylamide Gel Electrophoresis
SkMR	Skeletal muscle regeneration
SMTE	Skeletal muscle tissue engineering
SSC-A	Side scatter area
TBST	Tris-buffered saline tween
TE	Tissue engineering
TGA	Thermogravimetric analyses
TGF-β	Transforming growth factor-β
Th	T helper
TNF	Tumor necrosis factor
THA	Total hip arthroplasty
Treg	T regulatory cells
VCAM1	Vascular Cell Adhesion Molecule 1
VEGF	Vascular-Endothelial Growth Factor
α-MEM	Minimum essential medium alpha

- **Publications**

1) **Scala P.**, Manzo P., Longo R., Giudice V., Ciardulli M.C., Serio B., Selleri C., Guadagno L., Rehak L., Maffulli N., Della Porta G. *Contribution of Peripheral Blood Mononuclear Cells isolated by advanced filtration system to myogenesis of Human Bone Marrow Mesenchymal Stem Cells co-cultured with Myoblasts.* Heliyon, *accepted.*
2) **Scala P.,** Manzo P., Lamparelli E.P, Lovecchio J., Ciardulli M.C., Giudice V., Selleri C., Giordano E., Rehal L., Maffulli N., Della Porta G. *Peripheral Blood Mononuclear Cells contribute to myogenesis in a 3D bioengineered system of Bone Marrow Mesenchymal Stem Cells and Myoblasts.* Front. Bioeng. Biotechnol., 10 January 2023. Sec. Biomaterials, Volume 10-2022.
3) **Scala P.,** Manzo P., Giudice V., Gorrese M., Bertolini A., Morini D., D'Alto F., Pepe R., Pedicini A., Izzo B., Verdesca F., Langella M., Serio B., Della Porta G., Selleri C. *c-Kit M541L variant is related to ineffective hemopoiesis predisposing to clonal evolution in 3D in vitro biomimetic co-culture model of bone marrow niche*. Heliyon. 2022 Dec 1;8(12):e11998.
4) Lamparelli E.P., Ciardulli M.C., Giudice V., **Scala P.**, Vitolo R., Dale T.P., Selleri C., Forsyth N.R., Maffulli N., Della Porta G. *3D in-vitro cultures of human bone marrow and Wharton's jelly derived mesenchymal stromal cells show high chondrogenic potential.* Front Bioeng Biotechnol. 2022 Sep 26;10:986310.
5) Lamparelli E.P., Ciardulli M.C., **Scala P.**, Scognamiglio M., Charlier B., Di Pietro P., Izzo V., Vecchione C., Maffulli N., Della Porta G. *Lipid nano-vesicles for thyroid hormone encapsulation: A comparison between different fabrication technologies, drug loading, and an in vitro delivery to human tendon stem/progenitor cells in 2D and 3D culture.* Int J Pharm. 2022 Aug 25;624:122007.

6) Ciardulli M.C., **Scala P**., Giudice V., Santoro A., Selleri C., Oliva F., Maffulli N., Della Porta G. *Stem Cells from Healthy and Tendinopathic Human Tendons: Morphology, Collagen and Cytokines Expression and Their Response to T3 Thyroid Hormone*. Cells 2022, 11, 2545.

7) **Scala P.**, Lovecchio J., Lamparelli E.P., Vitolo R., Giudice V., Giordano E., Selleri C., Rehak L., Maffulli N., Della Porta G. *Myogenic commitment of human stem cells by myoblasts Co-culture: a static vs. a dynamic approach.* Artif Cells Nanomed Biotechnol. 2022 Dec;50(1):49-58.

8) **Scala P**., Rehak L., Giudice V., Ciaglia E., Puca A.A., Selleri C., Della Porta G., Maffulli N. *Stem Cell and Macrophage Roles in Skeletal Muscle Regenerative Medicine*. Int J Mol Sci. 2021 Oct 8;22(19):10867.

9) Ciardulli M.C., Lovecchio J., **Scala P.**, Lamparelli E.P., Dale T.P., Giudice V., Giordano E., Selleri C., Forsyth N.R., Maffulli N., Della Porta G. *3D Biomimetic Scaffold for Growth Factor Controlled Delivery: An In-Vitro Study of Tenogenic Events on Wharton's Jelly Mesenchymal Stem Cells.* Pharmaceutics. 2021 Sep 10;13(9):1448.

10) Lamparelli, E.P., Palazzo, I., Ciardulli, M.C., **Scala, P.**, Reverchon, E., Forsyth, N.R., Maffulli, N., Santoro, A., Della Porta, G. *Supercritical emulsion extraction fabricated PLA/PLGA micro/nano carriers for growth factor delivery: Release profiles and cytotoxicity*. International Journal of Pharmaceutics. 2021; 592, 120108.

- **Oral and poster presentations at conferences**

1) September 27-29, 2023. 31st Annual Meeting of the European Orthopaedic Research Society (EORS). Porto, Portugal. ***Oral presentation***. "2D static and 3D dynamic co-cultures of human bone marrow mesenchymal stem cells as novel in vitro bioengineered myogenic models".
2) September 11-13, 2023. 50th ADRITELF Anniversary. Trieste, Italy. ***Poster presentation.*** "Nano-carriers as microenvironment regulators for tissue engineering strategies".
3) May 17-19, 2023. 41st National Conference of the Italian Society of Cytometry GIC. Naples, Italy. ***Poster presentation***. "Human bone marrow 3D niche immunophenotyping".
4) April 21-22, 2023. 11° I.S.M.u.L.T. Congress: Open Mind and New Technologies in muscles, ligaments and tendons. Paestum (SA), Italy. ***Oral presentation*** "Myogenesis in vitro model: from 2D monolayer to 3D scaffold dynamic co-cultures".
5) April 21-22, 2023. 11° I.S.M.u.L.T. Congress: Open Mind and New Technologies in muscles, ligaments and tendons. Paestum (SA), Italy. ***Poster presentation***.
6) March 28-31, 2023. Tissue Engineering and Regenerative Medicine International Society (TERMIS) 8th world congress. ***Poster presentation*** "Peripheral blood mononuclear cell contribution to myogenic commitment of human Mesenchymal Stem Cells in a 2D and 3D Myoblast co-culture".
7) September 4-7, 2022. 1° Italian Chemistry Society: technology. Naples, Italy. ***Oral presentation*** "Advanced biopolymer filtration system for Peripheral Blood Mononuclear Cells collection: a study on filter composition and *in vitro* filtrate composition".

8) April 8-9, 2022. 10° I.S.M.u.L.T. Congress: Open Mind and New Technologies in muscles, ligaments and tendons. Rome, Italy. ***Poster presentation.*** "PBMC contribution in myogenesis events studied by an in-vitro 3D bioengineered system with human Bone Marrow-Stem Cells and Myoblasts".
9) April 8-9, 2022. 10° I.S.M.u.L.T. Congress: Open Mind and New Technologies in muscles, ligaments and tendons. Rome, Italy. ***Oral presentation*** "PBMC activity in myogenesis studied by a 3D co-culture bioengineered system with human stem cells and myoblasts*".*
10) November 15-19, 2021. Tissue Engineering and Regenerative Medicine International Society (TERMIS) 6th world congress. ***Poster presentation.*** "Tissue engineering strategies for the myogenic commitment of human stem cells by myoblasts co-culture".
11) November 29-30, 2019. 9° I.S.M.u.L.T. Congress: Open Mind and New Technologies in muscles, ligaments and tendons. Verona, Italy. ***Oral presentation*** "Skeletal muscle regeneration modulated by inflammation: an in vitro study on a 3D bioengineered system".

- **Acknowledgments**

At the end of my course of study, I would like to sincerely thank all people who contributed to reach this important achievement.

I would like to sincerely thank my PhD supervisors, Prof. Nicola Maffulli and Prof. Giovanna Della Porta for their support and encouragement along these years. Their expertise, constructive criticism, and intellectual contributions have been essential to my personal and professional growth, as well as to the successful completion of this research.

I am also grateful to Dr. Laura Rehak who believed in this project from the beginning with enthusiasm and passion.

I would like to thank Prof. Johannes Stöckl and his group for hosting me in his lab at Medical University of Vienna. Their kindness made me feel welcome and supported.

I am deeply thankful to Prof. Carmine Selleri of Hematology and Transplant Center, University Hospital "San Giovanni di Dio e Ruggi d'Aragona", for human stem cell supply, and to Dr. Valentina Giudice for stem cell characterization, constructive feedback, and for inspiring motivation.

I would like to thank Prof. Emanuele Domenico Giordano and Dr. Joseph Lovecchio, Department of Electrical, Electronic and Information "Guglielmo Marconi", University of Bologna, for design and development of perfusion bioreactors.

A heartfelt thanks to my colleagues who became true friends at the end of these years. Thanks for collaboration, support and for making everyday experiment a great fun.

CHAPTER 1. Skeletal muscle tissue engineering

1.1 Skeletal muscle: structure and function

Skeletal muscle is one of the most abundant tissues in human body comprising 40% of total body weight and containing 50-75% of all body proteins[1]. Skeletal muscles belong to musculoskeletal system that together with bones, cartilage, tendons and ligaments support correct posture, allow movements and protect vital inner organs of human body[2]. Skeletal muscle tissue is designed to generate contraction and movement under our voluntary control, with a well-organized and complex structure.

Muscle cells, also known as myofibers, have a cylindrical shape with diameters ranging from 10 μm to 100 μm and 1 cm in length, and are supported by a complex scaffold composed by a basal lamina rich in collagen and by multiple proteins termed as "muscle molecular fingerprint". Basal lamina together with cell membranes constitutes the sarcolemma. Each myofiber is surrounded by a collagenous mesh-like sheath called endomysium, that supports muscle tissue and play a central role in tension transmission from muscle fiber to tendon. Bundles of myofibers correspond to a muscle fascicle surrounded by a connective tissue known as perimysium. Bundles of fascicles are further enveloped by an epimysium[3].

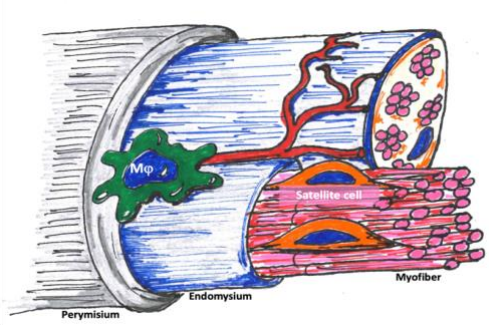

Figure 1. Schematic illustration of skeletal muscle architecture

Skeletal muscle tissue is composed by about 75% of water, 20% of proteins and the remaining 5% of inorganic salts, minerals, fat, and carbohydrates. Protein synthesis and degradation are well-balanced processes for controlling skeletal muscle mass, greatly influenced by other factors, such as nutritional status, hormones, physical exercises, injuries, and diseases[1]. After water, myofibers are mainly composed by proteins (80%) and sarcoplasma (8%). The most abundant proteins are actin and myosin, assembled as myofilaments, running in parallel to muscle fiber axis and forming the essential contractive muscle unit known as sarcomere. Remaining proteins contribute to cytoskeleton structure and finely regulate contraction process. For example, troponin is associated to actin filaments and regulates contraction once bound calcium (Ca^{2+}) ion, while titin and nebulin contribute to sarcomere integrity and cell stiffness.

Sarcomeres can be divided in areas and bands depending on protein filament content: myosin filaments constitute the M-band in the middle of sarcomere, while Z-discs border the ends and where actin filaments of adjacent sarcomeres are anchored. Z-discs are part of the I (isotropic)-band where only actin filaments are present. Between two I-bands, there is A (anisotropic)-band where actin and myosin filaments overlap.

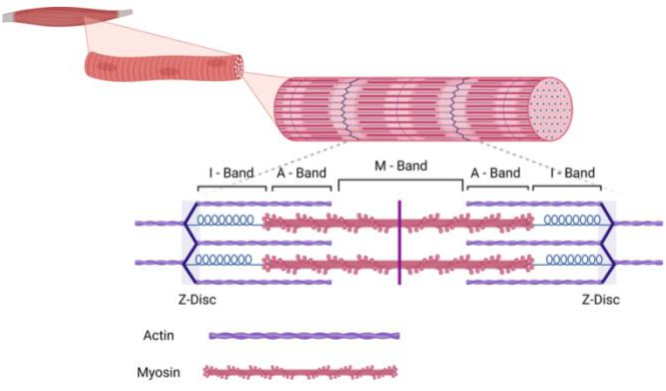

Figure 2. Sarcomere structure representation

Cyclic interactions between actin and myosin allow skeletal muscle contraction upon excitation by a nerve transmission signal. Excitation stimulus acts on sarcoplasmic reticulum where Ca^{2+} is stored, leading to ion release in sarcoplasma. Ca^{2+} binds to troponin-C on actin myofilaments. Tropomyosin protein covers active sites on actin filaments when muscles are relaxed. Ca^{2+}/Troponin-C binding induces a conformational change, exposing myosin binding sites on actin filaments. Myosin heads can bind and move along actin filament causing contraction. However, this process requires energy, produced by Adenosine triphosphate (ATP) hydrolysis. ATP is bound to myosin heads as well as ATPase, the enzyme required to hydrolyze ATP resulting in Adenosine diphosphate (ADP) and phosphate (Pi). When myosin head binds to actin filament, the cross-bridge angle is 45° relative to filaments, and ATPase can hydrolyze ATP. Myosin head swing over and binds to a new actin binding site; at this point the cross-bridge angle is 90° relative to filaments. With the release of Pi, a power stroke begins, myosin head rotates on its hinge scrolling through actin filament. At the power stroke end, myosin heads releases ADP and re-acquire a 45° angle configuration[1,4,5].

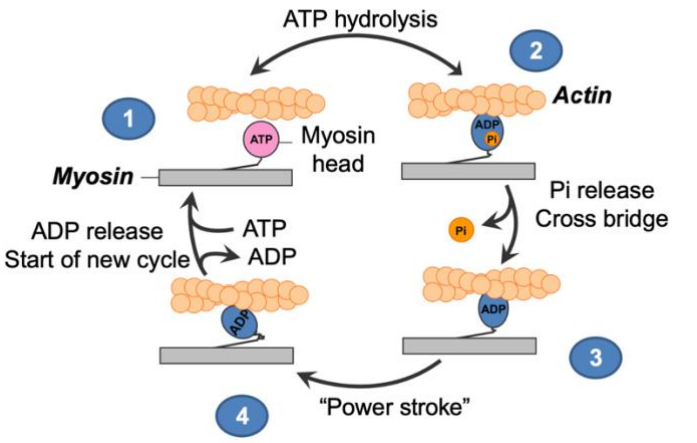

Figure 3. Scheme of skeletal muscle contraction
Zsolt R. The Physiology of Physical Training 2018.

1.2 Skeletal muscle injuries

Skeletal muscle injuries can commonly occur in everyday life, after physical activity, orthopaedic traumas, and diseases. Strains, contusions, and lacerations are the most common causes of skeletal muscle injuries where strains and contusions represent over 90% of all sports-related injuries while lacerations are less frequent. In case of strains, an excessive tensile force applied to muscle leads to an overtreading and rupture of myofibers at the myotendinous junction site, while heavy compressive force suddenly applied causes contusions[6]. Muscle can be damaged as consequences of acute compartment syndromes (ACS): a pressure increase within a confined closed fascial space causes a blood flow reduction ultimately leading to muscle necrosis[7]. After a trauma or surgery, skeletal muscle can be irreversibly damaged by a partial or total loss of muscle mass, also termed as volumetric muscle loss (VML), and muscle function is totally impaired and self-regeneration process is completely inefficient. VML affects adjacent muscle tissue, nerves, bones, tendons, and blood vessels destroyed by release of death molecules, ischemia/reperfusion injury, calcium ion influx, and mitochondria injuries. As consequences, chronic inflammation, fibrosis, and scar formation occur[8].

The current classification divides skeletal muscle injuries in mild, moderate, and severe, depending on severity of clinical impairment. Mild injuries, also defined as first-degree injuries, include strains and contusions where few muscle fibers are teared accompanied by minor swelling, minimal loss of strength, and movement restriction. Strains and contusions with contraction impairment are considered moderate injuries, or second-degree injuries, while when the entire muscle cross section is involved with a complete loss of contractile function, severe or third-degree injuries occur[9].

1.3 Skeletal muscle regeneration

Skeletal muscle can spontaneously heal in a finely regulated process, termed as skeletal muscle regeneration process (SkMR), that progresses in three phases: destruction, repair, and remodeling. In the destruction phase, cytoskeletal material condenses to a spatially confine necrotic tissue, and necrotic cells release their intracellular components from sarcolemma to bloodstream. Release of damage-associated molecular patterns, such as heat shock proteins and high mobility group box-1 proteins (HMGB1), quickly activates the complement system after injury. At the same time, resident mast cells rapidly release several inflammatory mediators, including tumor necrosis factor (TNF)-α, histamine, interleukin (IL)-1, IL-6, platelet-activated factor, and prostaglandins. Similarly, resident macrophages (MPs) release CXC-chemokine ligand 1 (CXCL1) and CC-chemokine ligand 2 (CCL2). Moreover, pro-inflammatory cytokines, including TNF-α, IL-1β and interferon (IFN)-γ, are quickly released by resident neutrophils. These initial steps aim to recruit immune cells at injured site and trigger inflammatory response. Indeed, in few hours post injury, neutrophils are massively recruited, reaching the maximum accumulation after 12-24 hours post injury, and contributing to oxidative and proteolytic modifications in damaged area. If activation of immune cells at this stage delays or is missing, as described in complement protein deficiency or neutrophil depletion, SkMR is irremediably impaired, with significantly decreased immune cell recruitment, and smaller myofiber formation. Within 24 hours, injured site is rich of MPs with a pro-inflammatory phenotype, known as M1-MPs, induced by T helper (Th)1-related cytokines, like IFN-γ and TNF-α, or lipopolysaccharide (LPS). M1-MPs are characterized by high expression of CD68, that mediates phagocytosis and pro-inflammatory cytokine secretion. The simultaneous

presence of neutrophils and M1-MPs amplify phagocytosis through oxidative modification of low-density lipoproteins that bind and activate CD68. In this first part of SkMR, necrotic debris are cleared within a strong pro-inflammatory microenvironment. After clearance of debris at the injured site by macrophages, M1-MPs secrete transforming growth factor (TGF)-β, and phagocytosis rate starts to reduce. As healing proceeds, within 2-4 days, M1-MPs switch to an anti-inflammatory phenotype (M2-MPs), upon Th2 cytokine (IL-4 and IL-13) stimulation or in the presence of IL-10 and IL-33. M2-MPs do not express CD68, while CD163 is highly present. CD163, a transmembrane glycoprotein, binds to haemoglobin-haptoglobin complexes and favors their internalization and degradation, and enhances IL-10 secretion. M2-MPs reach the maximum peak approximately after 4-7 days post injury. Moreover, pro-inflammatory cytokines are completely replaced by anti-inflammatory ones. MP phenotype and microenvironment by switching from pro- to anti-inflammatory marks the progression from destruction to repair and modeling phases. Both processes are strictly related and finely controlled. If this shift occurs too early or too late, SkMR is inefficient. Lymphoid cells are also involved in SkMR; however, their exact role is still under investigation. For example, $CD4^+$ T cells accumulate at injured site following M2-MPs kinetic, while T regulatory cells (Treg) damp inflammatory response and trigger M1-M2 switch, as Treg depletion is associated with slow healing process and prolonged inflammation status[10,11].

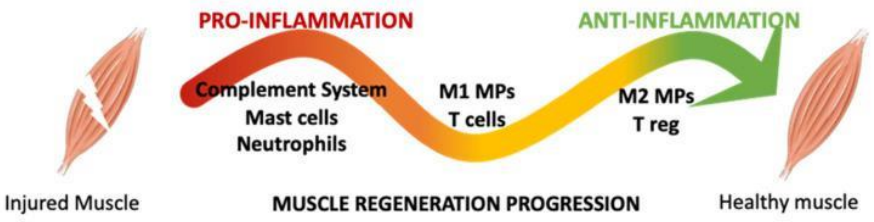

Figure 4. Schematic illustration of skeletal muscle regeneration progression

1.4 Satellite cells

SkMR involves different cell populations, such as muscle stem cells, muscle cells, and immune cells that work together to successfully achieve muscle healing. Muscle stem cells constitute a small cellular pool localized between connective tissue layers and sarcolemma; for this reason, these cells are commonly known as satellite cells (SCs)[10,12]. SCs are in a quiescent steady-state condition, characterized by expression of α7-Integrin and β1-Integrin, M-Cadherin, Syndecan-4, Calcitonin-Receptor (CALCR), C-X-C Chemokine Receptor type-4 (CXCR4), Vascular Cell Adhesion Molecule 1 (VCAM1), and CD34; while Paired box gene 7 (Pax 7) is an essential transcription factor for their postnatal maintenance. As other stem cells, SCs show self-renewal properties and differentiation potential to mature muscle cells. During the second phase of SkMR, SCs escape from quiescence, and first divide following the symmetric cell division criteria to expand stem cell pool. Subsequently, cell division becomes asymmetrical to generate a cell for the stem cell niche and another committed to differentiation. Asymmetrical division is regulated by Par complex, localized on the apical membrane, that selectively actives p38/MAPK pathway to directly regulate Myogenic regulatory factor (MRFs) expression. However, SCs can alternate symmetric and asymmetric cell division under an intrinsic counting mechanism. Upon activation, SCs co-express Pax 7 and Myoblast determination protein-1 (MyoD1), while a few SCs downregulate MyoD1 expression to avoid differentiation. At the same time, SCs migrate at injured site, and differentiate to myogenic progenitor cells (MPCs), also referred as myoblasts. MyoD1 is a member of MRF family, together with Myogenic factor 5 (Myf5), Myogenic factor 6 (Myf6) and Myogenin (Myog). Myf5 is overexpressed by myoblasts during proliferation, while MyoD1 expression is progressively replaced by Myf6 and Myog leading to terminal differentiation of myoblasts

to myocytes that fuse each other in multinucleated myotubes building mature myofibers. As the process progresses, MPCs morphologically change, become myocytes with elongated shape, and fuse each forming myotubes, that functionally mature into myofibers during the last stage of SkMR.

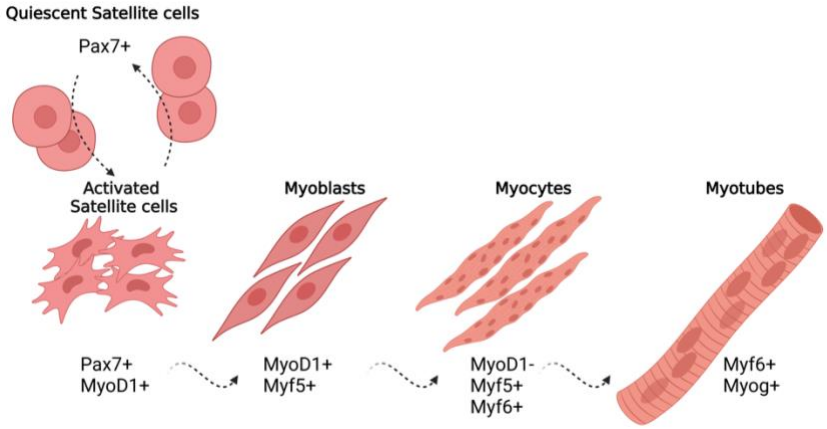

Figure 5. Satellite cell differentiation progression

Mechanisms that regulate SC proliferation and differentiation are still unclear. Some molecules, such as hepatocyte growth factor activator (HGFA), can induce SCs to escape from quiescence to an intermediate "G alert state" allowing faster cell cycle. Moreover, local interactions between SCs and surrounding cells in the niche can act as signals, as well as a complex crosstalk with immune cells. For example, M1-MPs release insulin-like growth factor 1 (IGF1), that act as mitogen on MPCs. SCs presence is essential for SkMR, as SC ablation or degenerative diseases totally impair healing process[10,13,14].

1.5 Conventional therapies

Clinical management of skeletal muscle injuries remains a major challenge. Available treatments are divided in conservative and surgical approaches.

Conservative management includes RICE protocol consisting of Rest, Ice (cold), Compression, and Elevation. Further retraction of muscle stumps is avoided by immobilization of injury area, preventing the formation of a large gap between muscle and connective scar tissue[6]. Ice application is immediately recommended after trauma, because of its effects in reducing the size of hematoma and inflammation, as well as tissue necrosis[15]. Compression application just after an injury is still a debated issue. Although compression reduces intramuscular blood flow at injured area, compression does not significantly reduce the size of hematoma nor accelerate healing process[6]. However, in common practice, combination of ice application and compression is currently adopted in bouts of 15-20 minutes, repeated at intervals of 30-60 minutes, resulting in limited hemorrhages and tissue necrosis[16]. Elevation of injured area above the heart level allows a better flow of interstitial fluid, leading to reduced fluid accumulation and lower hydrostatic pressure[6]. To date, in case of strains, more active treatments are also used, such as exercises aimed to agility recovery and trunk stabilization. These approaches show better outcomes in terms of faster return to sport activity and reduced re-injury rate compared to standard protocol focused on stretching and strengthening of injured muscles[17].

In severe injuries, muscles appear atrophic, and a specific sequence of rehabilitation exercises is recommended starting from isometric to isotonic and isokinetic trainings. Isometric training is characterized by contraction exercises where muscles are fixed in length but subjected to increasing loads. Isotonic training includes contraction exercises where muscle length changes while tension is constant. Both trainings are conducted without loads at the beginning, and tension force is progressively added. Once that isometric and isotonic trainings do not produce any pain, patients can start with isokinetic

dynamic training where specialized platforms provide increasing resistance force to movement performed at constant speed. Rehabilitation exercises are supported by other activities to train cardiovascular health[6].

If muscle injury does not successfully recover, a clinical re-examination is conducted and surgical procedure are evaluated[9]. Surgical interventions are required in large intramuscular hematoma, complete strains with few or absent agonist muscles, strains where more than a half of muscle is torn, and in patients with persisting pain and extension deficit. Expected outcomes are satisfying when surgery is early performed (e.g., within 3 weeks from injury)[18]. However, surgical procedures can cause muscle traumas, also called iatrogenic injuries. These procedures are required in case of aggressive tumor ablation or joint arthroplasties, such as total hip arthroplasty (THA) where a severe muscle laceration occurs, leading to the loss of muscle functionality, fatty degeneration, scar tissue formation, pain, and elevated re-injury rate[19,20].

1.6 Pharmacological therapies

Skeletal muscle injuries are always associated with pain and inflammation. Pharmacological treatments aim to relieve these symptoms using non-steroidal anti-inflammatory drugs (NSAIDs) and glucocorticoids. NSAIDs are commonly prescribed as cyclooxygenase 2 (COX-2) inhibitors, leading to reduction in prostaglandin levels and to inflammatory response arrest[21]. However, NSAIDs role in skeletal muscle injuries is still under debate, as NSAID use in animal models is associated with delayed muscle healing and increasing fibrosis rate[22], even if microcirculatory flow is completely restored in injured muscles[23].

Patients treated with NSAIDs show better recovery and reduced strength loss in less severe injuries, like exercise-induced muscle injury (EIMI) provoked by repeated eccentric contractions where few myofibers are damaged while connective sheaths are preserved[24,25]. NSAIDs and other drugs (e.g., analgesic or acetaminophen) do not show significant effects in Delayed Onset Muscle Soreness (DOMS) and muscle traumas, like strains or tears, without amelioration of pain, swelling, and muscle strenght[26]. Conversely, NSAIDs are recommended in severe skeletal muscle contusions, such as myositis ossificans (HO), because of their positive effects in preventing ossification after prosthetic replacement[27]. Glucocorticoids are a valid alternative to NSAIDs, even though their effects are still controversial. Intramuscular glucocorticoid injections in sportsmen is associated with faster muscle strength recovery and re-practice in fewer days[28]. On the other hand, intramuscular use of glucocorticoids is also related to atrophy, disruption of normal muscle architecture, and reduction in collagen fascicle stenght[29].

1.7 Alternative therapies

Current therapies are still controversial and seem not to completely restore muscle physiology, therefore, new therapies are required. PRP is defined as blood derivate with higher concentration of autologous growth factors and bioactive molecules obtained in a minimally invasive procedure. PRP is commonly used in orthopaedic filed. Patients treated with PRP injections can faster return to physical activity; however, patients treated with common therapies display similar outcomes with comparable re-injury rate, pain, and strength recovery[30–32].

Immune cell transplantation represents a potential solution to restore M1-M2-MPs transition and allow normal progression of SkMR process. Immune cells are usually harvested from peripheral blood in a non-invasive way and show regenerative potential in critical limb ischemia (CLI), where patients are not responsive to current therapies and can undergo to amputation. Peripheral blood mononuclear cell (PBMC) autologous transplantation is safe, easy, fast, and effective, as this procedure significantly decreases the risk of amputation, while improves oxygen pressure, and tissue regeneration[33–35].

Other novel therapeutic strategies for skeletal muscle injury treatment include stem cell transplantation of cells with both myogenic and non-myogenic origin. First studies on cell-based therapies have investigated efficacy of SCs in animal models. Once transplanted, SCs successfully engraft, proliferate, give rise to newly myofibers, and improve contractile function[36,37]. the number of SCs required to form hundreds of multinucleated myofibers is very low, as transplanted SCs undergo to proliferation, populate stem cell niche, and contribute to myofiber formation[38,39]. However, SC transplantation studies in human injury model are lacking due to the inability to harvest SCs from healthy human tissue since extraction and enzymatic degradation are required. Moreover, SCs are just a small fraction of whole skeletal muscle cellular content (2-7%), and spontaneously differentiate in *ex-vivo* conditions and lose their regenerative potential. For these reasons, stem cells of non-myogenic origin are preferred, such as mesenchymal stem cells (MSCs)[40].

Human mesenchymal stem cells (*h*MSCs) are the most versatile tool in regenerative medicine, because of their multi-lineage differentiation potential. *h*MSCs are potentially capable to differentiate in adipocytes, osteocytes, chondrocytes, and myocytes, and can be easily harvested from different tissues, such as umbilical cord, adipose tissue, and bone marrow

(BM)[41]. Mesenchymal and Tissue Stem Cell Committee of the International Society for Cellular Therapy developed the minimal criteria to universally define *h*MSCs: (i) adherence to plastic surfaces; (ii) specific surface antigen expression ($CD73^+$ $CD90^+$ $CD105^+$ $CD34^-$ $CD45^-$ $CD11b^-$ $CD14^-$ $CD19^-$ $CD79a^-$ $HLA\text{-}DR^-$); and (iii) multipotent differentiation potential[42]. *h*MSCs also exert immunomodulatory and anti-inflammatory activities by modulating T and B and natural killer (NK) lymphocytes, cytokine production, and dendritic cell (DC) differentiaiton[43–46]. Indeed, *h*MSCs secrete a wide range of cytokines and growth factors and establish an immunosuppressive microenvironment trough Treg stimulation and IL-10 secretion by plasmacytoid DCs[47,48]. *h*MSCs maintain their phenotype and their functional potential after *ex-vivo* expansion[49].

MSC therapies are popularly used in orthopaedic field, such as in bone, cartilage and cardiovascular diseases[50], however, few clinical trials have been conducted for skeletal muscle injury treatment. Moreover, the majority of these trials includes patients with damaged external skeletal muscle sphincter, an infrequent muscle injury, showing high tolerability of stem cell transplantation and scar tissue replacement with myofibers, without conclusive results muscle function improvement[51,52]. Conversely, allogenic intraoperative MSC transplantation for hip arthroplasty surgery-associated results in significant improvement of contractile function and muscle volume[53,54].

1.8 Skeletal muscle tissue engineering

Tissue engineering (TE) aims to develop an engineered tissue resembling its physiological counterpart in terms of regeneration potential and functions. TE

approach is based on combination of cells, scaffolds, and chemical or mechanical signals.

Stem cells are always subjected to stimuli from the surrounding environment (stem cell niche), including extracellular matrix (ECM), cell-cell-interactions, bioactive molecules (e.g., cytokines and hormones), and mechanical forces supplied by organism and physiological fluid movements. For this reason, engineered constructs are developed using biomaterials to reproduce physiological conditions, as these materials provide a comfortable environment to support stem cells in their differentiation toward functional tissue of interest. Natural polymers, such as collagen, chitosan, alginate, and fibrin, are commonly used for hydrogel scaffold formation, because of their biocompatibility, non-invasive administration, and high permeability to oxygen, nutrients and waste molecules[55,56]. Hydrogel can be chemically and structurally functionalized to better adapt to differentiation process requirements, such as hydrogel enriched in adhesion proteins favoring stem cell survival and differentiation[57–59]. Other hydrogel properties, including stiffness and topography, also influence stem cell behavior. Indeed, as stem cells better differentiate in hydrogels with high stiffness, or adipogenic commitment is enhanced in hexagonal scaffolds[60,61].

Chemical stimuli are provided by growth factors (GFs), bioactive molecules driving cell differentiation, that can be added to culture medium. Because of their short half-life, frequent medium exchange is required, or GFs can be alternatively embedded within hydrogels or loaded in micro-/nano-carriers to sustain their delivery for longer periods[62]. Mechanical inputs are provided by specific instruments, also known as bioreactors. Perfusion is one of the most diffused mechanical stimuli, characterized by continuous flow to supply oxygen and nutrients, favoring cell survival and differentiation[56,63,64].

Bone marrow-derived Mesenchymal stem cells (BM-MSCs) are frequently adopted in TE in orthopaedic field. Once seeded on a construct in a three-dimensional (3D) environment, chemically and mechanically stimulated, BM-MSCs successfully commit towards different phenotype, such as bone, tendon and cartilage[65–68].

In skeletal muscle tissue engineering (SMTE), early *in-vitro* studies have used muscle cells usually of animal origin, seeded on biocompatible and biodegradable materials[69–72]; however, some issues regarding myogenic stem cell harvesting have been highlighted, thus alternative source of stem cells has been investigated, (see Figure 6).

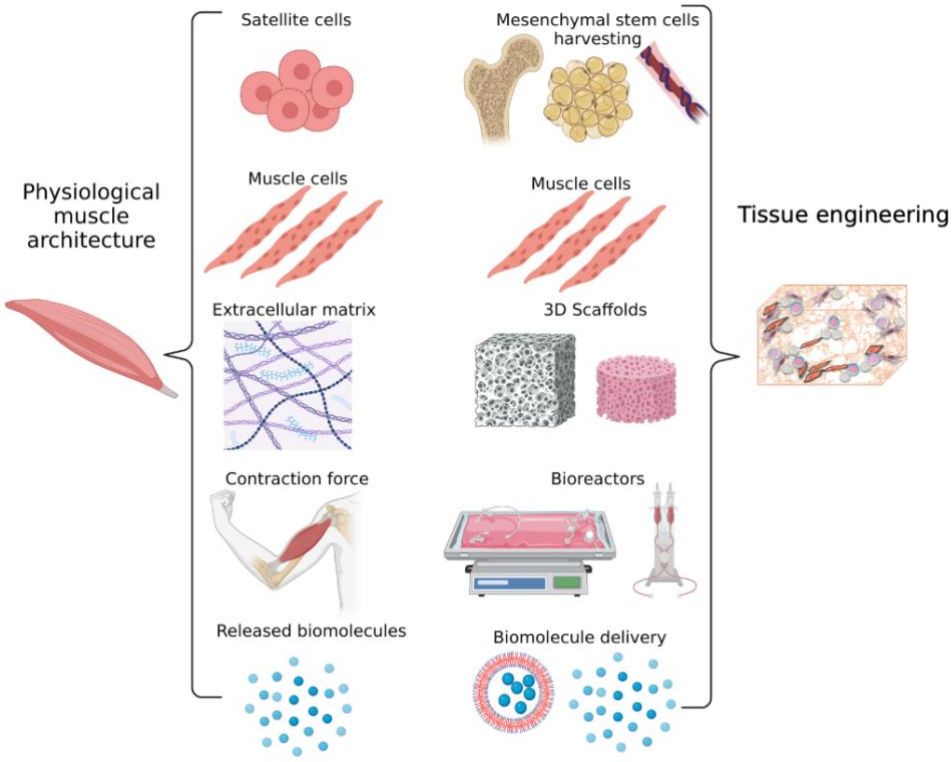

Figure 6. Skeletal muscle tissue engineering tools

BM-MSCs are the most utilized stem cell type in SMTE, although the exact composition of chemical *in-vitro* and *in-vivo* stimulation for myogenic commitment is still unclear. First *in-vitro* studies have investigated the role of 5-azacytidine (AZA), a DNA methyltransferase inhibitor, with some positive effects[73], not confirmed by addition of GFs, such as fibroblast growth factor (FGF) and amino acids with or without dexamethasone in culture medium[74]. Despite a wide range of GFs has been investigated for an optimal myogenic commitment, there are still no specific protocols to induce myogenesis. Therefore, co-culture systems could represent an alternative approach, as chemical and physical stimuli could be provided to MSCs by other co-cultured cells. Indeed, this method reproduces cell-cell interactions within stem cell niche, as co-cultured MSCs are pushed to acquire a myogenic fate as shown by MRF expression and the ability to fuse to myoblasts[75]. These effects can be increased in 3D co-culture conditions supplemented with bFGF and dexamethasone. In this model, MSCs show a better myotube formation and myogenic differentiation[76,77].

In SMTE, biomaterial choice to build hydrogel is not easy, as materials should display high biocompatibility and affinity for biological surfaces, and good elasticity to provide contractile function. Once fibrinogen is cleaved by thrombin enzyme, fibrin gels self-assemble and are considered the best material for myogenic stem cell 3D culture, showing high extensibility without stretch, and efficiently mimicking SC niche by favoring cell activation, proliferation, and differentiation[78,79]. Fibrin reproduce *in-vitro* the hierarchical structure of skeletal muscle tissue, and stem cells can easily engraft and regenerate muscle structure and function, without any fibrotic tissue deposition[80,81].

1.9 Thesis objective

Currently available treatments are still far from achieving complete skeletal muscle regeneration and tissue engineering strategies could represent an innovative approach for muscle trauma treatment. The aim of this PhD project was to develop a robust and reproducible *in-vitro* model of myogenic commitment by co-culturing different cell phenotypes in both 2D and in 3D environment, adopting static and dynamic conditions.

In more details, *h*BM-MSCs were co-cultured with differentiated human primary skeletal myoblasts (*h*SkMs) that could trigger myogenesis in stem cells through direct contacts and paracrine way. Moreover, co-culture system was implemented by adding immune cells from peripheral blood to investigate their contribution in myogenesis. Furthermore, a novel and versatile biomimetic 3D co-culture system was developed using fibrin-based scaffolds, PBMCs, and GFs, as a platform to efficiently reproduce *in-vitro* skeletal muscle environment.

CHAPTER 2. Myogenesis in 2D monolayer co-cultures: static and dynamic approach

2.1 Introduction

As described in Chapter 1, in case of severe injuries, spontaneous skeletal muscle healing process fails, and classical therapies do not provide a complete tissue restoration. *In-vitro* myogenic models are useful to represent this complex scenario to find out novel therapeutic approaches. *h*BM-MSCs are becoming the most utilized source of stem cells for *in-vitro* models to study healing and regeneration events, because of their high multi-differentiational potential.

To promote *h*BM-MSC myogenic commitment, culture medium can be supplemented with several GFs even if the best mix and related concentrations are still unknown and under investigation. Among them, FGF is widely added, usually at a concentration of 10 ng/mL. FGF family acts both at transcriptional and translational levels stimulating SC to enter cell cycle and favoring the transition from myoblast-to-myotube differentiation[82,83]. As previously indicated, combination of medium supplementation in a co-culture with mature skeletal muscle cells is the best strategy to commit MSCs to skeletal phenotype. However, seeding density ratios between BM-MSCs and skeletal muscle cells have not been well-defined and standardized yet.

During tissue regeneration, MSCs and immune cells strongly interact each other, favoring healing process. MSC immune-modulatory effect results in T/B lymphocyte and NK cell-mediated immune response damping. T-lymphocyte proliferation is strongly reduced, causing cell unresponsiveness by decreasing IFN-γ secretion and changing their expression profile[45,84]. B-lymphocyte proliferation is inhibited resulting in impairment of immunoglobulin secretion (Ig-M, Ig-G, Ig-A)[46]. MP polarization is also influenced by MSCs, as well as expression of anti-inflammatory cytokines, such as IL-10[85,86].

Perfusion bioreactor systems have been described to promote *in-vitro* stem cell differentiation models. These culture systems have been used to improve spatial uniformity of cardiac myocyte distribution in 3D scaffolds and to enhance expression of cardiac-specific markers[87]. Perfusion systems are also adopted to commit *h*BM-MSCs towards osteogenic and chondrogenic phenotypes, showing that medium perfusion allows a better distribution of soluble factors, as well as a more efficient mass transfer of nutrients[68,88].

2.2 Aim

The present work aimed to investigate myogenic commitment of *h*BM-MSCs, adopting a bFGF supplemented medium and a co-culture with human primary skeletal myoblasts (*h*SkMs) both in static and dynamic conditions. Cells were co-seeded in the same well in static culture, whereas *h*BM-MSCs and *h*SkMs were seeded in separated wells within a plate where culture medium continuously flows. *h*BM-MSC commitment was defined based on expression of skeletal muscle-related genes, such as *Pax3*, *MyoD1*, *Myf5*, *Myf6*, *Desmin* and *Myosin heavy Chain II* (*MYH2*); of Desmin and MYH2 protein expression levels by semi-quantitative immunofluorescence (qIF); and by western blotting in dynamic co-culture conditions.

2.3 Materials and Methods

2.3.1 *h*MSC isolation and harvesting

*h*BM-MSCs were obtained from bone marrow (BM) of two healthy donors (males aged 38 and 40) after informed written consent in accordance with the Declaration of Helsinki to the use of their residual BM aspirate for research purposes, with approval from the University Hospital (Review Board prot./SCCE n. 24988 achieved on April 09th, 2015). BM aspirate was cultured in Minimum Essential Medium Alpha (α-MEM) (Corning) supplemented

with 1% Glutagro (Corning), 10% Fetal Bovine Serum (FBS) (Gibco^{TM}), and 1% Penicillin/Streptomycin (Pen/Strep) (Corning) and incubated at 37°C in an atmosphere of 5% CO_2 and 95% relative humidity. After 48h, non-adherent cells and other residues were removed, and fresh media added. Adherent cells were fed twice a week till day 14 when colonies were detached and identified as MSCs. Cells were re-seeded at 4×10^3 cells/cm^2 in the same culture conditions, and cells were detached at 70–80% confluence using 0.05% trypsin-0.53 mM EDTA. After counting cells with Trypan Blue, MSCs were subcultured at a concentration of 4×10^3 cells/cm^2 and used at passage 2 for further experiments.

2.3.2 MSC flow cytometry characterization

A minimum of 1 x 10^5 cells were stained with surface markers for MSC immunophenotyping by flow cytometry according to International Society of Cellular Therapy guidelines[42]. Cells were incubated at room temperature (RT) for 20 min in the dark with the following directly conjugated mouse-anti human antibodies: 2.5 µL of fluorescein isothiocyanate (FITC)-conjugated anti-CD90 or 10 µL of FITC-conjugated anti-HLA-DR; 5 µL of allophycocyanin (APC)-conjugated anti-CD73; 10 µL of phycoerythrin (PE)-conjugated anti-CD105 or 10 µL of PE-conjugated anti-CD34; and 10 µL of phycoerythrin cyanin 7 (PC7)-conjugated anti-CD45 or 10 µL of PC7-conjugated anti-CD14. All isotype controls were immunoglobulin G type 1 (IgG1) conjugated to FITC, PE, APC, or PC7, and were used as negative controls. After incubation, cells were washed with 3 mL of PBS and resuspended in 300 µL of the same buffer for acquisition.

Sample acquisition was performed using a BD FACSVerse flow cytometer (Becton Dickinson, BD, NJ, USA) equipped with blue (488 nm) and red lasers (628 nm) and BD FACSuite software (BD Biosciences). Compensation

was calculated utilizing single-color controls for each fluorochrome and an unstained sample as negative control for setting PMT voltages.

All samples were run using the same PMT voltages. A minimum of 30,000 events were recorded. FlowJo software (v.10.7.1, LLC, BD Biosciences) was employed for post-acquisition compensation and flow cytometric analysis. In details, BM-MSCs were first identified using linear parameters (forward scatter area (FSC-A) vs side scatter area (SSC-A), double cells were excluded (area vs height, FSC-A vs FSC-H), and CD90 and CD45 expression was first investigated. Subsequently, CD105 and CD73 expression was further studied on $CD45^{-}CD90^{+}$ cells. Similarly, HLA-DR and CD34 expression was first investigated on single cells, and CD14 was further analysed on $CD34^{-}HLA\text{-}DR^{-}$ cells. Expression of each marker on single cells was also reported using histograms and using unstained samples as negative controls.

2.3.3 *h*BM-MSC-*h*SkM static co-culture

*h*BM-MSCs were co-seeded with *h*SkMs (Gibco™) at density of 4×10^{3} cell/cm^2 at 2:1 and 1:1 seeding density ratios. Culture medium was mixed according to cell ratio and composed of α-MEM (Corning) supplemented with 1% Glutagro (Corning), 10% FBS (Gibco™) and DMEM low glucose (Gibco™). Medium was enriched with 100 nM Dexamethasone and 100mM Ascorbic acid.

2.3.4 Dynamic culture condition

Cells were cultured within a perfusion bioreactor formed by a custom multi-well plate milled in polymethyl methacrylate (PMMA, AltuglasVR CN 100 10000, Altuglas International, La Garenne- Colombes Cedex, FR), a biocompatible material for biomedical applications[89]. This plate has two holes for silicon tube (TygonVR , Charny, France) insertion that allows the medium

to flow by peristaltic pumps at a constant flow rate of 1.0 mL/min. *h*BM-MSCs and *h*SkMs were seeded at a density of 4 x 10^3 cells/cm^2 in different wells always maintaining the ratios of 2:1 or 1:1. Medium ratios were adjusted accordingly, as described before.

2.3.5 Brightfield images

Brightfield images of *h*BM-MSC and *h*SkM cultures were captured using a LEICA DMIL LED microscope, at 10x magnification, and acquired by LEICA DFC425 C camera.

2.3.6 RNA isolation and gene expression profiling

Myogenic related genes such as *Pax3*, *MyoD1*, *Myf5*, *Myf6*, *Desmin* and *MYH2* were investigated, as well as pro- and anti-inflammatory cytokines Interleukin 6 (*IL6*), Tumor Necrosis Factor (*TNF*), Interleukin 12A (*IL12A*), Interleukin 1β (*IL1B*), Interleukin 10 (*IL10*) and *TGFB1*. Total RNA was extracted using Rneasy Micro Kit (Qiagen). For each sample, 1 μg of total RNA was reverse transcribed using the iScript™ cDNA synthesis kit (BioRad). Relative gene expression analysis was performed in a LightCycler® 480 Instrument (Roche), using the SsoAdvanced™ Universal SYBR® Green Supermix (BioRad) following MIQE guidelines[90]. Amplification was performed in a 10 μL final volume, including 2 ng of complementary DNA (cDNA) as template. Triplicate experiments were performed for each condition explored, and data were normalised to glyceraldehyde-3-phosphate dehydrogenase (*GAPDH*) applying the geNorm method[91] with CFX Manager software ($M < 0.5$), and fold changes in gene expression were determined by $2^{-\Delta\Delta Ct}$ method and presented as relative levels over day 0 = 1.

2.3.7 Immunofluorescence assays

Cells were fixed with 4% paraformaldehyde (PFA) for 30 min at RT, followed by permeabilization with 0.1% Triton X-100 for 5 min and blocked with horse serum solution for 1h. Cells were stained for Desmin (1:100; Abcam) and for MYH2 (1:50, Thermo Fisher Scientific). Then, cells were incubated for 1h at RT with the Alexa Fluor ™ 488 goat anti-rabbit IgG (1:400, Thermo Fisher Scientific) and with VectaFluor™ anti-mouse IgG Dylight 594 kit (VectorLaboratories) antibodies, and cell nuclei were counterstained using 4',6-diamidino-2-phenylindole (DAPI). Images were acquired by a fluorescence microscope with identical settings (Eclipse Ti Nikon Corporation). Signal intensity, related to the proteins of interest, was quantified using the software ImageJ (rel.1.52p National Institutes of Health, USA). Original images in RGB format were converted into a 16-bit (grey scale) format. Then, tagged areas were expressed as an average value of pixel intensity within a range from 0 (dark) to 255 (white). Data were normalized to the number of cells present in the whole field and reported as fold change relative to *h*BM-MSCs at day 0[92].

2.3.8 Western blotting

*h*BM-MSCs were lysed in ice-cold RIPA lysis buffer (50 mM Tris-HCl, 150 mM NaCl, 0.5% Triton X-100, 0.5% deoxycholic acid, 10 mg/mL leupeptin, 2 mM phenylmethylsulphonyl fluoride and 10 mg/mL aprotinin). About 10 μg of proteins were separated on 10% SDS-PAGE at 90V for 1h and at 120V for 1h and transferred on a nitrocellulose membrane. 5% non-fat dried milk powder (Sigma-Aldrich) in Tris-buffered saline containing 0.1% Tween-20 (TBST) was used for blocking for 1h at RT. Primary antibodies, Desmin (Abcam ab8592, rabbit, 1:3000) and MYH2 (Thermo Fisher Scientific, #PA5-116876, rabbit, 1:3000) were incubated overnight at 4°C. Horseradish

peroxidase-conjugated donkey anti-rabbit IgG (BioRad) was used to immunodetect proteins with chemiluminescence (ECL) system (Amersham Pharmacia Biotech) and exposed to X-ray film (Santa Cruz Biotechnology). The optical density (OD) of bands was analysed by Photoshop software and expressed as a ratio relative to actin-β protein.

2.3.9 Statistical analysis

Statistical analysis was conducted using Prism software (v.6.0, GraphPad Software, LLC, San Diego, California, United States). Results are presented as mean ± standard deviation (SD). Statistical analysis was performed using one-way analysis of variance (ANOVA) with Tukey's multiple comparison test, for comparison vs *h*BM-MSCs at day 0, selected as control. Two- way analysis of variance (ANOVA) with Tukey's multiple comparison test was also performed for comparison of data obtained in perfusion system culture vs *h*BM-MSCs at day 0. p values < 0.5 were accepted as significant[93].

2.4 Results

2.4.1 *h*BM-MSC and *h*SkM characterization

Mesenchymal phenotype was confirmed according to minimal criteria defined by International Society of Cellular Therapy[42]. Primary *h*BM-MSCs were positive for mesenchymal markers, such as CD90, CD105, and CD73, while negative for CD34, CD14, CD45, and HLA-DR by flow cytometry analysis, as shown in Figure 7.

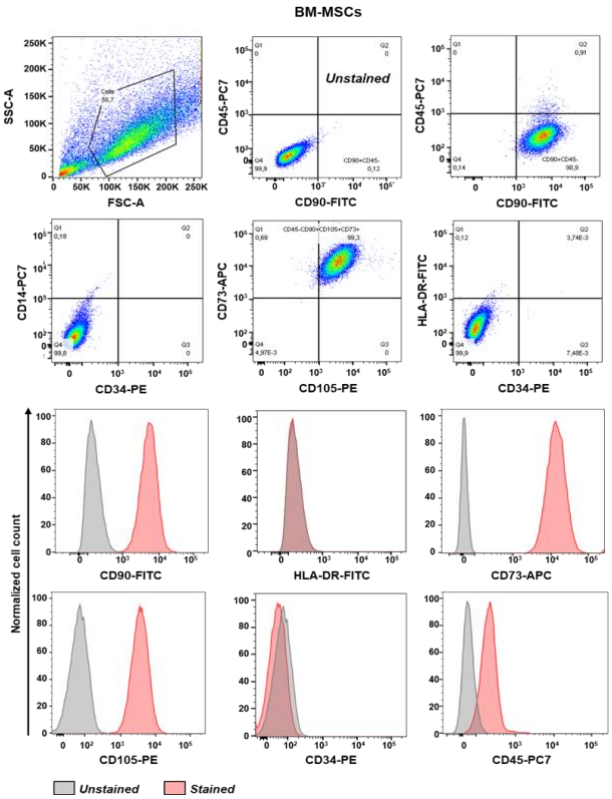

Figure 7. Flow cytometry and gating strategy of *h*BM-MSCs. Representative cytofluorimetric FSC vs SSC (cell size vs granularity index) cells scatter of *h*BM-MSCs is shown. Cells were first identified using linear parameters (forward scatter area [FSC-A] vs side scatter area [SSC-A], and double cells were excluded (FSC-A vs FSC-H). For antibody mix 1, CD90 and CD45 expression was investigated on single cells, and CD105 and CD73 expression was further studied on $CD45^{-}CD90^{+}$ cells. For antibody mix 2, HLA-DR and CD34 expression was first investigated on single cells, and CD14 was further studied on $CD34^{-}HLA\text{-}DR^{-}$ cells. Expression of each marker on single cells was also reported using histograms and using unstained samples as negative controls.

*h*SkMs showed their typical stretched shape, as observed by optical microscope images (see Figure 8a). q-IF analysis showed the two myogenic proteins, such as Desmin and MYH2. Desmin was better expressed in the first seven days of culture (41.7-fold), while MYH2 displayed an increasing trend up to day 21 (0.30-fold, *Pax3*, *MyoD1*, *Myf 5*, *Myf 6*, *Desmin*, and *MYH2* were expressed constitutively in *h*SkMs, (Figure 9).

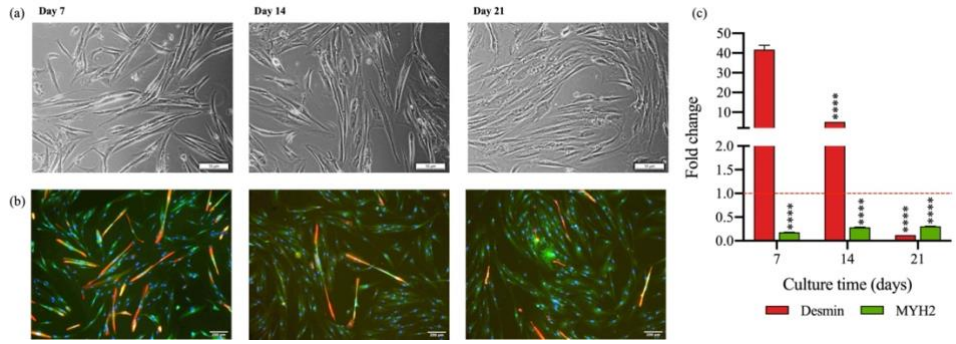

Figure 8. Brightfield images and immunofluorescence assay of *h*SkMs. Brightfield images of *h*SkMs, seeded at density of 120.000 cells/cm^2, at day 7, 14 and 21 of culture. All images were captured using 10x magnification; scale bar: 10 µm (a). IF assay at day 7, 14 and 21 of culture was performed by staining Desmin in red and MYH2 in green. All images were captured using 10x magnification, scale bar: 200µm (b). Semi-quantitative IF of Desmin and MYH2 protein signals is shown as mean±SD, and two-way ANOVA performed between time points, n=3, *$p < 0.05$, **$p < 0.01$, ***$p < 0.001$ and ****$p < 0.0001$ (c).

2.4.2 Myogenic commitment strategies of *h*BM-MSCs

bFGF at concentration of 10 ng/mL is recommended in literature as supplement in myogenic medium; however, when *h*BM-MSCs were cultured in static condition within this environment, they exhibited poor changes in myogenic gene expression (Figure 9). Indeed, *Pax3* reached the maximum expression after 7 days of culture (34-fold), and *MyoD1*, *Myf5* and *Myf6* sequentially picked the maximum of 30-fold, 23.6-fold, and 16.7-fold at day

7, respectively; then, these gene expressions were reduced. *Desmin* and *MYH2* genes were not up regulated at all throughout the whole culture time.

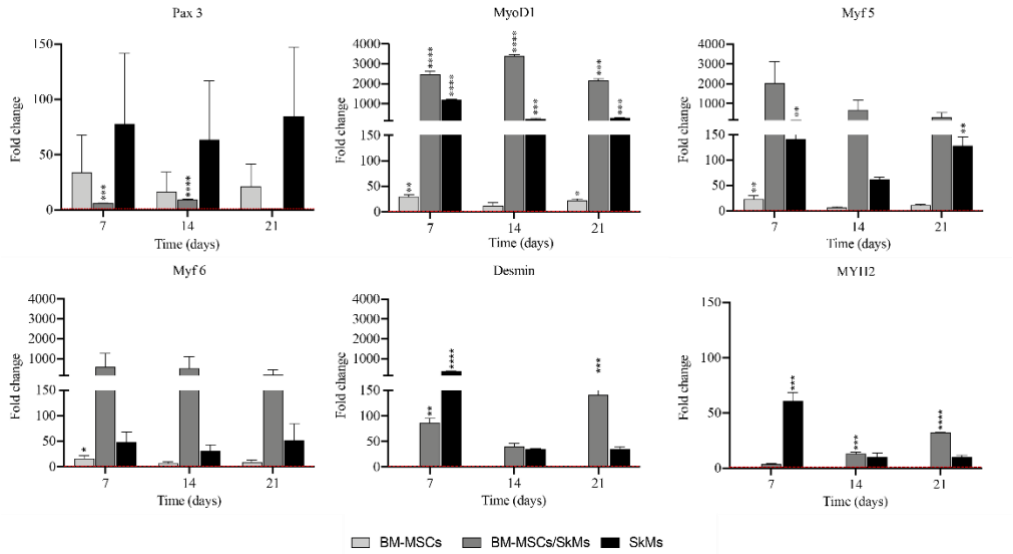

Figure 9. Gene expression profiling for myogenic markers by quantitative RT-PCR obtained from *h*BM-MSCs and *h*SkMs co-seeding culture in static condition with myogenic medium (10 ng/mL of bFGF). *h*BM-MSCs were co-seeded with *h*SkMs in ratio 2:1; *h*BM-MSCs and *h*SkMs were added, as controls. mRNA levels of myogenic markers: *Pax3*, *MyoD1*, *Myf5*, *Myf6*, *Desmin* and *MYH2* were assayed by qRT-PCR at days 7, 14 and 21 of culture. The relative quantification of each mRNA gene expression normalized to endogenous GAPDH (internal control) was calculated using the $2^{-\Delta\Delta Ct}$ method and presented as fold change over *h*BM-MSCs at day 0, selected as a control. All data were analyzed by one-way ANOVA, n=3; *$p < 0.05$, **$p < 0.01$, ***$p < 0.001$ and ****$p < 0.0001$.

Conversely, when *h*BM-MSCs were co-seeded with *h*SkMs at a 2:1 ratio, an excellent myogenic gene expression outcome was observed (Figure 9); *MyoD1* expression was remarkable with the maximum expression, statistically significant, at day 14 with 3400-fold, while *Myf5* and *Myf6* reached the highest expression at day 7, with 2000-fold and 590-fold, respectively. *Desmin* was up-regulated at day 7 of 88-fold and at day 21 of 141-fold ($p \leq 0.001$). *MYH2* increased to 13-fold at day 14 and up to 32-fold

($p \leq 0.0001$) at day 21. *h*SkMs gene expression, normalized on *h*BM-MSCs at day 0, were added to Figure 9, as a positive control.

By morphological analysis, co-seeded *h*BM-MSC-*h*SkMs showed a progressive elongated shape with an even more accurate orientation along paralleled line (brightfield images in Figure 10a).

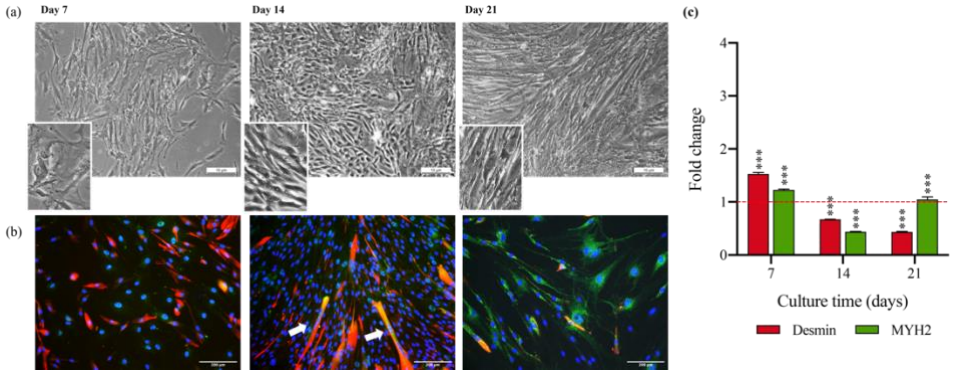

Figure 10. Brightfield and immunofluorescence images of *h*BM-MSCs and *h*SkMs co-seeded with ratio 2:1 in static condition with myogenic medium (10 ng/mL of bFGF). Brightfield images at day 7, 14 and 21 were captured using 10x magnification; scale bar: 10 µm; a zoomed area at 150% was added to better show the cells morphology and their elongation (**a**). IF assay was performed at same time points by staining Desmin in red and MYH2 in green. All images were captured using 20x magnification, scale bar: 200µm. Several *h*SkMs multinucleate cells are evident (see arrowheads); the Desmin protein (see red staining) is mainly localized nearby. MYH2 (see green staining) was more abundantly distributed over all cell population. From the images it was also clear the cells alignment and their longitudinally elongation (**b**). Semi-quantitative IF of Desmin and MYH2 protein signals is shown as mean±SD, and two-way ANOVA performed between time points, n=3, *$p < 0.05$, **$p < 0.01$, ***$p < 0.001$ and ****$p < 0.0001$ (**c**).

This behavior was particularly evident in the zoomed areas at 150% inserted in each image of Figure 10a. IF images showed the presence of Desmin, as confirmed by q-IF with 1.5-fold ($p \leq 0.001$) at day 7, and an increasing trend of MYH2 protein secretion, 1.1-fold ($p \leq 0.001$) at day 21. From IF images, *h*SkMs nuclei grouped clearly appeared at day 14, forming their typically polynuclear syncytia, that can aid to distinguish them from *h*BM-MSCs (Figure 10b). *h*BM-MSCs displayed a significantly high expression of MYH2

stained in green by IF. Poor *h*BM-MSC viability was observed when 1:1 cell ratio was adopted (data not shown).

To study immunomodulatory activity of *h*BM-MSCs on myogenic commitment, cytokine expressions were investigated (Figure 11).

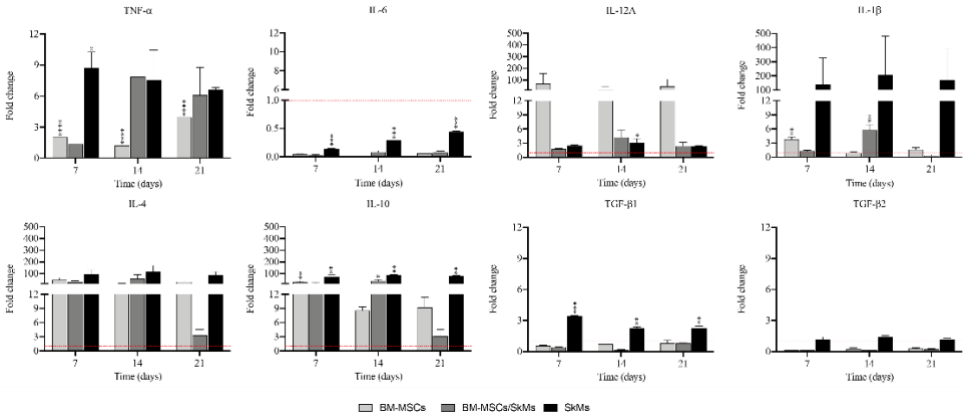

Figure 11. Gene expression profiling for pro- and anti- inflammatory cytokines by quantitative RT-PCR obtained from *h*BM-MSCs and *h*SkMs co-seeding culture in static condition with myogenic medium (10 ng/mL of bFGF). *h*BM-MSCs were co-seeded with *h*SkMs in ratio 2:1; *h*BM-MSCs under bFGF medium and *h*SkMs were added as controls. The mRNA levels of pro-inflammatory cytokines (*TNF-α, IL-6, IL-12A* and *IL-1β*) and anti-inflammatory cytokines (*IL-10, IL-4, TGF-β1* and *TGF-β2*) were assayed by qRT-PCR at day 7, 14 and 21 of culture. The relative quantification of each mRNA gene expression normalized to endogenous *GAPDH* (internal control) was calculated using the $2^{-\Delta\Delta Ct}$ method and presented as fold change over *h*BM-MSCs at day 0, chosen as control. All data were analyzed by one-way ANOVA, n=3; $*p < 0.05$, $**p < 0.01$, $***p < 0.001$ and $****p < 0.0001$.

*h*BM-MSCs cultured with bFGF supplemented medium upregulated *IL12A* at 67.5-fold at day 7; *IL1B* reached 4-fold at day 7, then those expressions were significantly reduced along culture. Among anti-inflammatory cytokines, *IL4* and *IL10* were the most overexpressed with the maximum fold reached by *IL4* of 44-fold and by *IL10* of 27-fold at day 7 (Figure 11). In static co-seeding culture, *TNFA* was the highest up-regulated pro-inflammatory cytokine,

followed by *IL1B* and *IL12A*. The maximum peak at day 14 was for *TNFA* (8-fold), *IL1B* (6-fold), and for *IL12A* (4-fold). All expressions returned close to baseline levels at day 21 (Figure 11).

Most significantly cytokines expressed by *h*SkMs were *TNFA* (9-fold) at day 7; *IL1B* (205-fold), *IL10* (90-fold), and *IL4* (117-fold) were overexpressed at day 14. *TGFB1* and *TGFB2* expression increased of 3.4-fold and 1.2-fold at day 7, respectively, showing a different behavior compared to co-seeding culture (Figure 11).

Therefore, *h*BM-MSCs showed low myogenic gene expression when cultured with bFGF supplemented medium; whereas static *h*BM-MSCs and hSkMs (ratio 2:1) co-seeding induced excellent expression of myogenic markers.

2.4.3 Dynamic culture system

When *h*BM-MSCs were cultured in bFGF supplemented medium in dynamic environment, total absence of myogenic gene expression was observed, IF observation confirmed the totally absence of myogenic proteins (data not shown). When *h*BM-MSCs and *h*SkMs dynamic co-culture was tested, two different cell populations were spatially separated, as they were seeded in separate wells, even if the same culture medium was flowing along the whole culture (Figure 12).

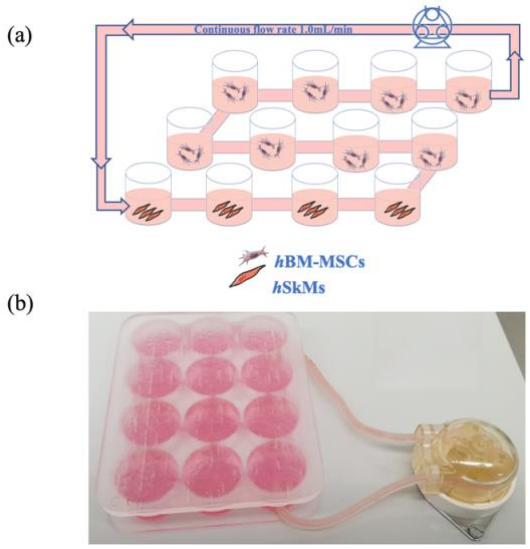

Figure 12. Schematic representation and image of perfused bioreactor system used for the dynamic co-culture of *h*BM-MSCs with *h*SkMs (2:1). *h*BM-MSCs were cultured in myogenic medium supplemented with 10 ng/mL of bFGF with perfused *h*SkMs medium up to 21 days. The number of well were loaded to maintain same cell ratio of 2:1, respectively, as studied in static culture. Each well has an internal diameter of 2 cm; the mean flow rate was of 1 mL/min.

In this dynamic arrangement, cell ratios explored was of 2:1 and 1:1 (*h*BM-MSCs:*h*SkMs). A poor cell survival was observed for 1:1 ratio (data not shown); conversely, an optimal cell viability was documented at 2:1 ratio. Indeed, *h*BM-MSCs showed an excellent up-regulation of myogenic genes (Figure 13a). *Pax3* was up-regulated 11-fold at day 7; myogenic regulation factors (MRFs) at day 7 showed the highest up-regulation of 9-fold for *MyoD1*, 38-fold for *Myf5* and 37-fold for *Myf6*. *Desmin* showed a constant up-regulation throughout dynamic culture, with 10-fold at day 7, 16-fold at day 14 and 9.5-fold at day 21. *MYH2* increase was of 4.4-fold at day 7.

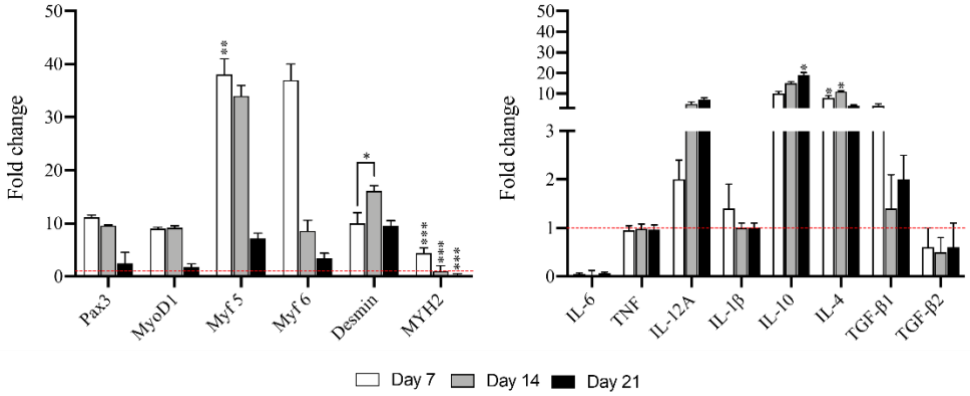

Figure 13. Gene expression profiling of myogenic markers and cytokines expressed by *h*BM-MSCs within perfusion bioreactor culture. mRNA levels of myogenic markers (*Pax3, MyoD1, Myf5, Myf6, Desmin* and *MYH2*), pro-inflammatory cytokines (*IL6, IL12A, IL1B*) and anti-inflammatory cytokines (*IL10, IL4, TGB1, TGFB2*) were monitored. Relative quantification of each mRNA gene expression normalized to endogenous *GAPDH* (internal control) was calculated using the 2^{-DDCt} method and presented as fold change over *h*BM-MSCs and *h*SkMs collected at day 0=1. Two-way analysis of variance (ANOVA) with Tukey's multiple comparison test was performed for comparison of data obtained at Day 0 in perfusion system culture. n=3. * $p < 0.05$, ** $p < 0.01$, *** $p < 0.001$.

Cytokines expression by *h*BM-MSCs, normalized over day 0, were also investigated (Figure 13b). Anti-inflammatory cytokines were upregulated compared to pro-inflammatory ones, similar to that observed in static co-seeding culture. More in detail, *IL12A* showed an increasing trend with 2-fold, 5-fold, and 7-fold at the investigated time points, while *IL-1B* expression was almost constant along culture (1-fold change). Other pro-inflammatory cytokines, such as *IL6*, *TNFA* and *IFNG* were not detected. Among anti-inflammatory cytokines, *IL10* and *IL4* were the most upregulated: i.e., *IL10* reached the maximum spike of expression at day 21 with 19.2-fold and *IL4* at day 14 with 11-fold. *TGFB* expression was low, except for *TGFB1* at day 7 (4-fold).

*h*BM-MSCs cultured within the perfusion system showed a significant signal for Desmin (stained in red) by IF at earlier time points and a significant more intense signal for MYH2 (stained in green) especially at day 21 (Figure 14b). q-IF confirmed a statistically significant increase of 2.4-fold ($p \leq 0.001$) at day 7 and 2.9-fold ($p \leq 0.01$) for Desmin and of 2.25-fold ($p \leq 0.001$) at day 7 and 2.5-fold ($p \leq 0.01$) at day 21 for MYH2 (Figure 14c). Furthermore, *h*BM-MSCs showed an extremely ordinate alignment with clearly elongated shape. When IF staining was performed on *h*BM-MSCs supplemented only with bFGF medium, neither Desmin nor MYH2 signals were observed (Figure 14a). In dynamic culture, *h*BM-MSCs and *h*SkMs were seeded independently, and Desmin and MYH2 production was monitored by western blot assay (Figure 15). Both proteins showed similar expression trends with a significant increase at day 7 and the maximum expression at day 14.

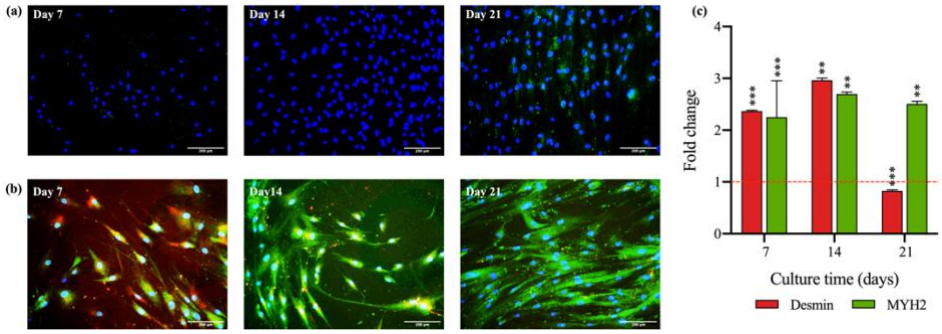

Figure 14. Immunofluorescence images of *h*BM-MSCs with myogenic medium and under co-culture within perfusion bioreactor. IF assay at day 7, 14 and 21 of culture was performed by staining Desmin in red and MYH2 in green. The images illustrated *h*BM-MSCs cultured in myogenic medium (a) and *h*BM-MSCs cultured in co-culture thanks to the perfusion system, in such case cells orientation and elongation and the presence of the myogenic protein are evident (b). All images were captured using 20x magnification. Scale bar: 200µm. Semi-quantitative IF of Desmin and MYH2 protein signals from *h*BM-MSCs is shown as mean±SD, and two-way ANOVA performed between time points, n=3, *$p < 0.05$, **$p < 0.01$, ***$p < 0.001$ and ****$p < 0.0001$ (c).

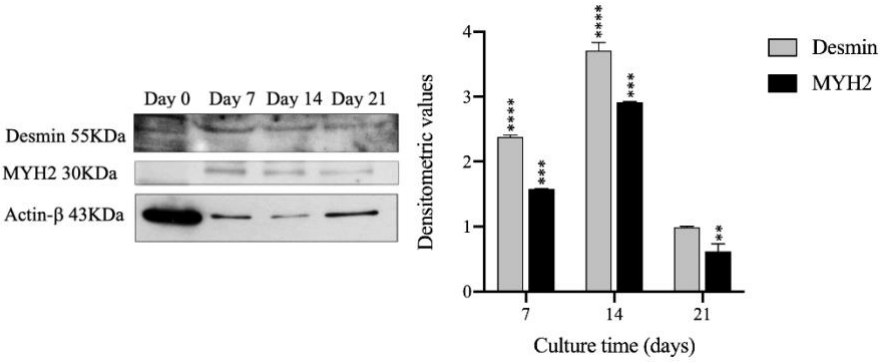

Figure 15. Western blot assay for Desmin and MYH2 proteins. Desmin and MYH2 proteins were detected trough western blot analysis in *h*BM-MSCs cultured in perfusion system at days 7, 14 and 21. Data were normalised against actin-β and reported as mean value ±SD (n=3). The blotting outcomes confirmed the presence of both proteins suggesting a clear *h*BM-MSCs commitment versus the myogenic phenotype. Two-way ANOVA was performed between time points, n=3, $^{**}p < 0.01$, $^{***}p < 0.001$ and $^{****}p < 0.0001$.

2.5 Discussion

bFGF supplemented medium showed low myogenic potential, whereas co-seeding *h*BM-MSCs with *h*SkMs promoted myogenic commitment events when a 2:1 ratio was adopted. This cell co-culture system was achieved by conventional static culture and by using a perfusion bioreactor to promote cell crosstalk by paracrine via. In both cases, the whole myogenic gene expression was progressively upregulated, probably due to a complex biochemical cells-to-cells crosstalk[94,95]. Expected commitment was checked by evaluating all MRFs gene expressions, that act in a concerted manner and with a specific spatio-temporal expression during myogenesis. Indeed, early factors (*MyoD1* and *Myf5*) are involved in commitment and proliferation of myogenic directed cells, and late factors (*Myf6*) regulate terminal differentiation of committed cells, even if they can functionally overlap[96]. In our system, *h*SkMs expressed these genes constitutively and constantly along the culture. Therefore, *h*BM-

MSCs upregulated the same genes, suggesting that an effective myogenic commitment of stem cells was achieved.

Co-seeding system in static culture environment promotes myogenic events but has poor versatility, and recovery of single cell population for further investigation is not possible. Conversely, co-culture adopting perfusion system ensured successful outcomes and allowed collection of each cell population independently. In addition, our system was an excellent model to investigate *in-vitro* myogenic commitment by paracrine via. Indeed, gene expression followed the same progression of commitment events of that observed in co-seeding experiments, suggesting that a paracrine effect could induce cell commitment versus a specific phenotype, probably due to complex crosstalk even in absence of direct cells-to-cells contact.

In perfused system, *h*BM-MSCs expressed and upregulated *Pax3* and all MRFs. *Pax3* was overexpressed at day 7 (11.1-fold) and then its expression decreased. The same behavior was observed for *Myf*5 and *Myf6*, significantly upregulated at day 7 of culture (38-fold, $p < 0.01$; 37-fold, respectively), followed by a decreasing trend at day 21. *Desmin* expression also significantly increased at day 14 (16-fold, $p < 0.05$), whereas *MYH2* started to be significantly overexpressed (4-fold, $p < 0.001$) at day 7. However, when protein characterization was performed by western blot assay, a clear presence of Desmin and MYH2 proteins was documented, confirming a proper myogenic commitment. Both proteins follow the same expression trend with the maximum peak at day 14, with Desmin more abundant than MYH2, likely because Desmin constitutes intermediate filaments, and its expression is temporarily earlier than MYH2, that is involved in contractile system.

How *h*BM-MSCs acquire a myogenic phenotype is complex and many aspects remain still unclear. The unique commitment of *h*BM-MSCs towards myogenic phenotype occurs when Pax3 signaling activates at expense of other potential mesenchymal differentiation events, such as adipogenesis, osteogenesis, and chondrogenesis[97]. In our study, in all experimental conditions, Pax3 showed a good expression, reducing over culture time in favor of MRFs expression; thus, we could assume that *h*BM-MSCs were successfully committed towards myogenic phenotype. In our system, the highest gene overexpression and protein production was observed at day 14 of culture, probably because long-term culture can affect biological activities of MSCs, as largely reported in literature[98].

*h*BM-MSCs have an immunomodulatory capacity. Therefore, a broad range of cytokines was investigated to understand which of them were expressed during commitment processes, considering that all of them play a pivotal role during myogenesis. For example, the role of TNF-α during myogenesis is still controversial; however, TNF-α is reported as an autocrine factor, is constitutively expressed by myoblasts and largely released under differentiation stimuli, and mostly contributes to myoblast proliferation by accelerating cell cycle progression[99–101]. In our study, *h*SkMs showed a low *TNFα* expression and was not detected in perfusion system even if it increased 8-fold in co-seeded static culture. IL-1β is involved in myogenesis and could favor myoblast mitosis, enhancing muscle protein synthesis[102]. *IL1β* was significantly high in *h*SkMs up to 205-fold, while *h*BM-MSCs under bFGF medium expressed *IL1β* only 4-fold (p <0.01) at 7 days. In co-seeded static culture, *IL1β* expression increased at 6-fold (p <0.01) at 14 days, and it was overexpressed 1-fold at day 7 in dynamic system.

IL-10 is an anti-inflammatory cytokine mostly involved in skeletal muscle regeneration, favoring newly regenerating myofibers[103]. The highest expression of *IL10* was detected in *h*SkMs (89.9-fold $p < 0.01$) at day 14, followed by co-seeding static culture (38-fold $p < 0.05$), at same time point. In perfusion system, *IL10* expression was lower than static co-seeding culture, but one of the most upregulated (19.2-fold, $p < 0.05$) at day 21. The same trend was observed for *IL4*. This cytokine promotes muscle differentiation[104]. In *h*BM-MSCs static co-seeding, *IL4* expression was high up to 55-fold and, in perfusion system, *IL4* was one of the most upregulated (11-fold; $p < 0.05$) at day 14. *TGFβ* family members did not exceed 4-fold, both in static and in perfusion system.

In static co-seeding culture, overall expression of pro-inflammatory cytokines was balanced by the high expression of anti-inflammatory ones, such as *IL10* (38-fold, $p < 0.05$) and *IL4* (55-fold). In perfusion system, pro-inflammatory cytokines showed an overall poor expression; conversely, anti-inflammatory ones were the most expressed. Our data indicated that the perfusion system promoted myogenic commitment, lower expression of pro-inflammatory cytokines, and overexpression of anti-inflammatory ones.

2.6 Conclusion

Our present work described myogenic commitment of *h*BM-MSCs by co-culture with *h*SkMs in a perfused system. Our data suggested that *h*BM-MSCs co-cultured in perfusion undergo to a successful myogenic commitment with significant upregulation of all gene markers and anti-inflammatory cytokines with Desmin and MYH2 protein production. Our proposed culture seemed more advantageous than the conventional static one, especially because of an

easy cell collection. Thus, our system opens perspectives for further studies on more complex crosstalk mechanisms involving multiple cell types. Indeed, the perfused system will easily allow a multiple cell culture with several cell types to better investigate their specific crosstalk and how they participate to activate molecular signals or cytokines exerting a fine regulation for muscle regeneration and healing. As an example, our proposed *in-vitro* model can be improved with Peripheral Blood Mononuclear Cells (PBMCs) to better understand the role of those cells in myogenic events. Alternatively, perfusion could allow circulation of biomimetic vesicles fabricated for targeted delivery of specific signals, in both physiological and pathological simulated conditions. A deep understanding of the whole biochemistry involved in stem cell differentiation is still a challenge, and our described model may open perspectives for a comprehensive exploration of stem cell behavior in myogenic commitment or to study a more complex crosstalk between stem cell and myoblast phenotype, in health and disease.

CHAPTER 3. Peripheral Blood Mononuclear Cell contribution in 2D myogenic co-culture system

3.1 Introduction

Alternative therapies in regenerative medicine include Peripheral Blood Mononuclear Cell (PBMC) transplantation. Several blood filtration systems are used in clinical practice to concentrate PBMC fraction from whole blood with extremely low residual red blood cells. These systems are safe, fast, sterile, and minimally invasive procedures for autologous transplantation of blood fraction. Autologous PBMCs are injected at the site of injury in patients suffering of critic limb ischemia (CLI) ineligible for revascularization procedures where myofiber regeneration significantly increases and limb rescue improves[33–35]. These very promising results are of particular interest in case of skeletal muscle severe injuries, where tissue self-renewal ability is limited and healing process fails[105]. Filtration system membranes can show different composition and pore size range, as indicated in the patent no. EPO 2602315A1, and be built using several types of polymers likely using melt-blowing technology. Filtration is possible because of membranes organized in multilayers, uncharged or functionalized with positive or negative surface charges that consequently influence system hydrophilicity and capacity to differentially retain or filter various cell types[106–108].

Exact mechanisms by which autologous PBMCs support both muscle and vascular healing in CLI are still unclear. Indeed, the exact role of PBMCs in influencing myogenic events is under debate, even though pharmacological targeting of inflammation and immune functions result in faster healing processes. In case of severe injuries, skeletal muscle capacity to spontaneously heal appears insufficient, and available treatments do not provide optimal restoration to preinjury status[109]. Therefore, biological treatments, including cell therapy and a biomimetic *in-vitro* model could be a precious tool to better understand the complex mechanism behind healing processes to improve clinical management. To date, BM-MSC clinical

application after severe muscle trauma are restricted to animal models where stem cells favor muscle regeneration, with successful improvement of contractile muscle force[110–112]. Autologous PBMC transplantation is another therapeutic option widely used in clinical practice for revascularization procedures, as those performed for lower limb ischemia treatments[113,114] or for non-healing ischemic ulcers[115].

3.2 Aim

The aim of this study was to investigate structure, morphology, and chemical composition of a commercial filter by optical and electron microscope, Fourier-transform infrared spectroscopy (FTIR), Differential Scanning Calorimetry (DSC), and Thermogravimetric analysis (TGA) analyses. Functional characterization was performed by flow cytometry immunophenotyping of filtered PBMCs. Subsequently, to better understand the role of PBMC collected fraction in myogenic events, filtered fractions were co-cultured with a previously described *in-vitro* myogenic model using a co-culture with BM-MSCs and SkMs[65]. BM-MSC myogenic commitment was monitored by gene expression profiling by RT-qPCR and by IF assay. Influence of PBMCs on modulation of cytokine levels during BM-MSC myogenic commitment events was also investigated by monitoring cytokine gene expression and protein concentration in culture medium.

3.3 Materials and Methods

3.3.1 Filter characterization

Filter system HeMaTrate® (CH-WB110C, Patent n. EP 2602315A1) was supplied by Pall Medistad B.V. (Medemblik; Netherlands) for Cook Regentec

(Indianapolis, Indiana, USA). Optical Microscope (mod. MZ6, Leica Microsystems GmbH, Wetzlar, Germany) and Field Emission Scanning Electron Microscope (FE-SEM, mod. LEO1550VP, Zeiss, Oberkochen, Germany) were used for morphological investigations. Fiber size and diameter were determined by ImageJ software by counting at least 300 fibers. Pore size distribution was obtained by converting FE-SEM images to binary using MATLAB software, as previously published[116,117]. FTIR was performed using a Bruker Vertex 70 FTIR-spectrophotometer (Bruker Optics Inc. Billerica, MA, USA) in the range of 500-4000 cm^{-1}. TGA was carried out in flowing air and N2 (50 mL/min) at a 10 K/min heating rate from 30° C to 700° C using a Mettler Toledo TC-10 thermobalance. DSC was performed in N_2 flowing atmosphere (50 mL/min) at 10 K/min heating rate using a Mettler Toledo DSC 822e from -60 °C to 300 °C.

3.3.2 PBMC concentration with filtration system and harvesting

Whole peripheral blood obtained from three healthy volunteers (a female and two males; age ranged from 38 to 45 years old) was concentrated using a blood filtration system (HeMaTrate®, Pall Medical Corporation) as per manufacturers' instructions. PBMCs were further isolated using Ficoll-Paque density gradient centrifugation (Cytiva), according to manufacturer's instructions. Isolated cells were directly used for experiments or stored in 70% RPMI (Gibco™), 20% Fetal Bovine Serum (FBS, Gibco™), and 10% DMSO (Sigma-Aldrich) at -80°C until use.

3.3.3 BM-MSC isolation, harvesting and characterization

BM specimens for isolation of BM-MSCs were obtained from three healthy male donors (aged 26, 24 and 28 years old) after informed written consent in accordance with protocols approved by our Institutional Review Board (Ethic Committee "Campania Sud", Brusciano, Naples, Italy; prot./SCCE n. 24988).

Isolation and characterization were performed as previously documented and according to the International Society of Cellular Therapy guidelines[42]. Whole BM aspirate was directly seeded at a density of 50,000 total nucleated cells/cm^2 in a T75 plastic flask containing α-MEM (Gibco™) supplemented with 1% Glutagro (Corning), 10% FBS (Gibco™) and 1% Pen/Strep (Corning) and incubated at 37°C in an atmosphere of 5% CO_2 and 95% relative humidity. After 48h, non-adherent cells were removed, and medium replaced twice a week. Cells were detached when 70-80% of confluence was reached, using 0.05% trypsin-0.53mM EDTA, washed with PBS (Corning), and counted using Trypan Blue (Sigma-Aldrich). BM-MSCs were subsequently seeded at 4,000 cells/cm^2 and expanded up to the third passage.

3.3.4 Flow cytometry

MSC and PBMC immunophenotype was investigated by flow cytometry. Briefly, for BM-MSCs, a minimum of 1 x 10^5 cells at the third passage was stained with the following antibodies: 2.5 µL of FITC-conjugated anti-CD90 or 5 µL of FITC-conjugated anti-HLA-DR; 5 µL of APC-conjugated anti-CD73; 10 µL of PE-conjugated anti-CD105 or 10 µL of PE-conjugated anti-CD34; and 10 µL of PC7-conjugated anti-CD45 or 10 µL of PC7-conjugated anti-CD14 (all antibodies were from Beckman Coulter, Fullerton, CA, USA). Cells were incubated at RT for 20 min in the dark, washed with PBS and resuspended in 300 µL of the same buffer for acquisition. For PBMC immunophenotyping, before and after filtering and separation procedures, a minimum of 2 x 10^5 cells were stained with the following antibodies: 5 µL of APC-conjugated anti-CD3; 5 µL PC7-conjugated anti-CD14; 5 µL of FITC-conjugated CD34; 5 µL of phycoerythrin cyanin 5 (PC5)-conjugated CD8; and 5 µL of PE-conjugated anti-CD4. For immunophenotyping of PBMCs in transwell at day 0, a minimum of 2 x 10^5 cells were stained with the following

antibodies: 5 µL of APC-conjugated anti-CD3; 5 µL PC7-conjugated anti-CD56; 5 µL of FITC-conjugated CCR7; 5 µL of PC5-conjugated CD45RA; and 5 µL of PE-conjugated anti-CD4. Cells were then incubated at RT for 20 min in the dark, washed with PBS and resuspended in 300 µL of the same buffer for acquisition. Sample acquisition was performed on a BD FACSVerse flow cytometer (Becton Dickinson, BD, NJ, USA) equipped with blue (488 nm) and red lasers (628 nm) and BD FACSuite software (BD Biosciences). PMT voltage setting, and compensation were carried out using single-color controls for each fluorochrome and an unstained sample as negative control. All samples were run with the same PMT voltages, and a minimum of 30,000 events were recorded. FlowJo software (v.10.7.1, LLC, BD Biosciences) was employed for post-acquisition compensation and analysis.

3.3.5 BM-MSC-SkM-PBMC static co-culture

BM-MSCs and SkMs were co-seeded at a density of 4,000 cells/cm^2 and at 2:1 ratio in a 12-well plate containing a differentiation medium composed by: 67% of α-MEM (Gibco™) supplemented with 1% Glutagro (Corning), 10% FBS (Gibco™), 100 nM Dexamethasone (Sigma-Aldrich), 100 µM Ascorbic Acid (Sigma-Aldrich), 10 ng/mL bFGF (Peprotech), and 1% Pen/Strep (Corning), and 33% of DMEM low glucose (Gibco™) supplemented with 2% Horse Serum (Gibco™), 100 nM Dexamethasone (Sigma-Aldrich), 100 µM Ascorbic Acid (Sigma-Aldrich), 10 ng/mL bFGF (Peprotech), and 1% Pen/Strep (Corning). PBMCs were seeded at a density of 10,000 cells/well in the upper chamber of transwell inserts, composed by a semi-permeable membrane with a pore size of 0.4 µm. Cells were incubated at 37°C in an atmosphere of 5% CO_2 and 95% relative humidity up to 21 days, fresh medium was changed every three days. Brightfield images of BM-MSC-SkM

co-cultures were captured at 5x magnification at 7, 14 and 21 days by LEICA DMIL LED microscope (Leica Microsystems GmbH, Wetzlar, Germany), and acquired using a LEICA DFC425 C camera.

3.3.6 RNA isolation and gene expression profiling

Myogenic genes, including *Pax3*, *MyoD1*, *Myf5*, *Myf6*, *Desmin*, and *MYH2*, and cytokines, such as *IL6*, *TNF*, *IL12A*, *IL1B*, *IFNG*, *IL10*, *IL4*, *TGFB1* and *TGFB2* (BioRad) expression were investigated by Reverse Transcription quantitative polymerase chain reaction (RT-qPCR). Total RNA at each time point was extracted using RNeasy Micro Kit (Qiagen). For each sample, 1 μg of total RNA was reverse transcribed using iScriptTM cDNA synthesis kit (BioRad), and relative gene expression analysis was performed on a LightCycler® 480 Instrument (Roche, Basel, Switzerland) using SsoAdvancedTM Universal SYBR® Green Supermix (BioRad). Specificity of formed products was assessed by melting curve analysis. Experiments were run in duplicate. Experiments were run in duplicate and were normalized to *GAPDH* expression (reference gene) applying the geNorm method[91] and using CFX Manager software ($M < 0.5$). Fold changes were determined by $2^{-\Delta\Delta Ct}$ method and presented as relative levels versus untreated cells.

3.3.7 Cytokine detection

For quantification of secreted cytokines in culture medium, a multiplex immunobead-based multiplex assay (Merck, Millipore) was employed for measurement of EGF, Eotaxin, GM-CSF, IFN-γ, IL-10, IL-12p70, IL-1RA, IL-1α, IL-1β, IL-2, IL-3, IL-4, IL-5, IL-7, MIP-1α, MIP-1β, TNF-α, bFGF, G-CSF, GRO, IL-6, IL-8, MCP-1, and VEGF, following manufacturer's instructions.

3.3.8 Immunofluorescence assay

Cells were fixed with 4% PFA for 30 min at RT, followed by permeabilization with 0.1% Triton X-100 for 5 min, and samples were blocked with horse serum solution for 1h. Cells were stained for Desmin (1:100; Abcam) and MYH2 (1:50; Thermo Fisher Scientific), and incubated overnight at 4°C. Subsequently, cells were incubated for 1h at RT with Alexa Fluor TM 488 goat anti-rabbit IgG (1:400; Thermo Fisher Sci.) and VectaFluorTM anti-mouse IgG Dylight 594® kit (Vector laboratories) antibodies, while cell nuclei were counterstained using DAPI. Separate images were acquired using identical settings of light intensity, exposure time, and gain using a fluorescence microscope (Eclipse Ti Nikon Corporation, Tokyo, Japan).

3.3.9 Statistical analysis

Data were analyzed using Prism software (v.9.0, GraphPad software, LLC, San Diego, California, United States). Results are presented as mean ± SD. Statistical analysis was performed using two-tailed independent Student's t-test for two group comparisons, or two-way analysis of variance (ANOVA) test for three or more group comparison with Tukey's test for multiple comparisons between group. For flow cytometry data, results are presented as percentage of positive cells, and expression of each marker on single cells is also reported as histograms and using unstained samples as negative controls. Percentage of positive cells and median fluorescence intensity (MFI) values were calculated for each marker. p value < 0.05 was considered statistically significant[93].

3.4 Results

3.4.1 Filter characterization

First, commercial filtration system routinely used in clinical practice for autologous transplantation procedures was physically and chemically studied to understand morphological characteristics and composition that make this system suitable for an efficient cell filtration starting from whole blood. The filter is composed by twelve polymeric membranes hermetically assembled in a plastic cylinder (diameter 5.7 cm, height 0.7 cm) and linked to two pipes required for blood flowing in and out, and for blood passage from one side to the other of the whole filtration system. Each filter slice (circular) is 5 cm in diameter and 3.2 mm in thickness, as shown in Figure 16.

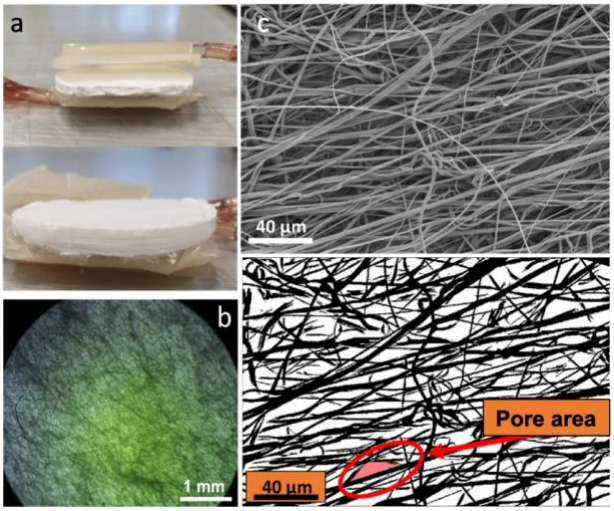

Figure 16. Filtration system membranes. Image of the whole filter assembly formed by 12 slices (a); single slice optical microscopy image (b); single slice FE-SEM microscopy image and related elaboration to evaluate the pore area with the illustration of the conversion of the images in binary and the evaluation of the pores.

Polybutylene terephthalate (PBT) fibers were identified in filter membranes by FTIR spectroscopy (Figure 17a), showing the presence of terephthalate group, aromatic group, and the stretching of C=O of carbonyl group[118,119].

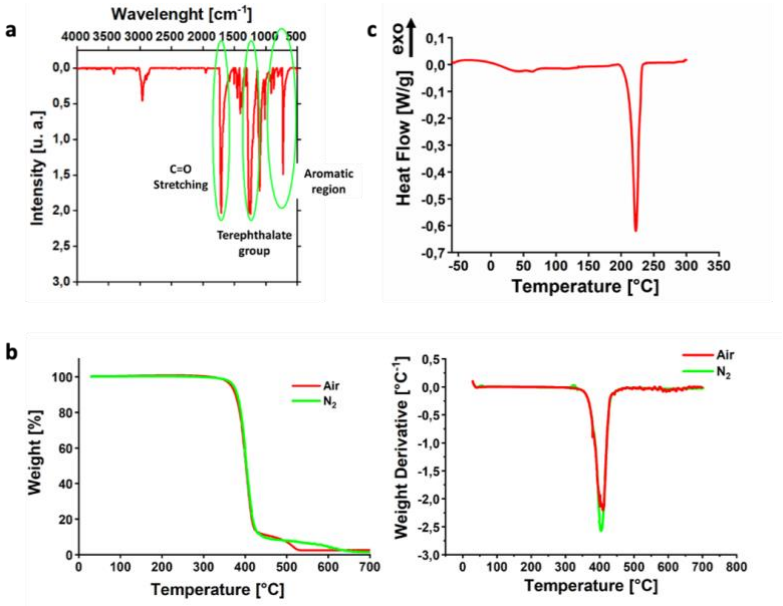

Figure 17. Filtration system characterization: physical and chemical properties. FTIR of the commercial filter (a); DSC of the filter disk (b); TGA and DTGA of the commercial filter (c). Polybutylene terephthalate (PBT) fibers were identified in filter membranes by FTIR spectroscopy (a) by the presence of the terephthalate group, the aromatic group and the stretching of C=O of the carbonyl group evident in the FT/IR spectrum, Profiles of TGA curves evidenced membrane stability up to 350°C both in reactive and inert environment (b), with the main degradation step occurring at around 400°C. DSC curve showed the glass transition of materials at around 30°C, and the melting temperature at about 223 °C (c).

Profiles of TGA curves evidenced membrane stability up to 350°C both in reactive and inert environment (Figure 17b), with the main degradation step occurring at around 400°C, due to the breakdown of the polymer in fragments and formation of combustible gases[119,120]. A very small second step of degradation occurred at around 500°C, more gradually in an inert environment, such as nitrogen flow environment, while abrupt in air. Residual profile values at 630°C were similar and almost irrisory. DSC curve showed

glass transition of materials at around 30°C and melting temperature at about 223°C[121] (Figure 17c).

Moreover, crystallinity degree was evaluated by integration of melting transition as indicated in eq. 1:

$$X_c = \frac{\Delta H_m}{\Delta H_{m,100\%}} = 30.2\% \qquad \text{(eq 1)}$$

where ΔHm is the integrating the melting transition in the DSC curve and ΔHm,100% is the melting enthalpy for 100% crystalline PBT, that according to literature is 145.5 J/g[122].

Filter morphology was investigated by FE-SEM (Figure 18a-b). Overall, filter structure was homogeneous, with fibers ranging from 0.9 to 4.0 μm obtainable with melt-blow technology (Figure 18c). Pore size distribution (Figure 18d) was extremely heterogeneous with pores ranging from 1 μm to > 20 μm of diameter.

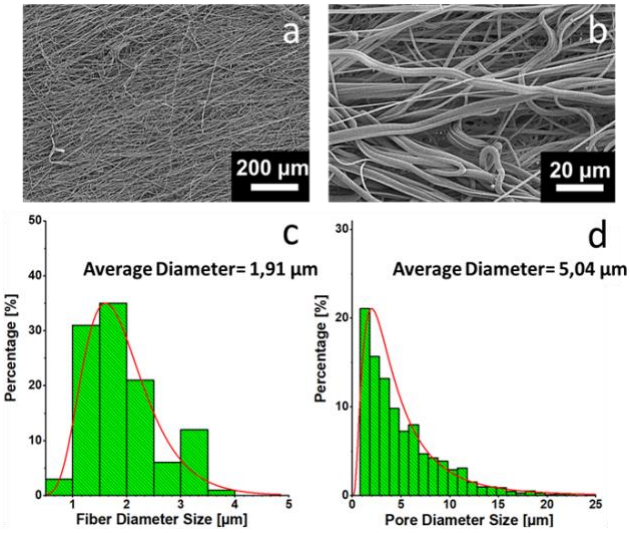

Figure 18. Filtration system characterization: morphology. SEM images of the filter (a-b); distribution of the fiber diameter size (c); distribution of the pore diameter size (d). Overall, filter structure was homogeneous, with fibers ranging from 0.9 to 4.0 μm (c). Pore size distribution (d) was extremely heterogeneous with pores ranging from 1 μm to 20 μm of diameter.

3.4.2 Filtrate composition

A total volume of 120 mL of whole blood was filtered through filtration system in few minutes and PBMCs were harvested in 10 mL of saline solution, see Figure 19.

Figure 19. Commercial filtration system.

To investigate filter efficacy to retrieve blood cell populations after filtration, PBMC immunophenotyping was carried out on whole blood, after filtration, and after separation by Ficoll-Paque density gradient, and results were compared (Figure 20a-b). As expected, no significant variations were described in percentage of positive cells for all studied cell populations, before and after filtration or separation, confirming filter efficiency in blood concentration and composition preservation (Figure 20c-d). Indeed, starting from a total blood volume of 120 mL, filtrated PBMCs were collected in a final volume of 10 mL of 0.9% saline solution. Therefore, because the relative percentage composition of positive cells was preserved after filtration, cells were concentrated in a final volume 10-times smaller than starting sample. No differences were observed in percentage of monocytes (p = 0.6490), total

T cells and T subpopulations ($CD3^+$ T cells, $p = 0.3762$; $CD4^+$ T cells, $p = 0.5062$; and $CD8^+$ T cells, $p = 0.4891$), or granulocytes ($p = 0.4901$), and in percentage of rare circulating cell populations in healthy conditions (e.g., $CD34^+$ hematopoietic stem cells, $p = 0.2875$). Those data confirmed filter efficiency in PBMC collection and concentration.

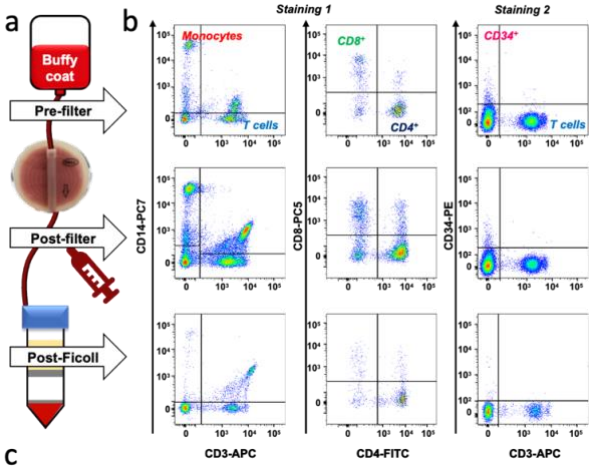

c

	Pre-filter	Post-filter	Post-separation	*P* value
Monocytes	15.1±16.9%	13.1±10.6%	6±4.5%	0.6490
$CD3^+$ T cells	22.9±12.7%	27.7±5.2%	40.6±22.7%	0.3762
$CD3^+CD4^+$ T cells	67.6±7.1%	68.2±4.9%	72.3±0.1%	0.5062
$CD3^+CD8^+$ T cells	21.1±0.1%	18.3±4.2%	15.1±8.3%	0.4891
$CD3^+CD4^+CD8^+$ T cells	2.8±1.8%	3.2±3.7%	3.5±4%	0.5107
$CD3^+CD4^-CD8^-$ T cells	8.5±5.5%	10.4±5.3%	9.1±4.2%	0.7477
$CD34^+$ cells	3.3±4.6%	1.5±1.7%	0.4±0.3%	0.2875
Granulocytes	66.3±27.4%	52.7±27.3%	57.5±20.6%	0.4901

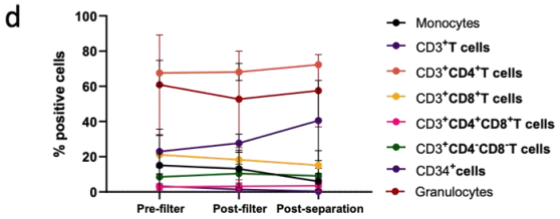

Figure 20. Flow cytometry immunophenotyping of peripheral blood mononuclear cells. Whole blood was collected and first subjected to filtration and subsequently to Ficoll-Paque density gradient separation (a). Flow cytometry immunophenotyping was performed at each step of the procedure, and frequencies of $CD14^+$ monocytes, $CD3^+$ T lymphocytes and relative $CD8^+$ and $CD4^+$ subsets and circulating $CD34^+$ hematopoietic stem cells were investigated (b). Percentage of each cell subset was compared before and after filtration and after separation to confirm filter efficacy without losing cells of a particular subset during the procedure (c-d). Data are shown as mean±SD. A $p < 0.05$ was considered statistically significant.

3.4.3 Effective myogenic commitment of BM-MSCs: flow cytometry evidence

After confirmed filter efficiency in preserving blood cell population composition, PBMCs were added to a well-established co-culture model of myogenesis to investigate the roles of immune cells on myogenic commitment. First, mesenchymal or myogenic phenotype was confirmed on each single population before further experiments. BM-MSCs were characterized according to minimal criteria of the International Society of Cellular Therapy[42] (Figure 21); while SkM phenotype was confirmed by gene expression profiling and IF analysis of myogenic markers (e.g., *Pax3*, *MyoD1*, *Myf5*, *Myf6*, *Desmin*, and *MYH2* genes, and Desmin and MYH2 proteins, respectively), as previously reported[65]. In single population cultures, BM-MSC mesenchymal phenotype was confirmed as cells showed positivity for CD90, CD73, and CD105, and negativity for CD45, and SkMs were $CD73^{+}CD45^{+}CD90^{+/-}CD105^{-}$ (Figure 21B).

Subsequently, BM-MSCs were co-cultured with SkMs because the presence of muscle cells highly improves myogenic commitment of mesenchymal cells, as documented[65]. Next, this well-established *in-vitro* myogenic commitment model was implemented with filtered PBMCs in transwell, and myogenic events were investigated by flow cytometry immunophenotyping and gene expression profiling at 0, 7, 14, and 21 days, and results were compared or normalized using BM-MSCs or SkMs cultured alone.

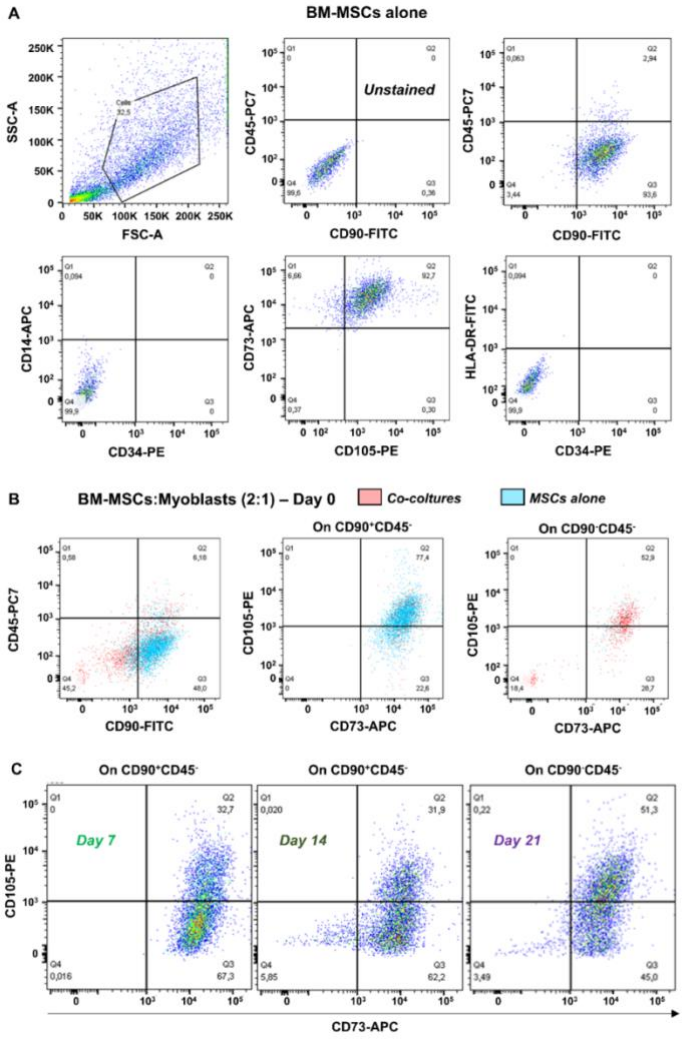

Figure 21. Flow cytometry and gating strategy of *h*BM-MSCs. The panel shows a representative cytofluorimetric FSC vs SSC (cell size vs granularity index) cells scatter of *h*BM-MSCs. Cells were first identified using linear parameters (forward scatter area [FSC-A] vs side scatter area [SSC-A], and double cells were excluded (FSC-A vs FSC-H). For antibody mix 1, CD90 and CD45 expression was investigated on single cells, and CD105 and CD73 expression was further studied on $CD45^{-}CD90+$ cells. For antibody mix 2, HLA-DR and CD34 expression was first investigated on single cells, and CD14 was further studied on $CD34^{-}HLA\text{-}DR^{-}$ cells. Expression of each marker on single cells was also reported using histograms and using unstained samples as negative controls (**A**). Flow cytometry immunophenotyping was performed on *h*BM-MSCs hSkMs co-culture and mesenchymal stem cells (MSCs) alone at day 0 (**A**), and CD90 expression was investigated on CD45- cells. Next, CD105 and CD73 expression was further studied on $CD45^{-}CD90^{+}$ and $CD45^{-}CD90^{+}$ cell populations (**B**).

At baseline, co-cultured cells were predominantly $CD90^{+}CD73^{+}CD105^{+}CD45^{-}$, and CD45 negativity and CD73 positivity were maintained throughout the culture (Figure 22a).

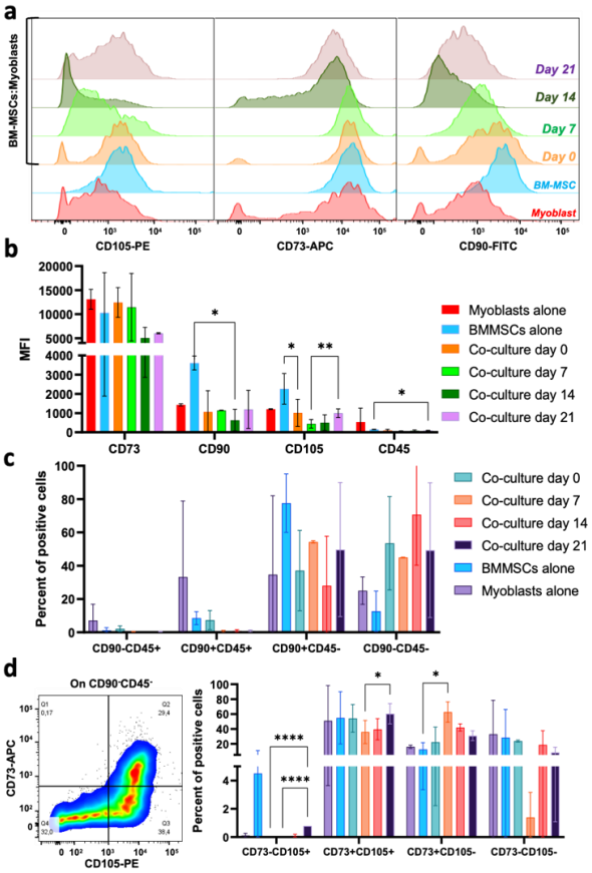

Figure 22. Myogenic commitment of bone marrow-derived mesenchymal stem cells (BM-MSCs) by flow cytometry analysis. BM-MSCs were co-cultured with myoblasts over 21 days, and myogenic commitment was monitored at day 0, 7, 14, and 21 by investigating variations in mesenchymal and myoblast marker expression. BM-MSCs and myoblasts alone were employed as control. Protein expression is reported as normalized cell count histograms (**a**) or as median fluorescence intensity (MFI) (**b**) for each studied marker and population over the culture period. MFI of each marker was calculated on single cells in each population and time point, and on BM-MSCs and myoblasts cultured alone. (**c**) Variations in frequencies of $CD90^{-}CD45^{+}$, CD90+CD45+, $CD90^{+}CD45^{-}$ (BM-MSC-like phenotype), and $CD90^{-}CD45^{-}$ (myocyte-like) cells were investigated throughout the culture, and BM-MSCs and myoblasts cultured alone were used as controls. (**d**) On myocyte-like population, CD73 and CD105 expression was compared at each time point. Data are shown as mean±SD. * $p < 0.05$; ** $p < 0.01$; **** $p < 0.0001$.

CD90 expression was significantly reduced at day 14 compared to BM-MSCs cultured alone ($p = 0.0310$) (Figure 22b). CD105 expression was significantly decreased at baseline compared to BM-MSCs cultured alone ($p = 0.0328$) likely because of the co-presence of $CD105^-$ myoblasts; however, CD105 levels increased again from day 7 to day 21 ($p = 0.0023$) (Figure 22b). Therefore, at the end of culture, BM-MSCs switched from a mesenchymal to a mature functional myocyte $CD90^-CD73^+CD105^{+/-}CD45^-$ phenotype[123].

Next, MSC subset composition variations were monitored throughout the culture by flow cytometry (Figure 22c-d and Figure 23). No differences in frequencies of $CD90^+CD45^+$, $CD90^+CD45^-$, $CD90^-CD45^+$, or $CD90^-CD45^-$ cells were observed, even though $CD90^-CD45^-$ cell subset tended to increase from day 7 of culture compared to BM-MSCs ($p = 0.1671$) or SkMs ($p = 0.1757$) cultured alone (Figure 23c). On each subset, CD73 and CD105 expression was further investigated, and percentage of positive cells were compared. On $CD90^+CD45^+$ cells (likely myoblasts), no significant variations in $CD73^-CD105^+$, $CD73^+CD105^+$, $CD73^+CD105^-$ (myoblast phenotype), or $CD73^-CD105^-$ cell subsets were observed (Figure 24a), suggesting that our 2D culture system did not alter myoblast phenotype. On $CD90^+CD45^-$ subset, $CD73^+CD105^+$ cells (BM-MSC phenotype) were significantly decreased already after 7 days of culture compared to baseline ($p = 0.0463$) and to BM-MSCs cultured alone ($p = 0.0062$); while $CD73^+CD105^-$ cell (committed BM-MSC) frequency was significantly increased starting from day 7 compared to baseline ($p = 0.0486$) and to BM-MSCs cultured alone ($p = 0.0236$) (Figure 24b), suggesting that after 7 days of culture, BM-MSCs lost their stemness and started to differentiate toward the myogenic lineage. Finally, on $CD90^-CD45^-$ subset, terminally differentiated $CD73^+CD105^+$ myocytes were significantly increased at the end of culture compared to day 7 ($p = 0.0351$);

however, immature functional $CD73^{+}CD105^{-}$ myocytes were already significantly augmented after 7 days of culture compared to BM-MSCs cultured alone ($p = 0.0417$) (Figure 23d).

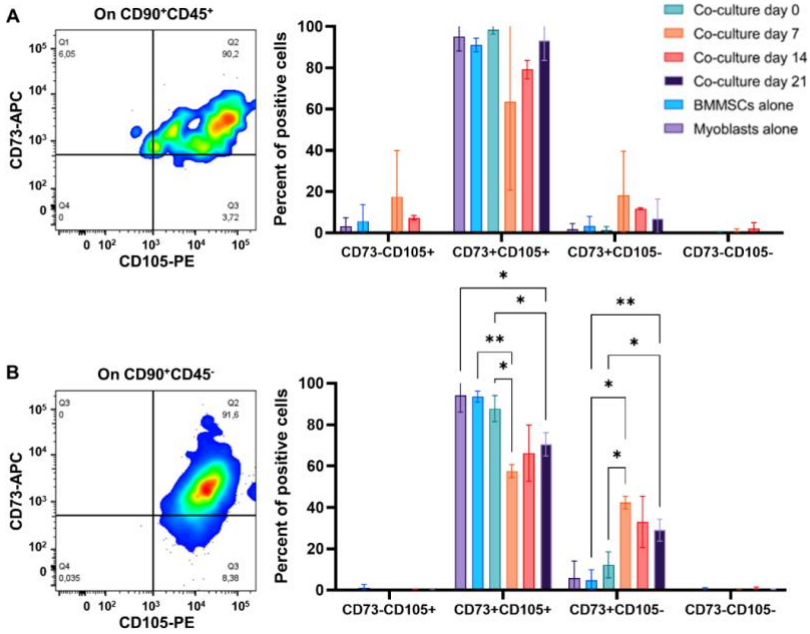

Figure 23. Myogenic commitment of mesenchymal subsets during co-culture. Variations in frequencies and expression of CD73 and CD105 on (A) CD90+CD45+ and (B) CD90+CD45- (bone-marrow-derived mesenchymal stem cell [BM-MSC] -like phenotype) were investigated throughout the culture, and BM-MSCs and myoblasts cultured alone were used as controls. Data are shown as mean±SD. * $p < 0.05$; ** $p < 0.01$.

3.4.4 Effective myogenic commitment of BM-MSCs: gene expression profiling

Subsequently, gene expression profiling of myogenic markers including *Pax3* and MRFs (*MyoD1*, *Myf5* and *Myf6)* was studied on BM-MSC-SkM co-seeding culture with and without PBMCs (Figure 24). *Pax3*, *Myf5*, and *MyoD1* were considered as satellite cell/myoblast markers, while *Myf6* and *MYH2* as mature myocyte markers. *Pax3*, the *Pax7* paralogue, is expressed in skeletal muscle cells in both quiescent and activated status[124]. P*ax3* was up-

regulated of 4- and 6-folds ($p < 0.05$) in the presence or absence of PBMCs at day 7, respectively. At day 14, gene expression resulted significantly higher without PBMCs (9.1-fold, $p < 0.01$) while at day 21, cells showed similar *Pax3* expression levels regardless the presence of PBMCs. *MyoD1* expression levels at day 7 was about 4124-fold, ($p < 0.0001$) then decreased at 1638-fold ($p < 0.05$) with PBMCs; whereas, in culture without PBMCs, *MyoD1* expression reached 2489-fold ($p < 0.01$) at day 7 but increased at 3397-fold ($p < 0.001$) at day 14. At day 21, in both conditions, gene expression showed a decreasing trend to 644.5-fold with PBMCs and 2165-fold without PBMCs with significant differences between the two data sets ($p < 0.05$). In the presence of PBMCs, *Myf5* was upregulated at 1709-fold, while without them expression was about 2640-fold ($p < 0.5$), at day 7. Then, gene expression decreased in both culture conditions, about 320-fold and 126-fold with PBMCs and 671-fold and 302-fold without, at day 14 and 21 respectively. The maximum fold-change of *Myf6* occurred at day 7, about 388-fold with PBMCs and 590-fold without PBMCs ($p < 0.5$). At day 14 and 21, expression was similar, 100-fold and 73-fold compared to 525-fold and 200-fold without PBMCs. *Desmin* was significantly up-regulated in the presence of PBMCs at day 7 with from 619-fold, ($p < 0.5$), to 200-fold at day 21, compared to cells cultured without PBMCs that showed an upregulation of 87.3-fold at day 7 and of 141-fold at day 21. Similarly, *MYH2* gene expression levels were significantly higher in the presence of PBMCs compared to cells cultured without PBMCs (192-fold vs 3.8-fold, $p < 0.0001$, at day 7; 116-fold vs 13-fold, $p < 0.01$ at day 14, and 89.6-fold vs 32.4-fold, $p < 0.5$, at day 21).

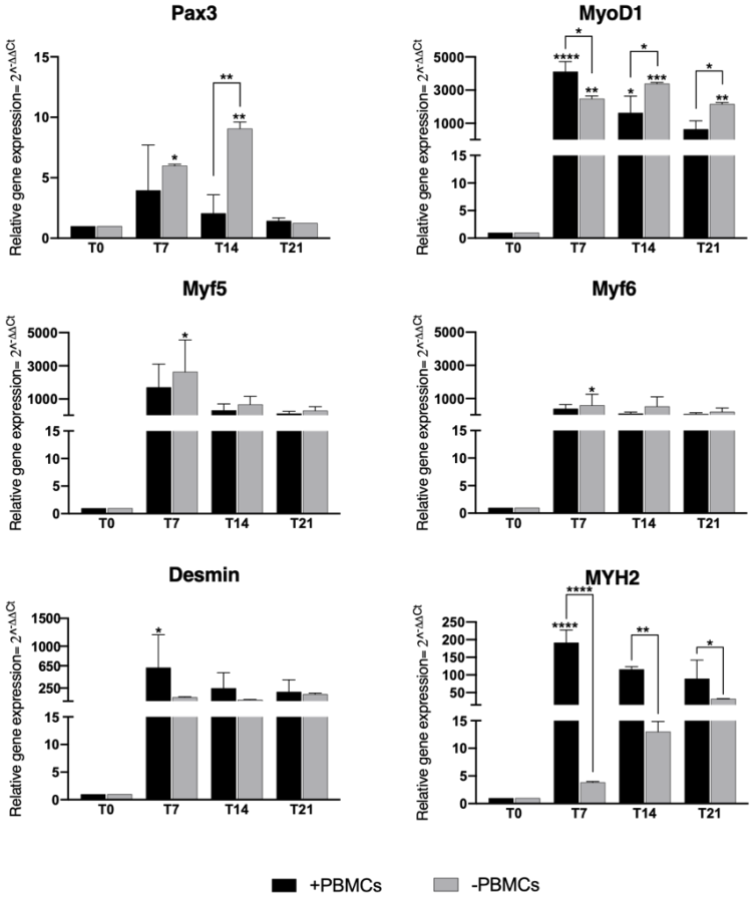

Figure 24. Gene expression profiling for myogenic markers by quantitative RT-PCR of BM-MSCs-SkMs-PBMCs in static culture. *h*BM-MSCs were co-seeded with *h*SkMs in ratio 2:1 and PBMCs were culture in the upper chamber of transwell inserts. mRNA levels of myogenic markers: *Pax3*, *MyoD1*, *Myf*5, *Myf6*, *Desmin* and *MYH2* were assayed by qRT-PCR at day 7, 14 and 21 of culture. The relative quantification of each mRNA gene expression normalized to endogenous GAPDH (internal control) was calculated using the $2^{-\Delta\Delta Ct}$ method and presented as fold change over *h*BM-MSCs at day 0, selected as a control.

BM-MSC-SkM cell morphology in the presence of PBMCs was monitored in brightfield optical microscope at each time point and elongated and proliferating cells were displayed starting from day 7 (Figure 25a). More growing cells, longitudinally organized in parallel bundles, were documented

along the culture period together with increasing protein expression of Desmin and MYH2, as observed by IF assay (Figure 25b).

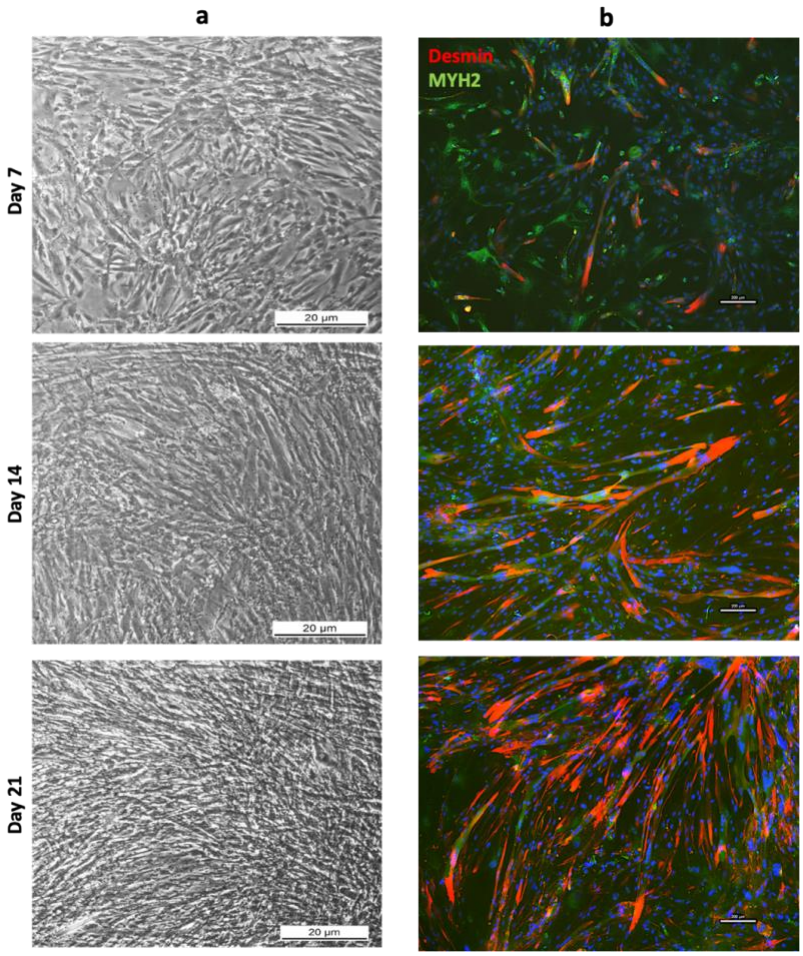

Figure 25. Brightfield and Immunofluorescence images of BM-MSCs:SkMs 2:1 co-seeded with PBMNCs in upper chamber of transwell insert. Brightfield images *h*BM-MSCs:*h*SkMs 2:1 co-seeding culture at day 7, 14 and 21 were captured using 5x magnification; scale bar: 20µm (a). IF assay was performed at same time points by staining Desmin in red and MYH2 in green (b). All images were captured using 10x magnification, scale bar: 200µm.

3.4.5 Pro-inflammatory activities of T effector memory lymphocytes and Natural Killer cells could negatively influence myogenic commitment

Based on our results showing a better myogenic commitment of BM-MSCs in the presence of PBMCs and on the role of immune system in modulating muscle injury repair, we explored the influence of PBMCs on myogenic commitment of co-cultured BM-MSCs and SkMs by flow cytometry immunophenotype of isolated PBMCs (post-separation) in transwell and gene expression profiling of pro- and anti-inflammatory cytokines.

$CD4^+$, $CD3^+CD4^-CD56^-$ (assumed as $CD8^+$ cells), Natural Killer (NK), and NKT cell frequencies were monitored throughout the culture (Figure 26a), and NK and NKT cells tended to decrease already after 7 days of culture, while $CD8^+$ and $CD4^+$ T cells tended to increase and to reach a plateau from day 14 to 21 of culture (Figure 26b). T cell central memory (TCM), T naïve (TN), T effector memory re-expressing CD45RA (TEMRA), and T effector memory (TEM) subset frequencies were monitored along the culture in $CD4^+$ and $CD8^+$ T lymphocytes (Figure 26c). On $CD4^+$ T cells, TEMRA and TEM cells tended to decrease after 7 or 14 days of culture, while TCM and TN cells increased, being TCM the predominant $CD4^+$ T cell subset (Figure 26d). On $CD8^+$ T cells, TN and TEMRA were almost absent at the end of culture, while TCM markedly increased from day 7 and TEM decreased, being these two subsets the most predominant in $CD8^+$ T cells at the end of culture (Figure 26e).

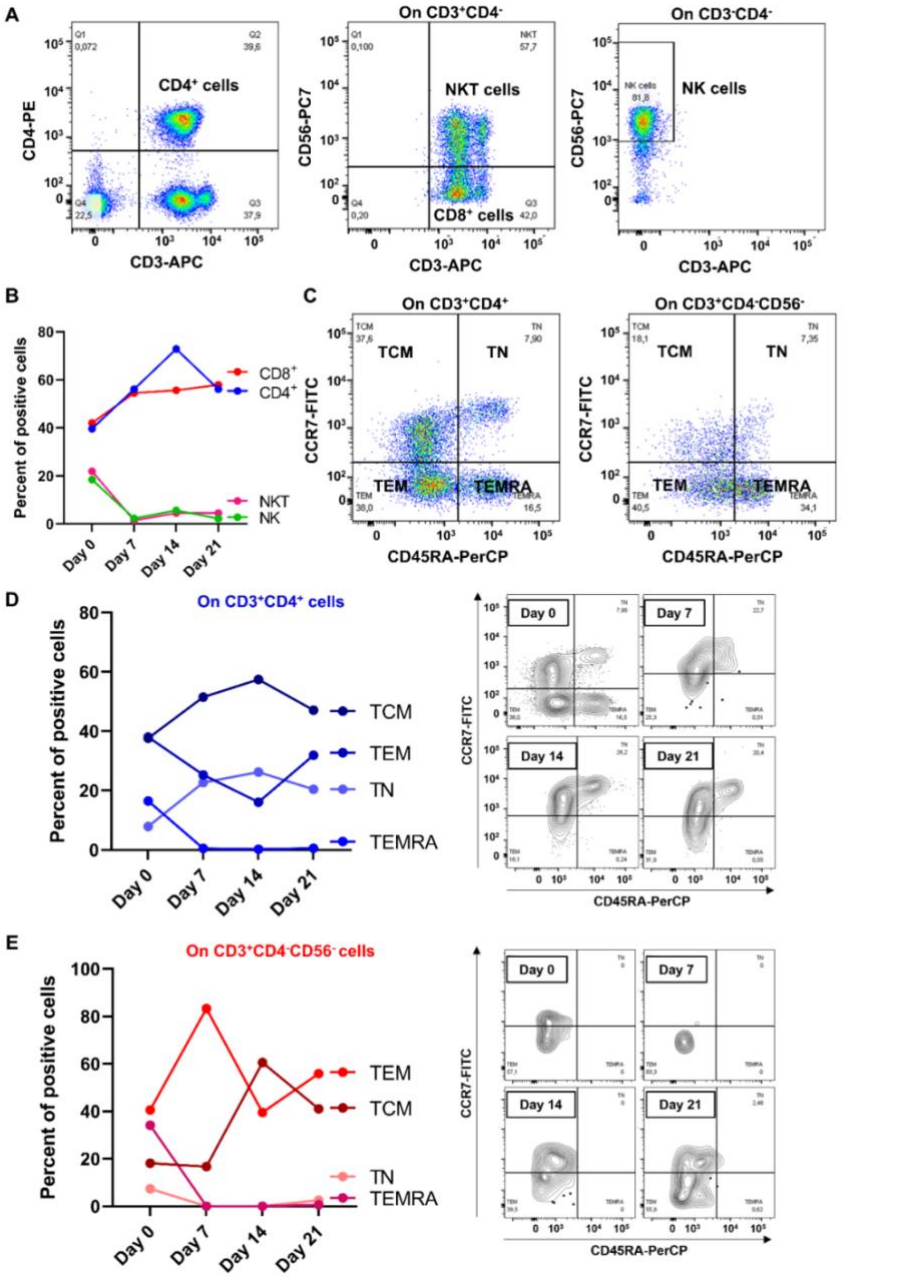

Figure 26. Flow cytometry immunophenotyping of peripheral blood mononuclear cells (PBMCs) in transwell. First, CD4+, CD3+CD4-CD56- (assumed as CD8+ T lymphocytes), CD3-CD56+ Natural Killer (NK), and CD3+CD56+ NKT cells were identified (**a**), and perturbations were monitored throughout the culture (**b**). On CD4+ and CD8+ T cells, T central memory (TCM), T naïve (TN), effector memory cells re-expressing CD45RA (TEMRA), and effector memory T (TEM) cell subsets were studied (**c**) and monitored along the culture (**d-e**).

Next, cytokine expression in co-culture system was investigated by qRT-PCR in the presence or not of PBMCs (Figure 27a). All pro-inflammatory cytokines showed very low expression levels in the presence of PBMCs, such as *IL12A* reached 1.3-fold vs 4.3-fold at day 7, $p < 0.5$, with and without PBMCs respectively. *TNF* was also significantly upregulated at day 14 in the absence of PBMCs (4.5-fold, $p < 0.1$, vs 0.35-fold without and with PBMCs, respectively); as well as at day 21, the presence of PBMCs resulted in a significantly *TNF* downregulation (6.6-fold vs 0.9-fold, with and without PBMCs, respectively; $p < 0.1$). Similarly, anti-inflammatory cytokines, such as *IL10*, were significantly upregulated in BM-MSCs-SkMs cultured in the absence of PBMCs (38.6-fold, $p < 0.0001$), completely lost in the presence of PBMCs. Interestingly, *TGFB1* showed a different expression profiling, compared to other investigated cytokines, as BM-MSCs-SkMs cultured in the presence of PBMCs displayed a significant upregulation of *TGFB1* throughout the culture period (from 1.6-fold at day 7 to 2.3-fold at day 21), while poorly expressed in the absence of PBMCs. *IL4*, *IL6*, *IFNG* and *TGFB2* were not detected in any conditions.

Cytokine secretion was also investigated by analyzing culture medium supernatants at 7, 14 and 21 days by magnetic bead-based immunoassay (Figure 27b). Among 24 cytokines studied, only monocyte chemoattractant protein-1 (MCP-1), growth-regulated alpha protein (GRO), and IL-8 were significantly high in culture medium starting from day 14, while vascular-endothelial growth factor (VEGF) reached the pick at the end of culture. All the other studied cytokines were not present in culture medium supernatants.

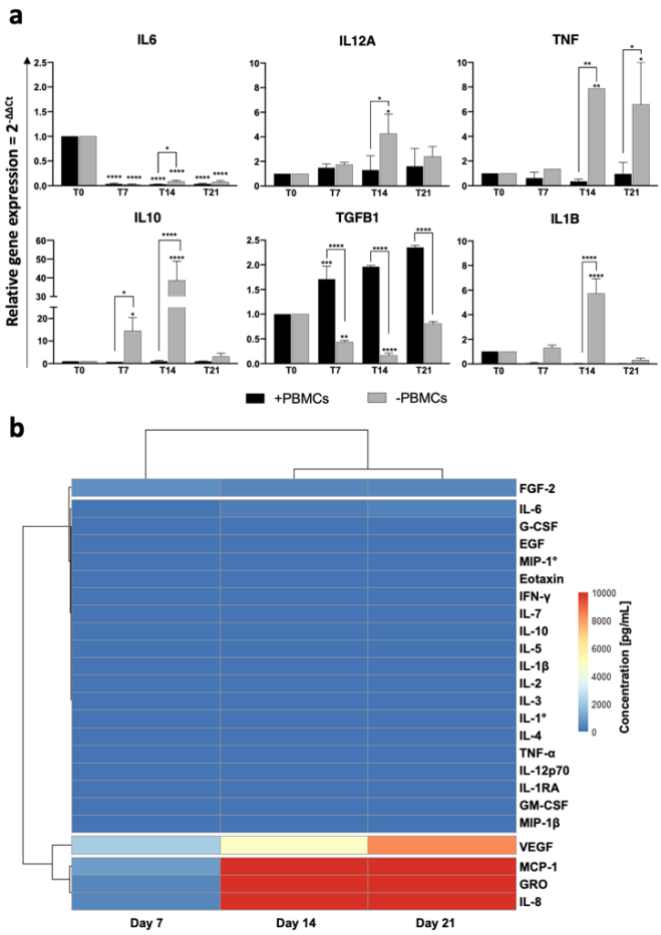

Figure 27. Pro- and anti- inflammatory cytokine expression by quantitative RT-PCR and immunoassay in static BM-MSC-SkM-PBMC co-culture. (a) BM-MSCs were co-seeded with SkMs in ratio 2:1 and PBMCs were culture in the upper chamber of transwell inserts. mRNA levels of pro-inflammatory (*TNF*, *IL12A*, and *IL1B*) and anti-inflammatory cytokines (*IL10*, *TGFB1*, and *IL4*) were assayed by qRT-PCR at day 7, 14 and 21 of culture. The relative quantification of each mRNA gene expression normalized to endogenous GAPDH (internal control) was calculated using the $2^{-\Delta\Delta Ct}$ method and presented as fold change over BM-MSCs at day 0, used as control. (b) Cytokine levels were also measured in culture medium supernatants at day 7, 14, and 21 by magnetic bead-based multiplex immunoassay. Data are reported as heatmap from blue (lowest value, 0 pg/mL of concentration) to red (highest value). Cytokines were hierarchical clustered based on expression pattern. Heatmap was made using *Pheatmap* and *ComplexHeatmap* packages in R Studio software (v. 2022.07.1+554; R Studio, Boston, MA, US). * $p < 0.05$; ** $p < 0.01$; **** $p < 0.0001$.

3.5 Discussion

Regenerative procedures are routinely used in clinical practice for supporting tissue healing. In CLI or other critical ischemic lesions, self-revascularization ability of resident stem cells is limited, and autologous transplantation of PBMCs concentrated by blood filtration with commercial filter systems can improve myofiber and vascular regeneration leading to limb rescue in CLI patients. However, exact mechanisms by which autologous PBMCs support both muscle and vascular healing in CLI are still unclear. Indeed, the exact role of PBMCs in influencing myogenic events is still under debate, even though pharmacological targeting of inflammation and immune functions result in faster healing processes. In case of severe injuries, skeletal muscle capacity to spontaneously heal appears insufficient, and available treatments do not provide optimal restoration to preinjury status. Therefore, biological treatments, including cell therapy and tissue engineering protocols, are of clinical interest, and a biomimetic *in-vitro* model could be a precious tool to better understand the complex mechanism behind healing processes to improve clinical management. In this work, we implemented our previously established myogenic model based on BM-MSC-SkM co-culture by adding PBMCs collected by a commercial filtration system to explore their potential contribution to myogenic commitment of BM-MSCs. In our experience, myogenic commitment is highly enhanced by the presence of myoblasts, likely because of cell-to-cell contacts and secreted factors favoring myogenic differentiation of MSCs. So that, PBMCs were implemented in this well-established *in-vitro* myogenic model adopting a transwell chamber to investigate the role of paracrine factors released by inflammatory cells in tissue repair.

First morphological, physical, and chemical properties of the filter were studied to highlight those characteristics that allow an efficient whole blood filtration. Based on filter characterization, cell suspension is retained within the continuous capillary network of the porous structure of the filter medium, likely because of combined actions of several factors, including sedimentation along tortuous capillary path, chemical-physical filter properties-related adsorption, and electrostatic attraction between opposite electric charges of cells and filter medium materials.

Filtered fractions were composed by all peripheral blood mononucleated populations, such as granulocytes, monocytes, lymphocytes, and stem cells (a rare circulating population in healthy individuals) without significative differences in relative percentage before and after filtration, even in T cell subpopulation distribution, as already described, confirming filter efficiency in filtration and blood composition preservation as well as blood concentration from a starting total whole blood volume of 98.2 mL $\pm$ 8.49 to a final enriched concentrate volume of 12.84 $\pm$ 1.29 mL (7 times enriched)[125]. Similarly, we efficiently concentrate whole blood starting from a total volume of 120 mL to a filtrated PBMC volume of 10 mL in 0.9% saline solution, with a higher yield of enrichment (10 times) compared to previously reported data.

Finally, isolated PBMCs were added to BM-MSC-SkM co-cultures developing a novel *in-vitro* three-cell co-culture myogenic model. More in details, PBMCs were added in the upper chamber of a transwell insert to study their potential paracrine effects in BM-MSC myogenic commitment; however, their presence did not significantly influence the expression of myogenic transcription factors, while *Desmin* and *MYH2* were significantly upregulated already after seven days of cultures compared to co-culture without PBMCs. Our data suggest that PBMCs might release factors that can

significantly speed-up BM-MSC commitment toward myogenic phenotype, as markers of a more mature myocytic phenotype (e.g., *MyoD1*, *Desmin*, and *MYH2*) were significantly upregulated just after seven days of culture compared to co-culture without PBMCs that upregulated later in culture myocytic markers (e.g., *MYH2* at 21 days of culture).

Successful myogenic commitment was also confirmed by flow cytometry immunophenotyping and IF analysis, as CD90 negativization mirrored lineage commitment of BM-MSCs toward $CD90^{-}CD73^{+}CD105^{+/-}$ mature myocytes as well as Desmin and MYH2 expression at protein level.

During myogenesis and skeletal muscle regeneration, a broad range of cytokines are secreted by stem cells, muscle cells and immune cells. First pro-inflammatory cytokines and then anti-inflammatory ones increase transiently triggering myogenesis cascade events. Cytokines coordinate inflammatory response, induce additional immune cell recruitment, and allow the complex cell-cell crosstalk, favoring muscle healing and maintaining healthy physiological condition.

Regarding cytokines, only *TGFB1* was significantly upregulated by co-cultured cells in the presence of PBMCs, while *IL12A*, *TNF*, *IL10*, and *IL1B* expression was significant increase in BM-MSC-SkM co-culture in the absence of peripheral blood cells. TGFB1 is considered an inhibitor of muscle differentiation through MyoD1 inactivation[126]; however, our results showed a high upregulation for MyoD1 along the culture, thus the modest upregulation of TGFB1 could be due to its contribution to a transient matrix deposit[127,128]. Conversely, macrophage chemoattracts and growth factors, such as GRO, MCP-1, IL-8, and VEGF, were increasingly present in medium along the culture. Indeed, during myogenesis and muscle healing,

chemoattractant factors play a pivotal role in cell recruitment like phagocytes, without which the process progression is destinated to stop[10]. VEGF, a well-known neovascularization growth factor and a therapeutic target in cancer treatments, is involved in muscle tissue regeneration by favoring blood vessel neoformation, and by muscle cell proliferation. Consequently, PBMCs might exert an anti-inflammatory paracrine effect on microenvironment composition that could favor BM-MSC myogenic commitment and might also create an optimal chemoattractant gradient that might favor macrophage and neutrophil recruitment for clearance of debris and for induction of healing processes after traumatic injuries.

3.6 Conclusion

In conclusion, this novel three-cell co-culture *in-vitro* system allowed investigation of paracrine effects of PBMCs on myogenic commitment of BM-MSCs. Our results show that the presence of immune cells could improve differentiation of BM-MSCs toward myogenic phenotype and could promote an anti-inflammatory and phagocyte-permissive microenvironment thus improving both cell proliferation and clearance of debris, especially in muscle injuries. Our *in-vitro* model also opens perspectives for a more comprehensive exploration of MSC behavior along myogenic commitment and for better studying the complex crosstalk between stem and immune cells, likely favoring regeneration events. However, our data need further *in-vivo* and *in-vitro* investigations to better understand the exact role of PBMCs or specific immune cell subsets on myogenesis and healing events, and to identify a possible pharmacological target. Moreover, our proposed data open perspectives for future use of these blood filtration systems to collect PBMC fraction for treatment of severe muscle injuries to accelerate healing events.

These filter devices could represent a valid and alternative therapeutic option in muscle regenerative medicine.

CHAPTER 4. Peripheral Blood Mononuclear Cell contribution in 3d bioengineered myogenic co-culture system

4.1 Introduction

In-vitro SkMR models are extremely challenging to reproduce because resident SCs - that mediate the entire process *in-vivo*- are very difficult to harvest from muscle tissue and lose their engraftment potential in *ex-vivo* conditions with progressive growth rate reduction[129–132]. BM-MSCs represent the gold standard for musculoskeletal regeneration study and research[67,68,133]. They were also proposed as a promising alternative in SkMR because of their ability to differentiate. towards various lineages, low immunogenicity, and high immunomodulatory activity[134,135]. However, BM-MSCs are still poorly investigated for *in-vitro* myogenic purpose because of the lack of standardized medium composition and appropriate culture system approaches, although BM-MSCs co-cultured with myoblasts show significant upregulation of muscle markers, such as MRFs, Desmin, and MYH2[65,77].

Myogenesis is also strongly influenced by cytokines secreted by PBMCs involved in tissue regenerative processes, like clearance of necrotic debris, inflammation, and remodeling processes[10]. Moreover, pro-inflammatory cytokines released by PBMCs, including IFN-γ, TNF, IL-6, and IL-1, influence SkMR fate by driving the first phase of repair process and by modulating immune responses and SCs. Conversely, anti-inflammatory cytokines, especially IL-10, are associated with the transition from proliferative to differentiation phase of myogenesis[103,136]. Indirect evidence of the essential role of PBMCs in SkMR is the efficacy of autologous transplantation of peripheral blood cells isolated by commercial blood filtration systems for treatment of critic limb ischemia by increasing regenerated myofibers and by improving clinical outcomes[34,125].

On the other hand, biomimetic 3D cultures of stem cell represent a versatile tool for the study of myogenic commitment events[76,137]. Indeed, BM-MSCs

are frequently cultured in 3D hydrogel scaffolds, like fibrin hydrogels[133,138,139] that efficiently mimic SC niche[79] and may reproduce *in-vitro* the hierarchical structure of skeletal muscle tissue. Moreover, fibrin-based scaffolds constitute a regenerative myogenic environment without fibrosis, as cells produce their own ECM proteins and degraded fibrin excess allowing long-term skeletal muscle cell culture[80,81,140]. When a perfusion bioreactor system is adopted for these 3D *in-vitro* cultures, the medium easily diffuses through a 3D structure enhancing metabolite mass transfer, nutrient transport, and oxygenation rate. In addition, 3D perfused cultures show excellent viability, high proliferation rates, and more efficient commitment processes[141–143].

4.2 Aim

In this study, we aimed to develop an *in-vitro* model of myogenic commitment using *h*BM-MSCs and *h*SkMs cultured in 3D dynamic conditions assembled within a fibrin scaffold. Moreover, PBMCs were added within the same 3D co-culture to investigate their activity on BM-MSC myogenic commitment. To our knowledge, 3D *in-vitro* models studying the effects of PBMCs on stem cell commitment has been proposed only in osteogenic events; whereas 3D dynamic co-cultures of BM-MSCs and PBMCs applied to SkMR are not reported yet. *h*BM-MSC myogenic events evolution was monitored by qRT- PCR and immunohistochemistry, and PMBC characterization was performed by flow cytometry.

4.3 Materials and Methods

4.3.1 PBMC harvesting

Whole peripheral blood (PB) obtained from three healthy volunteers (M/F, 2/1; age ranged from 38 to 45 years old) was concentrated using a HemaTrate® Blood Filtration System (CH-WB110C, Patent n. EP 2602315A1; Pall Medistad B.V. (Medemblik; Netherlands) from Cook Regentec (Indianapolis, Indiana, United States). After filtration, PBMCs were isolated by Ficoll-Paque density gradient centrifugation (Cytiva), according to manufacturer's instructions, for flow cytometer immunophenotyping. Conversely, filtrated PBMCs were directly used for 3D culture experiments, or were stored in 70% RPMI (Gibco™), 20% FBS (Gibco™), and 10% DMSO (Sigma-Aldrich) at -80°C until use.

4.3.2 *h*BM-MSC isolation, harvesting and characterization

BM specimens for *h*BM-MSC isolation were obtained from three healthy male donors (aged 26, 24, and 28 years old) after informed written consent in accordance with the Declaration of Helsinki and protocols approved by our Institutional Review Board (Ethic Committee "Campania Sud", Brusciano, Naples, Italy; prot./SCCE n. 24,988). Whole BM aspirate was directly seeded at a density of 50,000 total nucleated cells/cm^2 in a T75 plastic flask containing α-MEM (Gibco™) supplemented with 1% Glutagro (Corning), 10% FBS (Gibco™) and 1% Pen/Strep (Corning) and incubated at 37°C in an atmosphere of 5% CO_2 and 95% relative humidity. After 48h, non-adherent cells were removed, and medium replaced twice a week. Cells were detached when 70-80% of confluence was reached, using 0.05% trypsin-0.53mM EDTA, washed with PBS (Corning), and counted using Trypan Blue (Sigma-Aldrich). BM-MSCs were subsequently seeded at 4,000 cells/cm^2 and expanded up to the third passage. Mesenchymal phenotype was

confirmed according to the International Society of Cellular Therapy guidelines[42]. *h*BM-MSCs were co-cultured in a 3D system with *h*SkMs, with and without PBMCs. All experiments were performed in biological triplicates (n = 3).

4.3.3 *h*SkM characterization

*h*SkMs were purchased from Gibco™. *h*SkMs were embedded in fibrin scaffolds to investigate their behavior in a 3D environment through qRT-PCR. Then, *h*SkMs were co-cultured with *h*BM-MSCs with and without PBMCs. Seeding ratio between *h*BM-MSCs:*h*SkMs was 2:1, as previously optimized[65]. All experiments were performed in biological triplicates (n = 3).

4.3.4 Flow cytometry

MSC and PBMC immunophenotype was investigated by flow cytometry. Briefly, for BM-MSCs, a minimum of 1×10^5 cells at the third passage was stained with the following antibodies: 2.5 µl of FITC-conjugated anti-CD90 or 5 µl of FITC-conjugated anti-HLA-DR; 5 µl of APC-conjugated anti-CD73; 10 µl of PE-conjugated anti-CD105 or 10µl of PE-conjugated anti-CD34; and 10 µl of PC7-conjugated anti-CD45 or 10 µl of PC7-conjugated anti-CD14 (all antibodies from Beckman Coulter, Fullerton, CA, United States). Cells were incubated at RT for 20 min in the dark, washed with PBS, and resuspended in 300 µl of the same buffer for acquisition. For PBMC immunophenotyping, before and after filter and separation procedures, a minimum of 2×10^5 cells were stained with the following antibodies: 5 µl of APC-conjugated anti-CD3; 5 µl PC7-conjugated anti-CD14; 5 µl of FITC-conjugated CD34; 5 µl of PC5-conjugated CD8; and 5 µl of PE-conjugated anti-CD4. Cells were then incubated at RT for 20 min in the dark, washed with PBS and resuspended in 300 µl of the same buffer for acquisition. Sample acquisition was performed on a BD FACSVerse flow cytometer

(Becton Dickinson, BD, NJ, United States) equipped with blue (488nm) and red lasers (628nm) and BD FACSuite software (BD Biosciences). PMT voltage setting, and compensation were carried out using single-color controls for each fluorochrome and an unstained sample as negative control. All samples were run with the same PMT voltages, and a minimum of 30,000 events were recorded. FlowJo software (v.10.7.1, LLC, BD Biosciences) was employed for post-acquisition compensation and analysis.

4.3.5 3D fibrin scaffold preparation and characterization

Cylindrical 3D scaffolds were prepared by mixing fibrinogen at 50 or 100 mg/mL (Sigma-Aldrich), α-aprotinin 15,600 U/mL (Sigma-Aldrich), α-MEM (Corning), and thrombin at 100U/mL (Sigma-Aldrich), and then were incubated at 37°C for 30 min to allow fibrinogen polymerization. Samples were fixed in 4% PFA; 4°C, overnight and then dehydrated by multiple passages across ethanol:water solutions (10 min each) with increasing percentages of ethanol and dried using a dense CO_2 drying operating at 200 bar and 38°C for 4h; other details on the dense gas drying protocol were reported elsewhere[144]. Samples were immersed in liquid nitrogen and fractured with a needle, then placed on a double-sided adhesive carbon tape previously glued to an aluminum stub and coated with a gold film (250 A thickness) using a sputter coater (mod.108 A; Agar Scientific, Stansted, United Kingdom), before observation. Internal scaffold morphology was observed by field emission-scanning electron microscopy (FE- SEM, mod. LEO 1525; Carl Zeiss, Oberkochen, DE). Pore size frequency distribution was studied with ImageJ software (rel.1.52p National Institutes of Health, United States), and average perimeter and average Feret's diameter values were reported.

Cylindrical 3D scaffolds were prepared by mixing fibrinogen at 50 mg/mL (Sigma-Aldrich), α-aprotinin 15,600 U/mL (Sigma-Aldrich), and α-MEM (Corning) containing 1×10^6 cells. Two cell suspension solutions were prepared, composed by *h*BM- MSCs and *h*SkMs with PBMCs ([*h*BM-MSCs + *h*SkMs]: PBMCs, 1:1) and without PBMCs. This ratio was chosen based on previously published literature showing that lower PBMCs:co-cultured cells ratios are preferable[145,146].

Suspensions were pipetted in different wells of a 96-well plate, thrombin at 100 U/mL (Sigma-Aldrich) was added, and samples incubated at 37°C for 30 min to allow fibrinogen polymerization. 3D scaffolds were then transferred to a culture plate.

4.3.6 Dynamic culture

3D scaffolds were placed in a perfusion bioreactor, formed by a custom multi-well plate, milled in PMMA, (Altuglas® CN 100 10000, Altuglas International, La Garenne-Colombes Cedex, FR), a biocompatible material for biomedical application[89]. This plate has two holes allowing the insertion of silicon tubes (Tygon®, FR) for medium flowing at a constant flow rate of 1.0 mL/min maintained by peristaltic pumps[63]. This bioreactor system operates within a standard cell culture incubator.

4.3.7 Live&Dead assay

Cell viability was detected by fluorescence live and dead assay after preparation (day 0) and at each time point (day 7, 14, and 21). Calcein AM solution (Cat. No C1359, Sigma-Aldrich) was used to stain live cells, while cell membrane-impermeable Ethidium homodimer I solution (Cat. No E1903, Sigma-Aldrich) for nuclei of dead cells. Cells were incubated for 1h at 37°C, then washed in PBS, and imaged using a fluorescence microscope (Eclipse Ti Nikon Corporation, Tokyo, Japan). Signal intensity was quantified using

ImageJ software. Original RGB images were converted to 8-bit (grey scale) format and tagged area intensities were expressed as mean value of pixel intensity within a range from 0 (dark) to 255 (white), as previously reported (Spaepen et al., 2011).

4.3.8 RNA isolation and gene expression profile

Expression of myogenic genes, including *Pax3*, *MyoD1*, *Myf5*, *Myf6*, *Desmin*, and *MYH2* (Bio-Rad, Foster City, CA, United States), and cytokines, such as *IL6*, *TNF*, *IL12A*, *IL1B*, *IFNG*, *IL10*, *IL4*, *TGFB1*, and *TGFB2* (sequences are reported in Table 1) were investigated by reverse transcription quantitative polymerase chain reaction (RT-qPCR). Total RNA from 3D dynamic cultures at each time point was extracted using QIAzol Lysis Reagent (Qiagen), chloroform (Sigma-Aldrich), and RNeasy Micro Kit (Qiagen). For each sample, 1 μg of total RNA was reverse transcribed using iScript™ cDNA synthesis kit (BioRad), and relative gene expression analysis was performed on a LightCycler® 480 Instrument (Roche, Basel, Switzerland) using SsoAdvanced™ universal SYBR® Green Supermix (BioRad). Specificity of formed products was assessed by melting curve analysis. Experiments were run in triplicate. Data were normalized to *GAPDH* expression (reference gene) applying the geNorm method[91] and using CFX Manager software ($M < 0.5$). Fold changes were determined by $2^{-\Delta\Delta Ct}$ method and presented as relative levels versus *h*SkMs and *h*BM-MSCs at day 0. All experiments were performed in biological triplicates ($n = 3$), and each experiment in technical triplicate.

Gene symbol	Gene Bank accession number	Sequences	Size	Primer efficiency
IL6	NM-000600.5	Forward: ACTTGCCTGGTGAAAATCAT Reverse: CAGGAACTGGATCAGGACTT	135	106%
TNF	NM-000594.4	Forward: GCCCATGTTGTAGCAAACCC Reverse: TATCTCTCAGCTCCACGCCA	97	105%
IL12A	NM-000882.4	Forward: TCAGAATTCGGGCAGTGACT Reverse: AGTCCCAQTCCTTCTTTCCCC	163	110%
IL1B	NM-000576.3	Forward: GGAGAATGACCTGAGCACCT Reverse: GGAGGTGGAGAGCTTTCAGT	185	110%
IFNG	NM-000619.3	Forward: TGCAGAGCCAAATTGTCTCC Reverse: TGCTTTGCGTTGGACATTCA	194	110%
IL10	NM-000572.3	Forward: AAGACCCAGACATCAAGGCG Reverse: AATCGATGACAGCGCCGTAG	85	110%
IL4	NM-000589.4	Forward: CTGCTTCCCCCTCTGTTCTTC Reverse: TTCGCTCTGTGAGGCTGTT	117	110%
TGFB1	NM-000660.7	Forward: GCACTCGCCAGAGTGGTTAT Reverse: AAGCCCTCAATTTCCCCTCC	81	95%
TGFB2	NM-0001135599.4	Forward: CCCTAAGCGCAATTCCAC Reverse: CTGCTCCTCCTTCTCTTGCT	213	106%

Table 1. Cytokine RNA sequences.

4.3.9 Immunofluorescence assay

Fibrin scaffolds were fixed in 4% PFA for 2h at RT, cryo-protected in 30% sucrose (4°C, overnight), included in optimal cutting temperature (OCT) compound, and cut in slices of 10μm thickness using a cryostat (CM 1950, Leica, Wetzlar, Germany). Slices were permeabilized with 0.1% Triton X-100 for 10 min and blocked with horse serum solution for 1 h. Samples were then stained for Desmin (1:100; Abcam) and MYH2 (1:50, Thermo Fisher Scientific), incubated overnight at 4°C, and subsequently incubated for 1h at RT with Alexa Fluor 488 goat anti-rabbit IgG (1:400; Thermo Fisher Scientific), VectaFluor anti-mouse IgG Dylight 594® kit (Vector laboratories), and DAPI. Slices were also stained for FITC-conjugated CD90 and PE-conjugated CD105 (Beckman Coulter), incubated overnight at 4°C, and the cell nuclei were counterstained using DAPI. Separate images were acquired using identical settings of light intensity, exposure time, and gain using a fluorescence microscope (Eclipse Ti Nikon Corporation, Tokyo, Japan).

4.3.10 Cytokine detection

For quantification of secreted cytokines in culture medium, an immunobead-based multiplex assay (Merck, Millipore) was employed for measurement of EGF, Eotaxin, GM-CSF, IFN-γ, IL-10, IL-12p70, IL-1RA, IL-1a, IL-1β, IL-2, IL-3, IL-4, IL-5, IL-7, MIP-1 α, MIP-1β, TNF-α, bFGF, G-CSF, GRO, IL-6, IL-8, MCP-1, and VEGF, following manufacturer's instructions

4.3.11 Hematoxylin&Eosin staining

Scaffold slices (15 μm thickness) were hydrated using a decreasing ethanol gradient, washed for 5 min in water and incubated with hematoxylin and eosin for 60 min, then dehydrated using an increasing ethanol gradient and cleared in xylene for 5min. Sections were mounted using Eukitt (Sigma-Aldrich)

mounting medium. Images were acquired using an Olympus microscope BX53 equipped with ProgRes SpeedXT core five camera.

4.3.12 Statistical analysis

Data were analyzed using Prism software (v.9.0, GraphPad software, LLC, San Diego, California, United States). Results are presented as mean ± SD. Statistical analysis was performed using two-tailed independent Student's t-test for two group comparisons, or two-way analysis of variance (ANOVA) test for three or more group comparison with Tukey's test for multiple comparisons between group. For flow cytometry data, results are presented as percentage of positive cells, and expression of each marker on single cells is also reported as histograms and using unstained samples as negative controls. For characterization of mesenchymal cells in the co-culture system, percentage of positive cells and median fluorescence intensity (MFI) values were calculated for each marker. Surface marker expression variations were calculated as fold change normalizing MFI values for each marker and from each time point to MFI obtained from *h*BM-MSC cultured alone[147]. A *p*-value < 0.05 was considered statistically significant[93].

4.4 Results

4.4.1 3D scaffold characterization

50 and 100 mg/mL fibrinogen concentrations were tested to check the best concentration to simultaneously assure good scaffold integrity and void spaces to host cells. Polymerized fibrin scaffolds are shown in Figure 28a. Fibrinogen concentrations of 5 mg/mL was too low to induce polymerization, whereas scaffold obtained at 20 mg/ mL were difficult to be managed and were discharged (unpublished data). To better observe internal scaffold morphology obtained at 50 and 100 mg/mL, hydrogels were converted to

aerogels by dense gas drying process, a procedure already optimized procedure to avoid the natural shrinkage and collapsing of the 3D hydrated system[144]. Indeed, derived alcohol gels were processed with dense carbon dioxide for 4h at 38°C and 200 bar with a flow rate of 1.2 kg/h (system technology scheme is shown in Figure 28b.

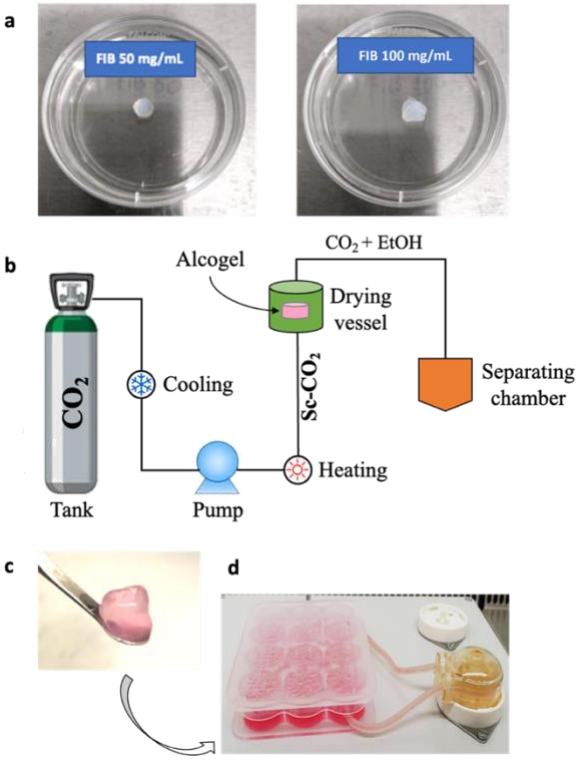

Figure 28. Fibrin scaffold, plant layout for drying and perfusion bioreactor images. Fibrin scaffold images at 50 mg/mL and 100 mg/mL of fibrinogen concentration (**a**); plant layout for hydrogel scaffold driyng by dense carbon dioxide at 200 bar and 38°C; using this protocol the 3D structure shrinkage was avoided, and scaffold internal structure was clearly observed (**b**); fibrin scaffold image (**c**); perfusion bioreactor that allows a constant medium flow rate of 1 mL/min (**d**).

Collected aerogels maintained the same volume with a shrinkage < 2%. Thanks to this extremely low shrinkage scaffold morphology was

investigated after their freeze-fracture and the internal void structure was observed by FE-SEM (Figure 29).

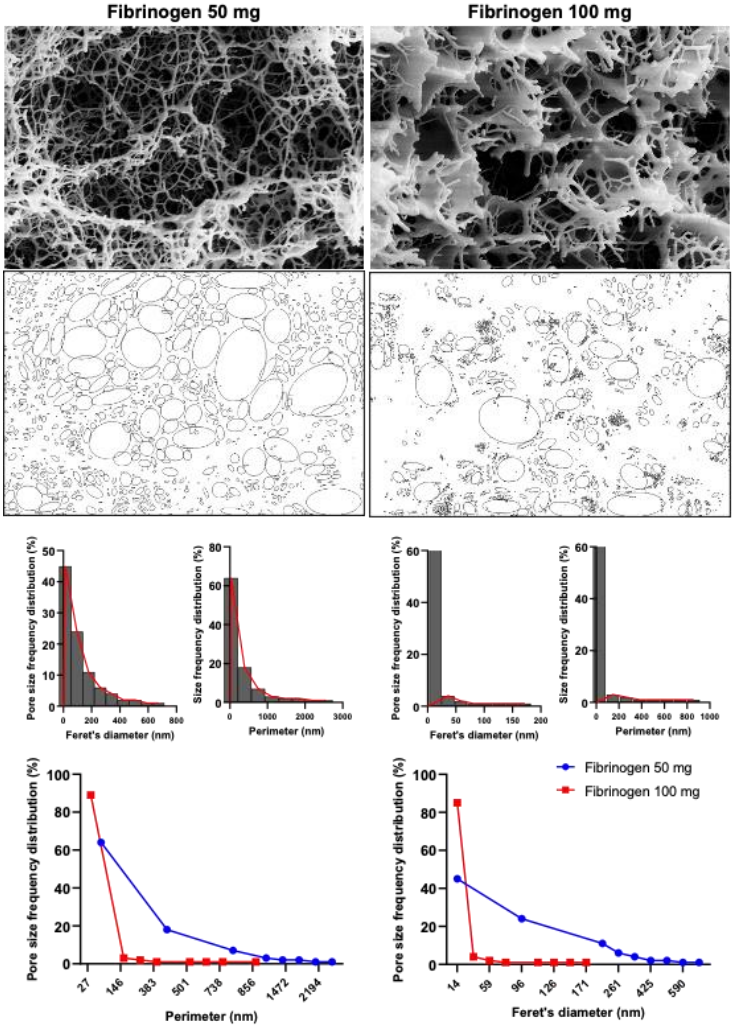

Figure 29. FE-SEM aerogel images and pore size measurement plots. After conversion in alcohol-gel, hydrogel scaffold was dried by dense carbon dioxide at 200 bar and 38°C; using this protocol the 3D structure shrinkage was avoided, and scaffold internal structure was clearly observed after freeze-fracturing in liquid nitrogen. Images and Field Emission-Scanning electron microscopy (FE-SEM) images of aerogels and of their internal structure morphology at two tested fibrinogen concentrations, (**a**) 100 mg/mL and (**b**) 50 mg/mL. Perimeter and Feret's diameter values were calculated with ImageJ software, and pores were automatically determined after threshold adjustment in (**c**) 100 mg/mL and (**d**) 50 mg/mL fibrinogen scaffolds. Size frequency distributions are shown for perimeter and Feret's diameter values in (**e**) 100 mg/mL and (**f**) 50 mg/mL fibrinogen scaffolds, and (**g**) compared between the two concentrations.

Scaffolds obtained using 50 mg/mL of fibrinogen showed thinner and wider meshes than those obtained with 100 mg/mL of fibrinogen. Pores of the 50 mg/mL of fibrinogen scaffold showed a mean perimeter of 548 nm and a mean Feret's diameter of 180 nm, while at 100 mg/mL of fibrinogen, pores had smaller perimeter (mean, 128 nm) and Feret's diameter (mean, 40 nm). Therefore, scaffolds made with 50 mg/m of fibrinogen were chosen for further experiments, because they displayed a more spacious microenvironment suitable for a better cell distribution and viability.

4.4.2 Dynamic culture by perfusion bioreactor

Next, a myogenic commitment model of *h*BM-MSCs-*h*SkMs co-cultured (ratio 2:1) with or without PBMCs was established using scaffolds composed by fibrinogen at 50 mg/mL as support for cell culture and placed in dynamic conditions using a custom-made perfusion bioreactor for maintaining a constant medium flow rate of 1 mL/min[148] (Figure 28c-d). To confirm suitability of this *in-vitro* system before performing further experiments, cell viability within fibrin scaffolds was assessed by live and dead assay over a culture period of 21 days. As expected, total cells were almost represented by live cells (> 80%) throughout the culture (Figure 30). Furthermore, fibrin scaffolds also maintained structure and integrity, as cells were homogenously distributed and were in close contact throughout the culture period. This regular distribution was also documented by histological evaluation of 3D scaffold culture slices using hematoxylin and eosin staining (Figure 31). Furthermore, fibrin matrix behaves as inert matrix not really influencing myogenic marker expression of *h*BM-MSCs-*h*SkMs co-culture; indeed, when, those cells were co-seeded in 2D culture, almost similar gene expression profile has been observed[65].

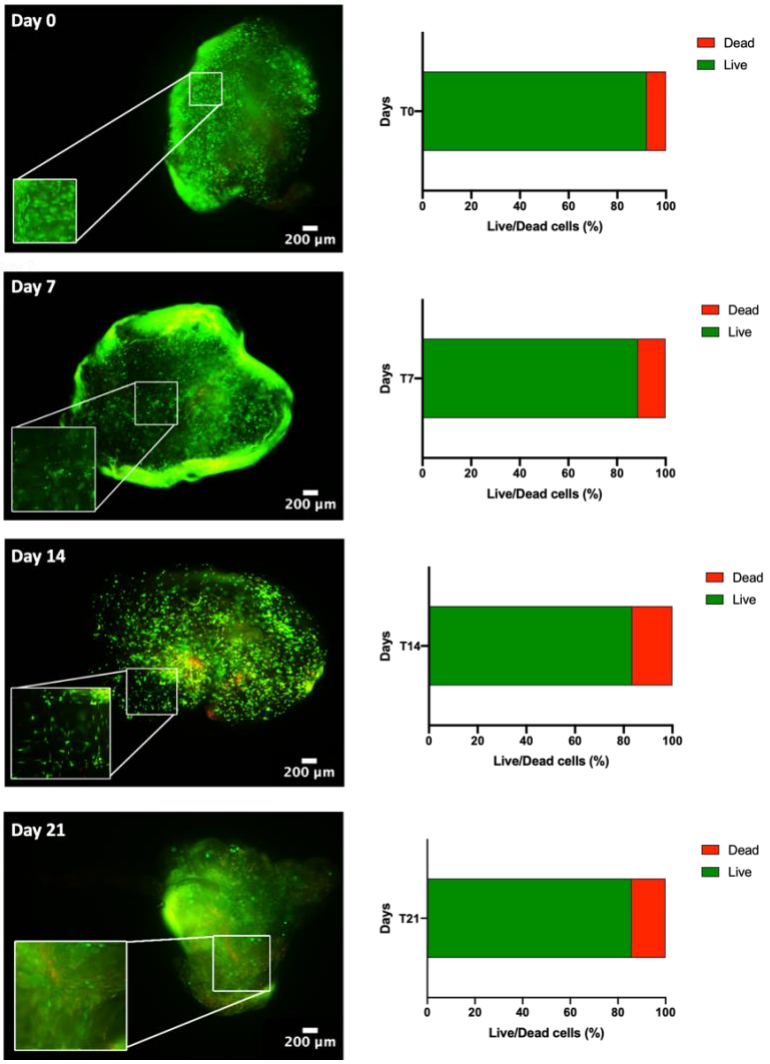

Figure 30. Live & Dead of *h*BM-MSC-*h*SkM-PBMC viability in a 3D fibrin scaffold cultured in perfusion system. Live cells are in green while dead cells in red. Images were captured at day 0, 7, 14 and 21 of culture, at 4x magnification, scale bar: 200µm, while zoomed areas are at 200%. Histograms report viability quantification.

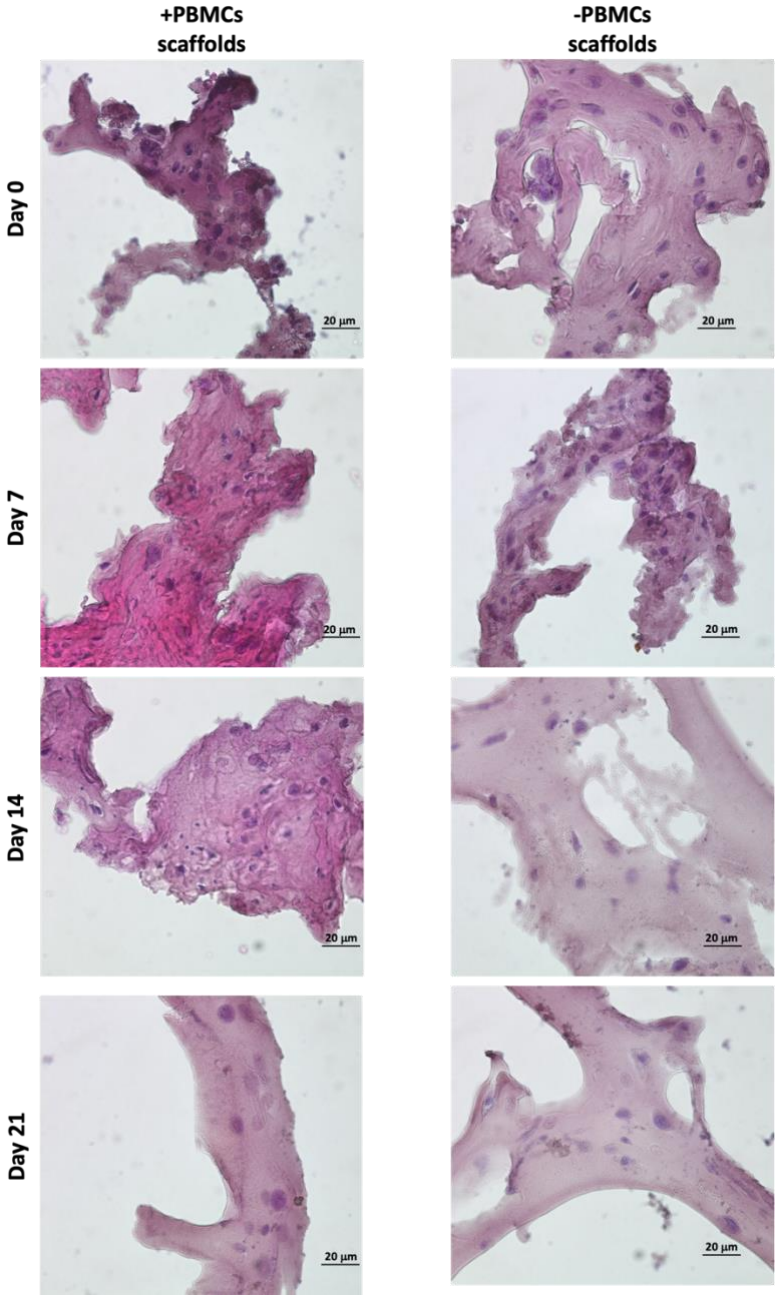

Figure 31. Hematoxylin & Eosin staining. Hematoxylin & Eosin staining on 3D fibrin scaffolds embedded with *h*BM-MSCs-*h*SkMs with and without PBMCs. Images were acquired at day 7, 14 and 21 at 40x magnification, scale bar: 20 µm.

4.4.3 *h*BM-MSC and PBMC characterization

First, mesenchymal phenotype of our primary *h*BM-MSCs was confirmed following International Society of Cellular Therapy criteria[42]: adherence to tissue culture plastics; fibroblast-like shape; positivity for CD90, CD105, and CD73 mesenchymal markers; and negativity for CD34, CD14, CD45, and HLA-DR by flow cytometry (Figure 32).

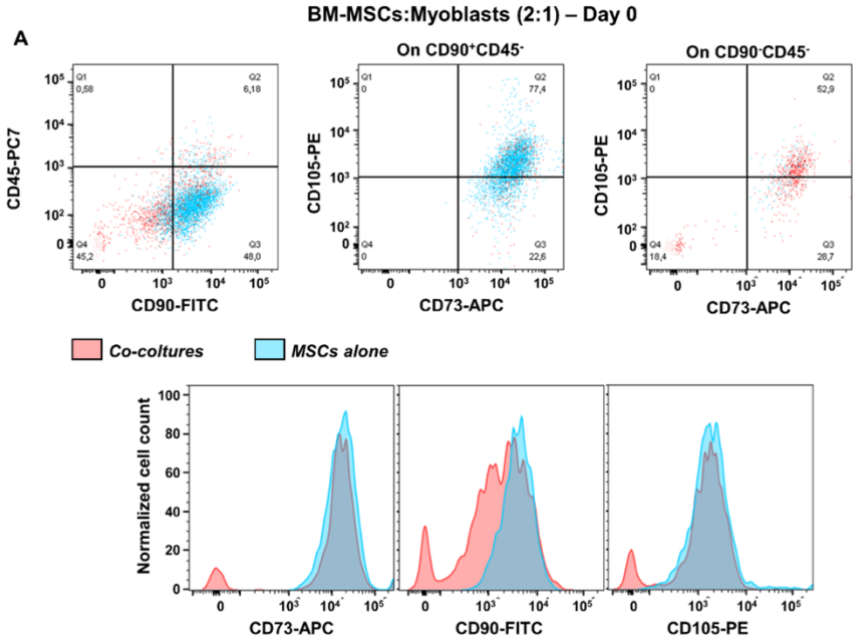

Figure 32. Immunophenotype of *h*BM-MSCs-*h*SkMs co-culture at day 0. Immunophenotype of *h*BM-MSCs-*h*SkMs co-culture at day 0 was performed by flow cytometry on *h*BM-MSCs-*h*SkMs co-culture and mesenchymal stem cells (MSCs) alone at day 0 (**A**), and CD90 expression was investigated on $CD45^-$ cells. Next, CD105 and CD73 expression was further studied on $CD45^-CD90^+$ and $CD45^-CD90^+$ cell populations (upper dot plots). Variations in marker expression are also displayed as normalized cell count histograms on single cells. On single cells, CD90 and CD45 expression was explored, and $CD90^+CD45^-$ cells were further studied for CD105 and CD73 expression. Similarly, on single cells, HLA-DR and CD34 expression was investigated, and $CD34^-HLA\text{-}DR^-$ cells were further studied for CD14 expression.

Then, PBMCs were collected by filtration of 120 ml of whole blood adopting a system conventionally used in clinical practice (HemaTrate® system), and nucleated cell fraction was concentrated in 10 mL of physiological solution. PBMC immunophenotyping and whole blood composition were investigated by flow cytometry on cells separated by Ficoll-Paque density gradient; filter waste bag was considered as a negative control for each donor employed (Figure 33). No significant variations were described in blood frequency and composition before and after filtration or separation, while no PBMCs were observed in specimens obtained from filter waste bags (Figure 33). Moreover, no differences were described for total $CD3^+$T Cells and $CD4^+$/$CD8^+$subpopulations (all $p > 0.05$), and for circulating $CD34^+$ hematopoietic stem cells ($p = 0.2875$), confirming that HemaTrate® filter was highly efficient in selective PBMC collection and concentration in 10 mL final volume of filtrate.

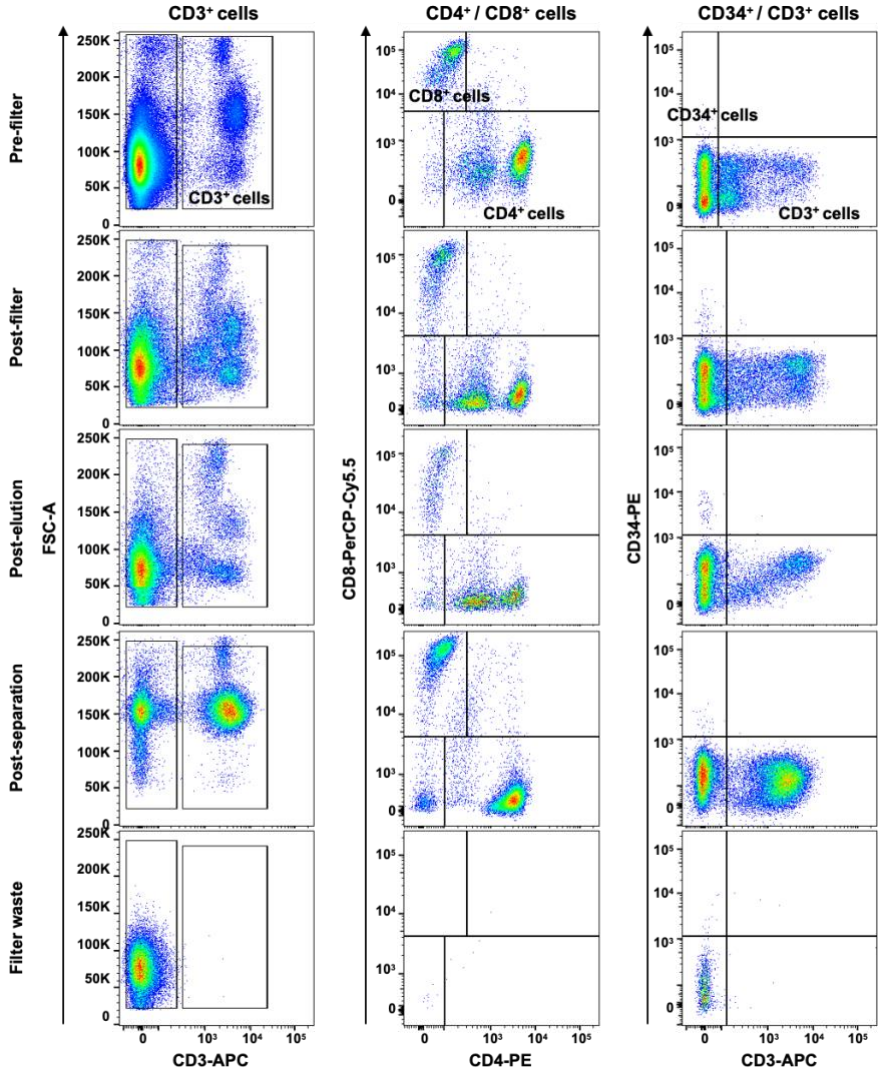

Figure 33. Flow cytometry immunophenotyping of peripheral blood mononuclear cells (PBMCs) obtained by a HemaTrate® Blood Filtration system. Peripheral blood mononuclear cells (PBMCs) obtained by whole blood by was collected and filtered by a HemaTrate® Blood Filtration system. PBMC different population fraction was subsequently separated by Ficoll-Paque density gradient separation to perform flow cytometry immunophenotyping on pre- and post-filtration, post-elution, post-separation, and on the filter bag waste, as negative control. Frequencies of $CD3^+$ T lymphocytes and $CD8^+$ and $CD4^+$ subsets and circulating $CD34^+$ hematopoietic stem cells were studied.

4.4.4 Myogenic commitment in co-culture system gene expression profile and immunofluorescence evidence

Myogenic commitment potential of our 3D system was investigated by gene expression profiling (Figure 34). First, *h*SkMs behavior in 3D culture was explored, as shown in Figure 34a *h*SkMs showed a significant upregulation of *Pax3* and *MYH2* at day 21 (258-fold and 261-fold, respectively, $p < 0.0001$), as well as *MyoD1*, *Myf5*, *Myf6*, and *Desmin* genes with an increasing trend from day 0–21. This behavior was reported for comparison purpose. Then, in Figure 34b gene expression profiling of *h*BM-MSCs-*h*SkMs in 3D co-culture with and without PBMCs is showed. *Pax3* expression levels significantly differed between the two culture conditions over time. In details, *Pax3* expression was upregulated at day 7 in the presence of PBMCs (20-fold), while decreased at day 14 (7-fold), and significantly upregulated at day 21 (27-fold, $p < 0.05$). A similar trend was described in the absence of PBMCs (from 8.6-fold at day 7 to 6.4-fold at day 14 and 11.3-fold at day 21). For MRF genes, *MyoD1* expression showed lower fold-change values than those without PBMCs at day 7 (28.35-fold vs. 70-fold); however, at day 14 in the presence of PBMCs a significant upregulation occurred (118-fold, $p < 0.05$) as well as at day 21 (81-fold vs. 51-fold). In cultures with PBMCs, *Myf5* expression was increased about 220-fold and without PBMCs about 329-fold ($p < 0.05$) at day 7, while at day 14 slightly decreased with PBMCs (152-fold with vs. 186-fold without PBMCs), remaining stable at day 21 (136-fold with vs. 99-fold without PBMCs). Generally, *Myf6* expression decreased along the culture with PBMCs, from 215-fold ($p < 0.5$) at day 7, to 75.2-fold at day 14, and 31-fold at day 21. Without PBMCs, the expression was of 165-fold at day 7, about 105-fold at day 14, and decreased at 64-fold at day 21. Desmin expression displayed an increasing trend with PBMCs about 3-fold at day 7, 5-fold at day 14, and 6-fold at day 21. When cultured without PBMCs,

Desmin expression was slightly upregulated at day 7 and 14 (10-fold and 9.5-fold, respectively; $p < 0.01$), and at day 21 of 8-fold ($p < 0.05$). MYH2 was also investigated but not detected at any time point along the culture. All these profiles were also different from those observed for the *h*SkMs alone in 3D culture, suggesting a fundamental role of the different cell population cross-talk within the 3D system.

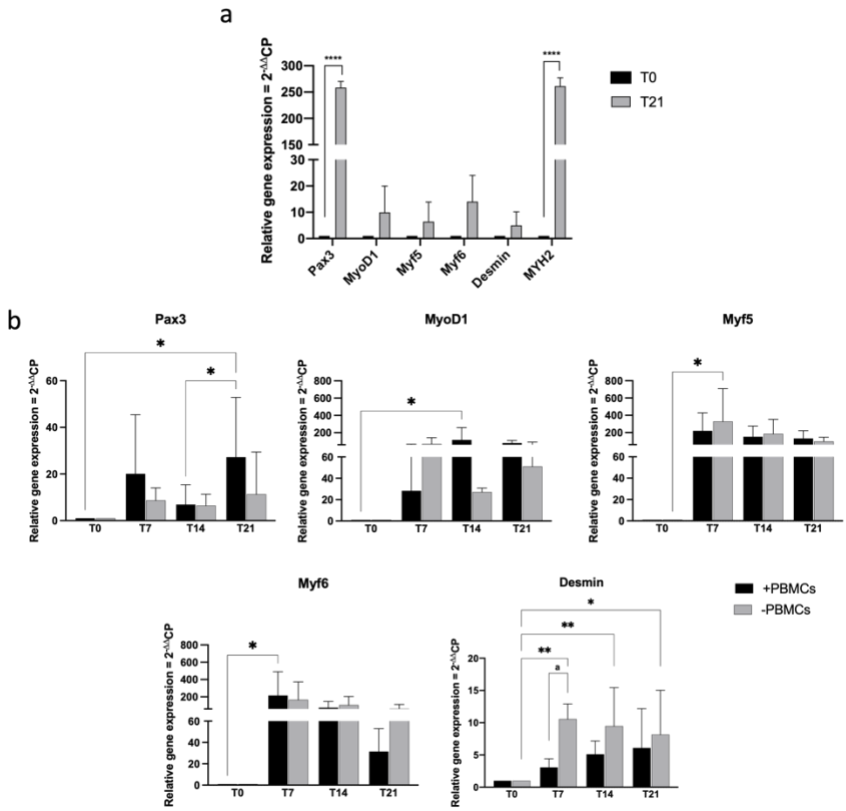

Figure 34. Gene expression profiling for myogenic markers by quantitative RT-PCR of *h*SkMs (a) and of *h*BM-MSCs-*h*SkMs-PBMCs (b), both within 3D fibrin scaffold. mRNA levels of myogenic markers (*Pax3*, *MyoD1*, *Myf5*, *Myf6* and *Desmin*) were assayed by qRT-PCR at day 7, 14 and 21 of culture. Relative quantification of each mRNA gene expression normalized to endogenous *GAPDH* (internal control) was calculated using the $2^{-\Delta\Delta Ct}$ method and presented as fold change over *h*SkMs at day 0 (**a**) and over *h*BM-MSCs at day 0 (**b**), selected as a control. All experiments were performed in biological triplicates (N=3) and each experiment in technical triplicates. *, significant compared to T0; a, significant comparison between +/- PBMCs at day 7. *, a $p < 0.05$; ** $p < 0.01$; **** $p < 0.0001$.

To further confirm myogenic commitment of *h*BM-MSCs with or without PBMCs in a 3D culture system, myogenic-related proteins, such as Desmin and MYH2, were assayed by IF (Figures 35, 36).

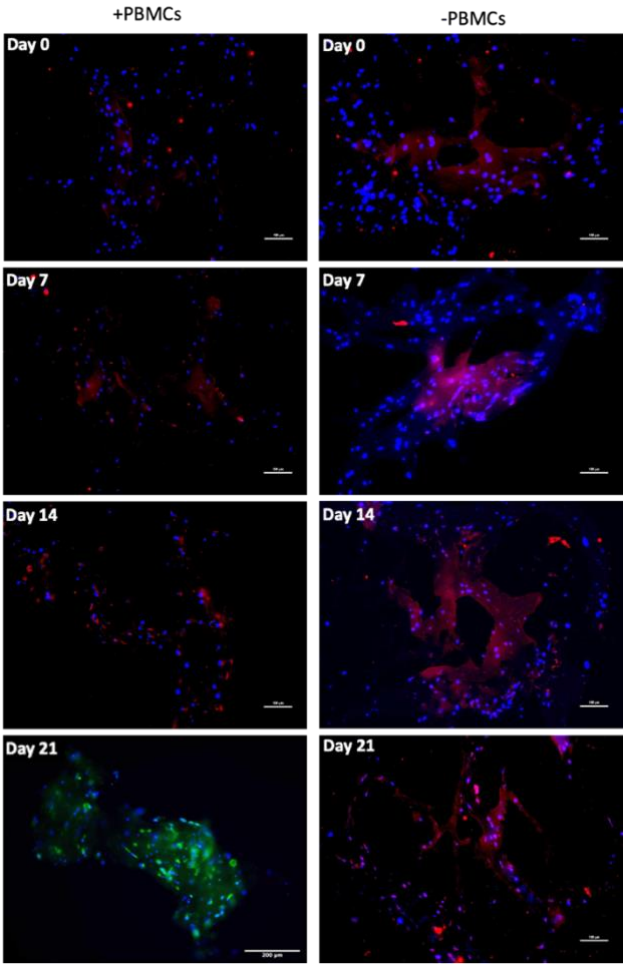

Figure 35. Immunofluorescence images of 3D fibrin scaffold for Desmin and MYH2. Immunofluorescence images of 3D fibrin scaffold for Desmin and MYH2 obtained by IF assay performed at day 7, 14 and 21 of culture. Desmin was stained in red and MYH2 in green; scaffolds embedded with *h*BM-MSCs-*h*SkMs-PBMCs (left column) and scaffolds embedded with *h*BM-MSCs-*h*SkMs (right column) are shown. MYH2 was not detected. All images were captured using 20x magnification, scale bar: 200 μm.

In the presence of PBMCs, Desmin was detectable from day 7 with a signal that became brighter throughout the culture. Despite not well detected by

qRT-PCR, MYH2 protein was highlighted by IF assay at day 21 days but only in the culture with PBMCs. Furthermore, almost all 3D cultures of *h*BM-MSCs-*h*SkMs without PBMCs displayed IF signals less intense at each time point compared to cultures with PBMCs (Figure 35). CD90 and CD105 protein expression was also investigated to confirm mesenchymal phenotype at baseline. Signals were clearly detected at day 0, confirming the mesenchymal phenotype of cultured *h*BM-MSCs, while very low or undetectable expression was observed at day 21 (Figure 36).

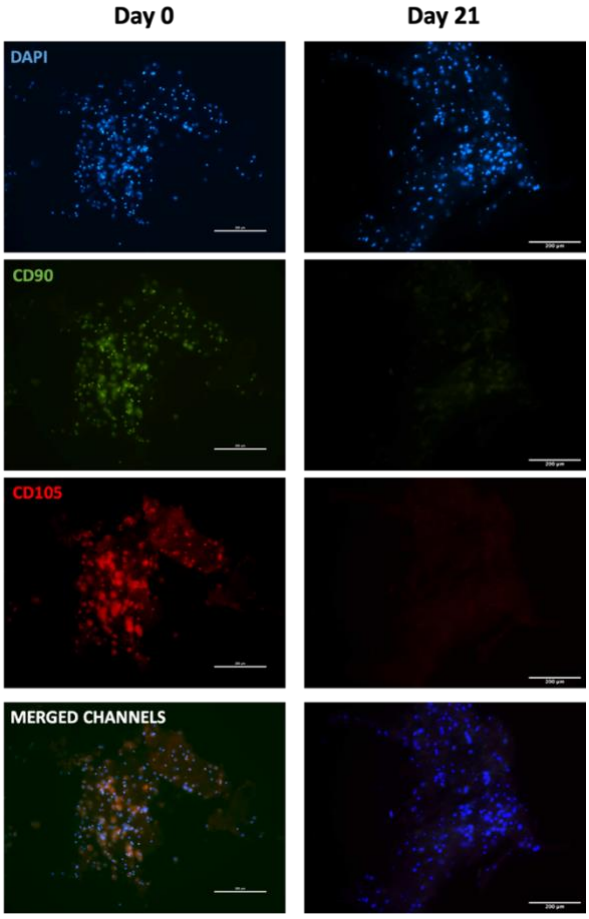

Figure 36. Immunofluorescence images of 3D fibrin scaffold for stemness markers. Immunofluorescence images of 3D fibrin scaffold for stemness markers by IF assay performed staining FITC-conjugated CD90 and PE-conjugated CD105 fibrin scaffolds embedded with *h*BM-MSCs-*h*SkMs-PBMCs at day 0 and 21. All images were captured using 20x magnification, scale bar: 200 μm.

4.4.5 Cytokine expression

We next explored paracrine and cell-to-cell contact effects of PBMCs on cytokine expression in *h*BM-MSCs-*h*SkMs cultured in a 3D *in-vitro* perfused model (Figure 37). *h*SkMs showed a significant upregulation of pro-inflammatory cytokine as *TNF*, 478-fold ($p < 0.0001$) and *IL12A*, 14-fold ($p < 0.5$) (Figure 37a). In co-culture system, pro-inflammatory cytokines were downregulated with PBMCs, especially *IL6* (0.04-fold at day 7, 0.1-fold at day 14, and 0.05-fold at day 21; $p < 0.01$). At day 14 and 21, *IL12A* increased of 6-fold and 17-fold with PBMCs, and of 75-fold and 13-fold without PBMCs; similarly, *IL1B* increased at 6-fold and 15-fold with PBMCs, while 20.5-fold and 8-fold without PBMCs. Conversely, among investigated anti-inflammatory cytokines, *IL10* was the most expressed and was higher in the presence of PBMCs (23.3-fold vs 11.5-fold at day 7, or 9-fold vs 5-fold at day 14, with vs without PBMCs, respectively). *TGFB1* showed an increasing trend in the presence of PBMCs from 1.8-fold at day 7 to 9.5-fold at day 14 and 12-fold at day 21. *TGFB2* displayed the maximum expression at day 14, about 7-fold without PBMCs. *TNF*, *IL4*, and *IFNG* were not detected (Figure 37b). Cytokine secretion was also investigated by analyzing culture medium supernatants at 7, 14 and 21 days by multiplex bead-based immunoassay (Figure 37c). Among 24 cytokines studied, growth- regulated alpha protein (GRO; 2.5 ng/ml), IL-6, granulocyte-colony stimulating factor (G-CSF), IL-8, monocyte chemoattractant protein-1 (MCP-1), and vascular epidermal growth factor (VEGF; 0.1 ng/mL) were detected in culture medium at day 7. Remaining cytokines were not present in culture medium supernatants at day 7, and no cytokines were detected at day 14 and 21.

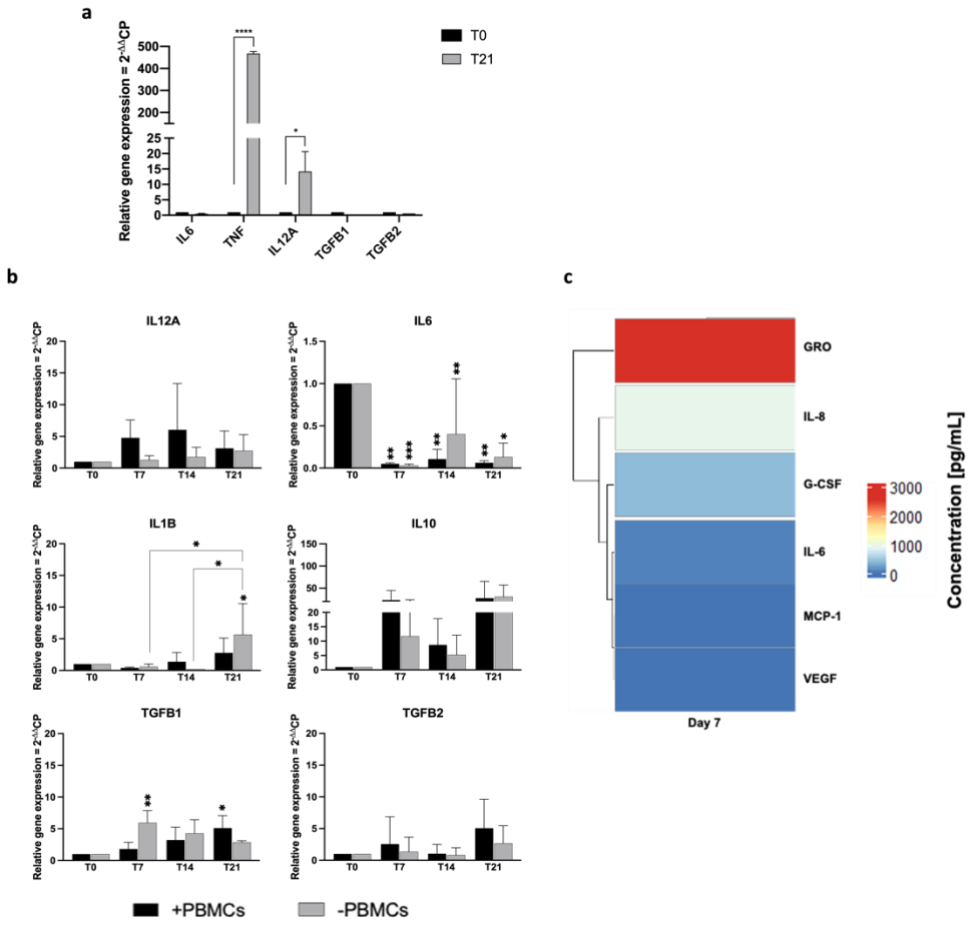

Figure 37. Gene expression profiling for pro- and anti-inflammatory cytokines by quantitative RT-PCR of *h*SkMs (a) and of *h*BM-MSCs-*h*SkMs-PBMCs (b), both within 3D fibrin scaffold. The mRNA levels of pro-inflammatory cytokines (*IL12A*, *IL6* and *IL1B*) and anti-inflammatory cytokines (*IL10*, T*GFB1* and *TGFB2*) were assayed by qRT-PCR at day 7, 14 and 21 of culture. The relative quantification of each mRNA gene expression normalized to endogenous GAPDH (internal control) was calculated using the $2^{-\Delta\Delta Ct}$ method and presented as fold change over *h*SkMs at day 0 (a) and over *h*BM-MSCs at day 0 (b), selected as a control. Cytokine levels measured in culture medium supernatants at day 7, 14, and 21 by magnetic bead-based multiplex immunoassay (c). Data are reported as heatmap from blue (lowest value, 0 pg/mL of concentration) to red (highest value). Cytokines were hierarchical clustered based on expression pattern. Heatmap was made using Pheatmap and ComplexHeatmap packages in R Studio software (v. 2022.07.1 + 554; R Studio, Boston, MA, US). All experiments were performed in biological triplicates (n = 3) and each experiment in technical triplicates. *$p < 0.05$; **$p < 0.01$; ****$p < 0.0001$.

4.5 Discussion

Development of accurate *in-vitro* myogenic commitment models from *h*BM-MSCs is still challenging, and the exact role of PBMCs in influencing myogenic events is under debate, despite clinical reports indicated that the pharmacological targeting of inflammation and immune functions results in faster healing processes. Spontaneous healing skeletal muscle capacity in case of severe injuries appears insufficient, and conventional injury management, including RICE protocol, drug therapies with NSAIDs drugs and intramuscular corticosteroids do not provide optimal restoration to preinjury status[149]. Therefore, biological treatments, like cell therapy, are of high clinical interest. In this sense, the development of biomimetic *in-vitro* SkMR models are precious tools to better understand the complex mechanism of muscle healing process, as recently reported using an *in-vitro* model of myogenic commitment by co-culture *h*BM-MSCs with *h*SkMs[65].

In this work, we implemented our previously described *h*BM-MSC-*h*SkM co-culture system with PBMCs in a 3D fibrin scaffold to investigate their potential roles in muscle injury resolution through paracrine and cell- to-cell contact effects. Indeed, indirect evidence of PBMCs contribution in muscle tissue regeneration is in the clinical efficacy of autologous peripheral cell transplantation in critic limb ischemia treatments[35]. In this case, PBMCs are collected from patient by blood filtration using a commercial filter device (HemaTrate®), are concentrated in a smaller volume, and are then reinfused without any external cell manipulation. However, exact mechanisms underlying clinical efficacy of autologous filtered peripheral blood cell transplantation are still under debate. Here, we sought to investigate the role of PBMCs in myogenesis using a 3D biomimetic *in-vitro* model where PBMCs were added to a myogenic model composed by a co-culture of *h*BM-MSCs and *h*SkMs.

Scaffold porosity is another important parameter when setting up a 3D scaffold-based *in-vitro* system, as cells require an appropriate void volume to locate and to permit oxygen and mass exchange[68,150]. Fibrinogen concentration can affect internal porosity with formation of irregular geometric areas. At the lowest fibrinogen concentrations tested (e.g., 5 mg/mL), polymerization reaction did not occur, while scaffold obtained at 20 mg/mL were difficult to be managed (unpublished data). Therefore, 50 mg/mL concentration was chosen to build fibrin scaffold because scaffold structure showed larger porosity with higher interconnectivity, whereas, higher fibrinogen concentrations decreased the scaffold pore size diameters, even if an increase in tensile strength is documented in literature[151]. However, because tensile strength was not the focus of our study, fibrinogen concentration at 50 mg/mL was selected for our 3D system, allowing a better nutrient and gas exchange, confirmed by excellent cell viability up to 21 days of culture. Furthermore, to assure proper oxygen and metabolite mass transfer into the 3D high-density culture, scaffolds were placed within a close system in which culture medium re-circulated at a constant flow rate of 1 mL/min, maintained by a perfusion bioreactor. Indeed, even in standard 2D conditions, dynamic cultures assured a better myogenic commitment, as previously shown in our optimized co-culture system. Fibrin is widely used in tissue engineering and derives from thrombin-mediated fibrinogen monomer polymerization. Fibrin is naturally degraded by serine protease, and α-aprotinin, a serine protease inhibitor, is usually added to fibrinogen mix to prevent fibrin scaffold degradation *in-vitro* and *in-vivo* conditions, as previously demonstrated[152,153].

*h*BM-MSCs cultured in 3D fibrin scaffold displayed upregulation of myogenic genes with conserved kinetics, as MRFs, such as *Myf5* and *Myf6*, were expressed earlier than *Desmin*, upregulated at later time points[96]. When

PBMCs were embedded in the 3D fibrin scaffold together with *h*BM-MSCs and *h*SkMs, *h*BM-MSCs differentiated toward myogenic phenotype, although less efficiently when in the absence of PBMCs. In both conditions, *h*BM-MSCs lost their mesenchymal for a mature myocyte phenotype with $CD90^{-}CD73^{+}CD105^{+/-}$ [123] and showed Desmin and Myosin Heavy Chain II protein production. In our IF analysis, cells appeared in a spherical shape and immunofluorescence signals were detected as single dots, because cells in a 3D system were in close contact with fibrin and embedded in pores, as already reported[154,155].

The use of complex co-cultures could create a bias in gene expression normalization, as different cell populations were embedded together in the same scaffold and could not be separately recovered for gene expression analysis. For this reason, cultures with single populations, including *h*BM-MSCs and *h*SkMs alone, were used as controls and for gene expression normalization. Moreover, *h*SkMs were seeded at a lower density compared to *h*BM-MSCs (seeding ratio, 2:1, *h*BM-MSCs:*h*SkMs) in our 3D fibrin system, as previously optimized[65] thus, gene expression from co-culture experiments can be reconducted to *h*BM-MSC behavior. PBMCs were added to this well-established myogenic model at the lowest possible ratio (1:1), as lower PBMC ratios are the optimal solution in co-culture systems[145,146].

Based on our results, PBMCs played an effective role in myogenic commitment, while their main activity was the influence on cytokine expression by *h*BM-MSCs. Fibrin can also induce synthesis of pro-inflammatory cytokines, especially from PBMCs[156]; however, pro-inflammatory cytokines were detected at very low levels in our 3D system throughout the culture period at both gene and protein levels, suggesting that fibrin scaffold did not influence gene and protein expression of BM-MSCs.

Moreover, in our system, *TGFB2* was increased, contributing to a transient matrix deposit[127,128], while *IL-10* upregulation, especially in the first 14 days of culture at gene and protein levels, could suggest a possible anti-inflammatory paracrine effect of PBMCs on microenvironment composition, promoting *h*BM-MSC commitment[157]. Secretion of chemoattracts and growth factors in culture medium could co-adjuvate physiological myogenic differentiation by triggering cell recruitment and neovascularization.

To our knowledge, this is the first study using a complex co-culture system composed by mesenchymal stem cells, muscle cells, and immune cells in a 3D microenvironment, representing a novelty in the tissue engineering field. In this *in-vitro* myogenic model, immune cells exerted their effects only in paracrine manner, while not influencing myogenic gene expression. Indeed, immune cells could reduce pro-inflammatory cytokines early in the healing process, while later induce anti-inflammatory molecules favoring muscle cell differentiation and regeneration[11].

4.6 Conclusion

The present work described myogenic commitment of *h*BM-MSCs using a 3D scaffold of fibrin hydrogel bioengineered with different cell populations, such as *h*SkMs and PBMCs in a perfused bioreactor system. Our proposed system could be successfully employed for further studies on more complex crosstalk mechanisms involving multiple cell types. Furthermore, our *in-vitro* biomimetic 3D model could allow to better understand the role of PBMCs in myogenic events in both physiological and pathological simulated conditions. Indeed, despite several clinical reports indicated that filtrated PBMC fraction could be useful in case of muscle severe injuries, biological mechanisms

underlying stem cell differentiation and muscle regenerative events are still poorly understood. Therefore, our described 3D *in-vitro* model might open perspectives for further exploration of the role of PBMCs behavior in myogenic healing events.

CHAPTER 5. CONCLUSIONS

Skeletal muscle injuries are a frequent cause of muscle impairment requiring conservative or surgical treatment; however, severe traumas never completely repair and are a major challenge in the orthopaedic field. Indeed, muscle tissue has an intrinsic ability to regenerate damaged tissue and to restore injured areas structurally and functionally. This regenerative potential is limited, and severe injuries are unlikely to completely restore. Commonly used therapies, including RICE protocol and anti-inflammatory drug prescription, as well as surgical managements, promote only a partial healing, negatively impacting on patients' quality of life. Alternative therapies employ stem cells, because of their multi-differentiation potential and of their ability to secrete GFs and anti-inflammatory molecules supporting regeneration processes. Routinely use of stem cells in clinical practice is limited, because muscle stem cells constitute only a small percentage of total cellular muscle content, their harvesting is an invasive procedure, and *in-vitro* expansion can affect differentiation potential. Conversely, *h*BM-MSCs can be more easily harvested thus representing a valid alternative source of stem cells. Moreover, immune cells are critical for successful repair and recovery of injured skeletal muscles, as they remove necrotic tissue and provide a supportive environment for the remodeling phase. However, exact mechanisms behind immune cell contribution in muscle healing are complex and still unclear.

Upon biochemical stimulation and appropriate cell-to-cell contacts, *h*BM-MSCs can be successfully committed towards myogenic phenotype. Chemical stimulation is provided by supplementing culture media with bFGF at a concentration of 10 ng/mL; whereas, co-culture systems can be composed by *h*BM-MSCs and SkMs. Cell-to-cell direct interactions and/or paracrine effects of differentiated cells helped stem cells to escape from their stemness status and trigger myogenesis.

Cells cultured in 2D standard conditions do not strictly mirror cell behavior in physiological conditions, as cells grow on a flat surface, completely different from ECM support, structure, and organization in living tissues. In contrast, 3D culture approach better reproduces the complex *in vivo* environment, as 3D biomaterial-based scaffolds offer a more physiological support to cells allowing cell-to-cell contacts and paracrine interactions. Moreover, scaffold-based systems can be cultured in dynamic conditions, such as perfusion, where culture media continuously flows assuring better nutrient and gas exchange, as well as excellent cell viability. Our fibrin-based model represents a novelty in the tissue engineering field because we embedded three different cell populations (*h*BM-MSCs, SkMs, and PBMCs) within a fibrin-based scaffold cultured under perfusion. In 3D, stem cells can successfully achieve myogenic phenotype, while immune cells exert their main function in influencing cytokine expression and in establishing an anti-inflammatory microenvironment. Our co-culture *in vitro* model simultaneously allowed a close interaction between stem cells, myoblast, and immune cells, and cytokine-mediated paracrine effects resulting in the establishment of anti-inflammatory and pro-myogenic conditions. Indeed, when immune cells isolated from whole blood were added to co-culture models, *h*BM-MSC myogenic commitment was fastened, and muscle tissue microenvironment showed anti-inflammatory and phagocyte-permissive characteristics.

In conclusion, our data provided advances in *in vitro* skeletal muscle tissue engineering by describing novel 3D *in vitro* models for better understanding of myogenic process, and by identifying an anti-inflammatory potential of immune cells in co-culture systems that might improve *h*BM-MSC myogenic commitment both *in vitro* and *in vivo*.

References

(1) Frontera, W. R.; Ochala, J. Skeletal Muscle: A Brief Review of Structure and Function. *Calcif Tissue Int* **2015**, *96* (3), 183–195. https://doi.org/10.1007/s00223-014-9915-y.

(2) Balestri, W.; Morris, R. H.; Hunt, J. A.; Reinwald, Y. Current Advances on the Regeneration of Musculoskeletal Interfaces. *Tissue Engineering Part B: Reviews* **2021**, *27* (6), 548–571. https://doi.org/10.1089/ten.teb.2020.0112.

(3) Lieber L. Richard. *Skeletal Muscle Structure, Function, and Plasticity.*, Seconda edizione.; Lippincott Williams & Wilkins.

(4) Wang, Z.; Grange, M.; Wagner, T.; Kho, A. L.; Gautel, M.; Raunser, S. The Molecular Basis for Sarcomere Organization in Vertebrate Skeletal Muscle. *Cell* **2021**, *184* (8), 2135-2150.e13. https://doi.org/10.1016/j.cell.2021.02.047.

(5) Mukund, K.; Subramaniam, S. Skeletal Muscle: A Review of Molecular Structure and Function, in Health and Disease. *WIREs Mechanisms of Disease* **2020**, *12* (1). https://doi.org/10.1002/wsbm.1462.

(6) Järvinen, T. A. H.; Järvinen, T. L. N.; Kääriäinen, M.; Äärimaa, V.; Vaittinen, S.; Kalimo, H.; Järvinen, M. Muscle Injuries: Optimising Recovery. *Best Practice & Research Clinical Rheumatology* **2007**, *21* (2), 317–331. https://doi.org/10.1016/j.berh.2006.12.004.

(7) Guo, J.; Yin, Y.; Jin, L.; Zhang, R.; Hou, Z.; Zhang, Y. Acute Compartment Syndrome: Cause, Diagnosis, and New Viewpoint. *Medicine* **2019**, *98* (27), e16260. https://doi.org/10.1097/MD.0000000000016260.

(8) Downing, K.; Prisby, R.; Varanasi, V.; Zhou, J.; Pan, Z.; Brotto, M. Old and New Biomarkers for Volumetric Muscle Loss. *Current Opinion in Pharmacology* **2021**, *59*, 61–69. https://doi.org/10.1016/j.coph.2021.05.001.

(9) Järvinen, T. A. H.; Järvinen, T. L. N.; Kääriäinen, M.; Kalimo, H.; Järvinen, M. Muscle Injuries: Biology and Treatment. *Am J Sports Med* **2005**, *33* (5), 745–764. https://doi.org/10.1177/0363546505274714.

(10) Scala, P.; Rehak, L.; Giudice, V.; Ciaglia, E.; Puca, A. A.; Selleri, C.; Della Porta, G.; Maffulli, N. Stem Cell and Macrophage Roles in Skeletal Muscle Regenerative Medicine. *IJMS* **2021**, *22* (19), 10867. https://doi.org/10.3390/ijms221910867.

(11) Tidball, J. G. Regulation of Muscle Growth and Regeneration by the Immune System. *Nat Rev Immunol* **2017**, *17* (3), 165–178. https://doi.org/10.1038/nri.2016.150.

(12) Mauro, A. SATELLITE CELL OF SKELETAL MUSCLE FIBERS. *The Journal of Biophysical and Biochemical Cytology* **1961**, *9* (2), 493–495. https://doi.org/10.1083/jcb.9.2.493.

(13) Schmidt, M.; Schüler, S. C.; Hüttner, S. S.; von Eyss, B.; von Maltzahn, J. Adult Stem Cells at Work: Regenerating Skeletal Muscle. *Cell. Mol. Life Sci.* **2019**, *76* (13), 2559–2570. https://doi.org/10.1007/s00018-019-03093-6.

(14) Sousa-Victor, P.; García-Prat, L.; Muñoz-Cánoves, P. Control of Satellite Cell Function in Muscle Regeneration and Its Disruption in Ageing. *Nat Rev Mol Cell Biol* **2022**, *23* (3), 204–226. https://doi.org/10.1038/s41580-021-00421-2.

(15) Deal et al. The Journal of Bone & Joint Surgery. *Ice Reduces Edema: A Study of Microvascular Permeability in Rats.* **2002**, *84* (9), 1573–1578.

(16) Schaser, K.-D.; Disch, A. C.; Stover, J. F.; Lauffer, A.; Bail, H. J.; Mittlmeier, T. Prolonged Superficial Local Cryotherapy Attenuates Microcirculatory Impairment, Regional Inflammation, and Muscle Necrosis after Closed Soft Tissue Injury in Rats. *Am J Sports Med* **2007**, *35* (1), 93–102. https://doi.org/10.1177/0363546506294569.

(17) Sherry, M. A.; Best, T. M. A Comparison of 2 Rehabilitation Programs in the Treatment of Acute Hamstring Strains. *J Orthop Sports Phys Ther* **2004**, *34* (3), 116–125. https://doi.org/10.2519/jospt.2004.34.3.116.

(18) Äärimaa, V.; Rantanen, J.; Heikkilä, J.; Helttula, I.; Orava, S. Rupture of the Pectoralis Major Muscle. *Am J Sports Med* **2004**, *32* (5), 1256–1262. https://doi.org/10.1177/0363546503261137.

(19) Tan, J.; Chen, H.; Chen, C.; Liang, X.; Huang, W. The Strength and Function of Hip Abductors Following Anterolateral Minimally Invasive Total Hip Arthroplasty. *Chin J Traumatol* **2014**, *17* (2), 73–78.

(20) Whiteside, L. A.; Nayfeh, T.; Katerberg, B. J. Gluteus Maximus Flap Transfer for Greater Trochanter Reconstruction in Revision THA. *Clinical Orthopaedics & Related Research* **2006**, *453*, 203–210. https://doi.org/10.1097/01.blo.0000246538.75123.db.

(21) Constantinescu, D. S.; Campbell, M. P.; Moatshe, G.; Vap, A. R. Effects of Perioperative Nonsteroidal Anti-Inflammatory Drug Administration on Soft Tissue Healing: A Systematic Review of Clinical Outcomes After Sports Medicine Orthopaedic Surgery Procedures. *Orthopaedic Journal of Sports Medicine* **2019**, *7* (4), 232596711983887. https://doi.org/10.1177/2325967119838873.

(22) Shen, W.; Li, Y.; Tang, Y.; Cummins, J.; Huard, J. NS-398, a Cyclooxygenase-2-Specific Inhibitor, Delays Skeletal Muscle Healing by

Decreasing Regeneration and Promoting Fibrosis. *The American Journal of Pathology* **2005**, *167* (4), 1105–1117. https://doi.org/10.1016/S0002-9440(10)61199-6.

(23) Gierer, P.; Mittlmeier, T.; Bordel, R.; Schaser, K.-D.; Gradl, G.; Vollmar, B. Selective Cyclooxygenase-2 Inhibition Reverses Microcirculatory and Inflammatory Sequelae of Closed Soft-Tissue Trauma in an Animal Model: *The Journal of Bone & Joint Surgery* **2005**, *87* (1), 153–160. https://doi.org/10.2106/JBJS.C.01510.

(24) O???Grady, M.; Hackney, A. C.; Schneider, K.; Bossen, E.; Steinberg, K.; Douglas, J. M.; Murray, W. J.; Watkins, W. D. Diclofenac Sodium (Voltaren) Reduced Exercise-Induced Injury in Human Skeletal Muscle: *Medicine & Science in Sports & Exercise* **2000**, *32* (7), 1191–1196. https://doi.org/10.1097/00005768-200007000-00001.

(25) Baldwin Lanier, A. Use of Nonsteroidal Anti-Inflammatory Drugs Following Exercise-Induced Muscle Injury: *Sports Medicine* **2003**, *33* (3), 177–186. https://doi.org/10.2165/00007256-200333030-00002.

(26) Ziltener, J.-L.; Leal, S.; Fournier, P.-E. Non-Steroidal Anti-Inflammatory Drugs for Athletes: An Update. *Annals of Physical and Rehabilitation Medicine* **2010**, *53* (4), 278–288. https://doi.org/10.1016/j.rehab.2010.03.001.

(27) Fijn, R.; Koorevaar, R. Th.; Brouwers, J. R. B. J. Prevention of Heterotopic Ossification after Total Hip Replacement with NSAIDs. *Pharmacy World and Science* **2003**, *25* (4), 138–145. https://doi.org/10.1023/A:1024830213832.

(28) Levine, W. N.; Bergfeld, J. A.; Tessendorf, W.; Moorman, C. T. Intramuscular Corticosteroid Injection for Hamstring Injuries: A 13-Year Experience in the National Football League. *Am J Sports Med* **2000**, *28* (3), 297–300. https://doi.org/10.1177/03635465000280030301.

(29) Linklater, J.; Hamilton, B.; Carmichael, J.; Orchard, J.; Wood, D. Hamstring Injuries: Anatomy, Imaging, and Intervention. *Semin Musculoskelet Radiol* **2010**, *14* (02), 131–161. https://doi.org/10.1055/s-0030-1253157.

(30) A Hamid, M. S.; Mohamed Ali, M. R.; Yusof, A.; George, J.; Lee, L. P. C. Platelet-Rich Plasma Injections for the Treatment of Hamstring Injuries: A Randomized Controlled Trial. *Am J Sports Med* **2014**, *42* (10), 2410–2418. https://doi.org/10.1177/0363546514541540.

(31) Grassi, A.; Napoli, F.; Romandini, I.; Samuelsson, K.; Zaffagnini, S.; Candrian, C.; Filardo, G. Is Platelet-Rich Plasma (PRP) Effective in the Treatment of Acute Muscle Injuries? A Systematic Review and Meta-Analysis. *Sports Med*

2018, *48* (4), 971–989. https://doi.org/10.1007/s40279-018-0860-1.

(32) Reurink, G.; Goudswaard, G. J.; Moen, M. H.; Weir, A.; Verhaar, J. A. N.; Bierma-Zeinstra, S. M. A.; Maas, M.; Tol, J. L. Platelet-Rich Plasma Injections in Acute Muscle Injury. *N Engl J Med* **2014**, *370* (26), 2546–2547. https://doi.org/10.1056/NEJMc1402340.

(33) Persiani, F.; Paolini, A.; Camilli, D.; Mascellari, L.; Platone, A.; Magenta, A.; Furgiuele, S. Peripheral Blood Mononuclear Cells Therapy for Treatment of Lower Limb Ischemia in Diabetic Patients: A Single-Center Experience. *Annals of Vascular Surgery* **2018**, *53*, 190–196. https://doi.org/10.1016/j.avsg.2018.05.036.

(34) Rigato, M.; Monami, M.; Fadini, G. P. Autologous Cell Therapy for Peripheral Arterial Disease: Systematic Review and Meta-Analysis of Randomized, Nonrandomized, and Noncontrolled Studies. *Circ Res* **2017**, *120* (8), 1326–1340. https://doi.org/10.1161/CIRCRESAHA.116.309045.

(35) De Angelis, B.; Gentile, P.; Orlandi, F.; Bocchini, I.; Di Pasquali, C.; Agovino, A.; Gizzi, C.; Patrizi, F.; Scioli, M. G.; Orlandi, A.; Cervelli, V. Limb Rescue: A New Autologous-Peripheral Blood Mononuclear Cells Technology in Critical Limb Ischemia and Chronic Ulcers. *Tissue Engineering Part C: Methods* **2015**, *21* (5), 423–435. https://doi.org/10.1089/ten.tec.2014.0245.

(36) Cerletti, M.; Jurga, S.; Witczak, C. A.; Hirshman, M. F.; Shadrach, J. L.; Goodyear, L. J.; Wagers, A. J. Highly Efficient, Functional Engraftment of Skeletal Muscle Stem Cells in Dystrophic Muscles. *Cell* **2008**, *134* (1), 37–47. https://doi.org/10.1016/j.cell.2008.05.049.

(37) Webster, M. T.; Manor, U.; Lippincott-Schwartz, J.; Fan, C.-M. Intravital Imaging Reveals Ghost Fibers as Architectural Units Guiding Myogenic Progenitors during Regeneration. *Cell Stem Cell* **2016**, *18* (2), 243–252. https://doi.org/10.1016/j.stem.2015.11.005.

(38) Sacco, A.; Doyonnas, R.; Kraft, P.; Vitorovic, S.; Blau, H. M. Self-Renewal and Expansion of Single Transplanted Muscle Stem Cells. *Nature* **2008**, *456* (7221), 502–506. https://doi.org/10.1038/nature07384.

(39) Collins, C. A.; Olsen, I.; Zammit, P. S.; Heslop, L.; Petrie, A.; Partridge, T. A.; Morgan, J. E. Stem Cell Function, Self-Renewal, and Behavioral Heterogeneity of Cells from the Adult Muscle Satellite Cell Niche. *Cell* **2005**, *122* (2), 289–301. https://doi.org/10.1016/j.cell.2005.05.010.

(40) Qazi, T. H.; Duda, G. N.; Ort, M. J.; Perka, C.; Geissler, S.; Winkler, T. Cell Therapy to Improve Regeneration of Skeletal Muscle Injuries. *Journal of Cachexia, Sarcopenia and Muscle* **2019**, *10* (3), 501–516. https://doi.org/10.1002/jcsm.12416.

(41) Elahi, K. C.; Klein, G.; Avci-Adali, M.; Sievert, K. D.; MacNeil, S.; Aicher, W. K. Human Mesenchymal Stromal Cells from Different Sources Diverge in Their Expression of Cell Surface Proteins and Display Distinct Differentiation Patterns. *Stem Cells International* **2016**, *2016*, 1–9. https://doi.org/10.1155/2016/5646384.

(42) Dominici, M.; Le Blanc, K.; Mueller, I.; Slaper-Cortenbach, I.; Marini, F. C.; Krause, D. S.; Deans, R. J.; Keating, A.; Prockop, D. J.; Horwitz, E. M. Minimal Criteria for Defining Multipotent Mesenchymal Stromal Cells. The International Society for Cellular Therapy Position Statement. *Cytotherapy* **2006**, *8* (4), 315–317. https://doi.org/10.1080/14653240600855905.

(43) Jiang, X.-X.; Zhang, Y.; Liu, B.; Zhang, S.-X.; Wu, Y.; Yu, X.-D.; Mao, N. Human Mesenchymal Stem Cells Inhibit Differentiation and Function of Monocyte-Derived Dendritic Cells. *Blood* **2005**, *105* (10), 4120–4126. https://doi.org/10.1182/blood-2004-02-0586.

(44) Spaggiari, G. M.; Capobianco, A.; Abdelrazik, H.; Becchetti, F.; Mingari, M. C.; Moretta, L. Mesenchymal Stem Cells Inhibit Natural Killer–Cell Proliferation, Cytotoxicity, and Cytokine Production: Role of Indoleamine 2,3-Dioxygenase and Prostaglandin E2. *Blood* **2008**, *111* (3), 1327–1333. https://doi.org/10.1182/blood-2007-02-074997.

(45) Glennie, S.; Soeiro, I.; Dyson, P. J.; Lam, E. W.-F.; Dazzi, F. Bone Marrow Mesenchymal Stem Cells Induce Division Arrest Anergy of Activated T Cells. *Blood* **2005**, *105* (7), 2821–2827. https://doi.org/10.1182/blood-2004-09-3696.

(46) Corcione, A.; Benvenuto, F.; Ferretti, E.; Giunti, D.; Cappiello, V.; Cazzanti, F.; Risso, M.; Gualandi, F.; Mancardi, G. L.; Pistoia, V.; Uccelli, A. Human Mesenchymal Stem Cells Modulate B-Cell Functions. *Blood* **2006**, *107* (1), 367–372. https://doi.org/10.1182/blood-2005-07-2657.

(47) Di Ianni, M.; Del Papa, B.; De Ioanni, M.; Moretti, L.; Bonifacio, E.; Cecchini, D.; Sportoletti, P.; Falzetti, F.; Tabilio, A. Mesenchymal Cells Recruit and Regulate T Regulatory Cells. *Experimental Hematology* **2008**, *36* (3), 309–318. https://doi.org/10.1016/j.exphem.2007.11.007.

(48) Choi, Y.-S.; Jeong, J.-A.; Lim, D.-S. Mesenchymal Stem Cell-Mediated Immature Dendritic Cells Induce Regulatory T Cell-Based Immunosuppressive Effect. *Immunological Investigations* **2012**, *41* (2), 214–229. https://doi.org/10.3109/08820139.2011.619022.

(49) Wang, Y.; Han, Z.; Song, Y.; Han, Z. C. Safety of Mesenchymal Stem Cells for Clinical Application. *Stem Cells International* **2012**, *2012*, 1–4. https://doi.org/10.1155/2012/652034.

(50) Kim, N.; Cho, S.-G. Clinical Applications of Mesenchymal Stem Cells. *Korean J Intern Med* **2013**, *28* (4), 387. https://doi.org/10.3904/kjim.2013.28.4.387.

(51) Sarveazad, A.; Newstead, G. L.; Mirzaei, R.; Joghataei, M. T.; Bakhtiari, M.; Babahajian, A.; Mahjoubi, B. A New Method for Treating Fecal Incontinence by Implanting Stem Cells Derived from Human Adipose Tissue: Preliminary Findings of a Randomized Double-Blind Clinical Trial. *Stem Cell Res Ther* **2017**, *8* (1), 40. https://doi.org/10.1186/s13287-017-0489-2.

(52) Park, E. J.; Kang, J.; Baik, S. H. Treatment of Faecal Incontinence Using Allogeneic-Adipose-Derived Mesenchymal Stem Cells: A Study Protocol for a Pilot Randomised Controlled Trial. *BMJ Open* **2016**, *6* (2), e010450. https://doi.org/10.1136/bmjopen-2015-010450.

(53) Winkler, T.; Costa, M. L.; Ofir, R.; Parolini, O.; Geissler, S.; Volk, H.-D.; Eder, C.; On behalf of the HIPGEN Author Consortium. HIPGEN: A Randomized, Multicentre Phase III Study Using Intramuscular PLacenta-EXpanded Stromal Cells Therapy for Recovery Following Hip Fracture Arthroplasty: A Study Design. *Bone & Joint Open* **2022**, *3* (4), 340–347. https://doi.org/10.1302/2633-1462.34.BJO-2021-0156.R1.

(54) Winkler, T.; Perka, C.; von Roth, P.; Agres, A. N.; Plage, H.; Preininger, B.; Pumberger, M.; Geissler, S.; Hagai, E. L.; Ofir, R.; Pinzur, L.; Eyal, E.; Stoltenburg-Didinger, G.; Meisel, C.; Consentius, C.; Streitz, M.; Reinke, P.; Duda, G. N.; Volk, H.-D. Immunomodulatory Placental-Expanded, Mesenchymal Stromal Cells Improve Muscle Function Following Hip Arthroplasty: Placental-Derived Cells Improve Muscle Regeneration. *Journal of Cachexia, Sarcopenia and Muscle* **2018**, *9* (5), 880–897. https://doi.org/10.1002/jcsm.12316.

(55) Liu, G.; Zhou, Y.; Zhang, X.; Guo, S. Advances in Hydrogels for Stem Cell Therapy: Regulation Mechanisms and Tissue Engineering Applications. *J. Mater. Chem. B* **2022**, *10* (29), 5520–5536. https://doi.org/10.1039/D2TB01044E.

(56) Ashammakhi, N.; GhavamiNejad, A.; Tutar, R.; Fricker, A.; Roy, I.; Chatzistavrou, X.; Hoque Apu, E.; Nguyen, K.-L.; Ahsan, T.; Pountos, I.; Caterson, E. J. Highlights on Advancing Frontiers in Tissue Engineering. *Tissue Engineering Part B: Reviews* **2022**, *28* (3), 633–664. https://doi.org/10.1089/ten.teb.2021.0012.

(57) Kim, I. L.; Khetan, S.; Baker, B. M.; Chen, C. S.; Burdick, J. A. Fibrous Hyaluronic Acid Hydrogels That Direct MSC Chondrogenesis through Mechanical and Adhesive Cues. *Biomaterials* **2013**, *34* (22), 5571–5580. https://doi.org/10.1016/j.biomaterials.2013.04.004.

(58) Salinas, C. N.; Anseth, K. S. The Influence of the RGD Peptide Motif and Its Contextual Presentation in PEG Gels on Human Mesenchymal Stem Cell

Viability. *J Tissue Eng Regen Med* **2008**, *2* (5), 296–304. https://doi.org/10.1002/term.95.

(59) Wang, X.; Yan, C.; Ye, K.; He, Y.; Li, Z.; Ding, J. Effect of RGD Nanospacing on Differentiation of Stem Cells. *Biomaterials* **2013**, *34* (12), 2865–2874. https://doi.org/10.1016/j.biomaterials.2013.01.021.

(60) Guvendiren, M.; Burdick, J. A. The Control of Stem Cell Morphology and Differentiation by Hydrogel Surface Wrinkles. *Biomaterials* **2010**, *31* (25), 6511–6518. https://doi.org/10.1016/j.biomaterials.2010.05.037.

(61) Zhan, X. Effect of Matrix Stiffness and Adhesion Ligand Density on Chondrogenic Differentiation of Mesenchymal Stem Cells. *J Biomed Mater Res* **2020**, *108* (3), 675–683. https://doi.org/10.1002/jbm.a.36847.

(62) Caballero Aguilar, L. M.; Silva, S. M.; Moulton, S. E. Growth Factor Delivery: Defining the next Generation Platforms for Tissue Engineering. *Journal of Controlled Release* **2019**, *306*, 40–58. https://doi.org/10.1016/j.jconrel.2019.05.028.

(63) Pasini, A.; Lovecchio, J.; Ferretti, G.; Giordano, E. Medium Perfusion Flow Improves Osteogenic Commitment of Human Stromal Cells. *Stem Cells International* **2019**, *2019*, 1–10. https://doi.org/10.1155/2019/1304194.

(64) Pasini, A.; Lovecchio, J.; Cortesi, M.; Liverani, C.; Spadazzi, C.; Mercatali, L.; Ibrahim, T.; Giordano, E. Perfusion Flow Enhances Viability and Migratory Phenotype in 3D-Cultured Breast Cancer Cells. *Ann Biomed Eng* **2021**, *49* (9), 2103–2113. https://doi.org/10.1007/s10439-021-02727-w.

(65) Scala, P.; Lovecchio, J.; Lamparelli, E. P.; Vitolo, R.; Giudice, V.; Giordano, E.; Selleri, C.; Rehak, L.; Maffulli, N.; Della Porta, G. Myogenic Commitment of Human Stem Cells by Myoblasts Co-Culture: A Static vs. a Dynamic Approach. *Artificial Cells, Nanomedicine, and Biotechnology* **2022**, *50* (1), 49–58. https://doi.org/10.1080/21691401.2022.2039684.

(66) Trucillo, E.; Bisceglia, B.; Valdrè, G.; Giordano, E.; Reverchon, E.; Maffulli, N.; Della Porta, G. Growth Factor Sustained Delivery from Poly-lactic-co-glycolic Acid Microcarriers and Its Mass Transfer Modeling by Finite Element in a Dynamic and Static Three-dimensional Environment Bioengineered with Stem Cells. *Biotechnology and Bioengineering* **2019**, *116* (7), 1777–1794. https://doi.org/10.1002/bit.26975.

(67) Ciardulli, M. C.; Marino, L.; Lovecchio, J.; Giordano, E.; Forsyth, N. R.; Selleri, C.; Maffulli, N.; Porta, G. D. Tendon and Cytokine Marker Expression by Human Bone Marrow Mesenchymal Stem Cells in a Hyaluronate/Poly-Lactic-Co-

Glycolic Acid (PLGA)/Fibrin Three-Dimensional (3D) Scaffold. *Cells* **2020**, *9* (5), 1268. https://doi.org/10.3390/cells9051268.

(68) Lamparelli, E. P.; Lovecchio, J.; Ciardulli, M. C.; Giudice, V.; Dale, T. P.; Selleri, C.; Forsyth, N.; Giordano, E.; Maffulli, N.; Della Porta, G. Chondrogenic Commitment of Human Bone Marrow Mesenchymal Stem Cells in a Perfused Collagen Hydrogel Functionalized with HTGF-B1-Releasing PLGA Microcarrier. *Pharmaceutics* **2021**, *13* (3), 399. https://doi.org/10.3390/pharmaceutics13030399.

(69) Rossi, C. A.; Flaibani, M.; Blaauw, B.; Pozzobon, M.; Figallo, E.; Reggiani, C.; Vitiello, L.; Elvassore, N.; De Coppi, P. *In Vivo* Tissue Engineering of Functional Skeletal Muscle by Freshly Isolated Satellite Cells Embedded in a Photopolymerizable Hydrogel. *FASEB j.* **2011**, *25* (7), 2296–2304. https://doi.org/10.1096/fj.10-174755.

(70) Vandenburgh, H.; Kaufman, S. In Vitro Model for Stretch-Induced Hypertrophy of Skeletal Muscle. *Science* **1979**, *203* (4377), 265–268. https://doi.org/10.1126/science.569901.

(71) Strohman, R. C.; Bayne, E.; Spector, D.; Obinata, T.; Micou-Eastwood, J.; Maniotis, A. Myogenesis and Histogenesis of Skeletal Muscle on Flexible Membranes in Vitro. *In Vitro Cell Dev Biol* **1990**, *26* (2), 201–208. https://doi.org/10.1007/BF02624113.

(72) Dennis, R. G.; Kosnik, Ii, P. E. EXCITABILITY AND ISOMETRIC CONTRACTILE PROPERTIES OF MAMMALIAN SKELETAL MUSCLE CONSTRUCTS ENGINEERED IN VITRO. *In Vitro Cell Dev Biol Anim* **2000**, *36* (5), 327. https://doi.org/10.1290/1071-2690(2000)036<0327:EAICPO>2.0.CO;2.

(73) Meligy, F. Y.; Shigemura, K.; Behnsawy, H. M.; Fujisawa, M.; Kawabata, M.; Shirakawa, T. The Efficiency of in Vitro Isolation and Myogenic Differentiation of MSCs Derived from Adipose Connective Tissue, Bone Marrow, and Skeletal Muscle Tissue. *In Vitro Cell.Dev.Biol.-Animal* **2012**, *48* (4), 203–215. https://doi.org/10.1007/s11626-012-9488-x.

(74) Stern-Straeter, J.; Bonaterra, G. A.; Juritz, S.; Birk, R.; Goessler, U. R.; Bieback, K.; Bugert, P.; Schultz, J.; Hörmann, K.; Kinscherf, R.; Faber, A. Evaluation of the Effects of Different Culture Media on the Myogenic Differentiation Potential of Adipose Tissue- or Bone Marrow-Derived Human Mesenchymal Stem Cells. *International Journal of Molecular Medicine* **2014**, *33* (1), 160–170. https://doi.org/10.3892/ijmm.2013.1555.

(75) Kowalski, K.; Dos Santos, M.; Maire, P.; Ciemerych, M. A.; Brzoska, E. Induction of Bone Marrow-Derived Cells Myogenic Identity by Their Interactions with the Satellite Cell Niche. *Stem Cell Res Ther* **2018**, *9* (1), 258.

https://doi.org/10.1186/s13287-018-0993-z.

(76) Witt, R.; Weigand, A.; Boos, A. M.; Cai, A.; Dippold, D.; Boccaccini, A. R.; Schubert, D. W.; Hardt, M.; Lange, C.; Arkudas, A.; Horch, R. E.; Beier, J. P. Mesenchymal Stem Cells and Myoblast Differentiation under HGF and IGF-1 Stimulation for 3D Skeletal Muscle Tissue Engineering. *BMC Cell Biol* **2017**, *18* (1), 15. https://doi.org/10.1186/s12860-017-0131-2.

(77) Beier, J. P.; Bitto, F. F.; Lange, C.; Klumpp, D.; Arkudas, A.; Bleiziffer, O.; Boos, A. M.; Horch, R. E.; Kneser, U. Myogenic Differentiation of Mesenchymal Stem Cells Co-Cultured with Primary Myoblasts. *Cell. Biol. Int.* **2011**, *35* (4), 397–406. https://doi.org/10.1042/CBI20100417.

(78) Grasman, J. M.; Zayas, M. J.; Page, R. L.; Pins, G. D. Biomimetic Scaffolds for Regeneration of Volumetric Muscle Loss in Skeletal Muscle Injuries. *Acta Biomaterialia* **2015**, *25*, 2–15. https://doi.org/10.1016/j.actbio.2015.07.038.

(79) Pollot, B. E.; Rathbone, C. R.; Wenke, J. C.; Guda, T. Natural Polymeric Hydrogel Evaluation for Skeletal Muscle Tissue Engineering. *J. Biomed. Mater. Res.* **2018**, *106* (2), 672–679. https://doi.org/10.1002/jbm.b.33859.

(80) Matthias, N.; Hunt, S. D.; Wu, J.; Lo, J.; Smith Callahan, L. A.; Li, Y.; Huard, J.; Darabi, R. Volumetric Muscle Loss Injury Repair Using in Situ Fibrin Gel Cast Seeded with Muscle-Derived Stem Cells (MDSCs). *Stem Cell Research* **2018**, *27*, 65–73. https://doi.org/10.1016/j.scr.2018.01.008.

(81) Gilbert-Honick, J.; Iyer, S. R.; Somers, S. M.; Lovering, R. M.; Wagner, K.; Mao, H.-Q.; Grayson, W. L. Engineering Functional and Histological Regeneration of Vascularized Skeletal Muscle. *Biomaterials* **2018**, *164*, 70–79. https://doi.org/10.1016/j.biomaterials.2018.02.006.

(82) Kästner, S.; Elias, M. C.; Rivera, A. J.; Yablonka–Reuveni, Z. Gene Expression Patterns of the Fibroblast Growth Factors and Their Receptors During Myogenesis of Rat Satellite Cells. *J Histochem Cytochem.* **2000**, *48* (8), 1079–1096. https://doi.org/10.1177/002215540004800805.

(83) Conte, C.; Ainaoui, N.; Delluc-Clavières, A.; Khoury, M. P.; Azar, R.; Pujol, F.; Martineau, Y.; Pyronnet, S.; Prats, A.-C. Fibroblast Growth Factor 1 Induced during Myogenesis by a Transcription–Translation Coupling Mechanism. *Nucleic Acids Research* **2009**, *37* (16), 5267–5278. https://doi.org/10.1093/nar/gkp550.

(84) Ribeiro, A.; Laranjeira, P.; Mendes, S.; Velada, I.; Leite, C.; Andrade, P.; Santos, F.; Henriques, A.; Grãos, M.; Cardoso, C. M. P.; Martinho, A.; Pais, M. L.; da Silva, C. L.; Cabral, J.; Trindade, H.; Paiva, A. Mesenchymal Stem Cells from Umbilical Cord Matrix, Adipose Tissue and Bone Marrow Exhibit Different

Capability to Suppress Peripheral Blood B, Natural Killer and T Cells. *Stem Cell Res Ther* **2013**, *4* (5), 125. https://doi.org/10.1186/scrt336.

(85) El-Sayed, M.; El-Feky, M. A.; El-Amir, M. I.; Hasan, A. S.; Tag-Adeen, M.; Urata, Y.; Goto, S.; Luo, L.; Yan, C.; Li, T.-S. Immunomodulatory Effect of Mesenchymal Stem Cells: Cell Origin and Cell Quality Variations. *Mol Biol Rep* **2019**, *46* (1), 1157–1165. https://doi.org/10.1007/s11033-018-04582-w.

(86) Kudlik, G.; Hegyi, B.; Czibula, Á.; Monostori, É.; Buday, L.; Uher, F. Mesenchymal Stem Cells Promote Macrophage Polarization toward M2b-like Cells. *Experimental Cell Research* **2016**, *348* (1), 36–45. https://doi.org/10.1016/j.yexcr.2016.08.022.

(87) Carrier, R. L.; Rupnick, M.; Langer, R.; Schoen, F. J.; Freed, L. E.; Vunjak-Novakovic, G. Perfusion Improves Tissue Architecture of Engineered Cardiac Muscle. *Tissue Engineering* **2002**, *8* (2), 175–188. https://doi.org/10.1089/107632702753724950.

(88) Kim, J.; Ma, T. Perfusion Regulation of HMSC Microenvironment and Osteogenic Differentiation in 3D Scaffold. *Biotechnol. Bioeng.* **2012**, *109* (1), 252–261. https://doi.org/10.1002/bit.23290.

(89) Samavedi, S.; Poindexter, L. K.; Van Dyke, M.; Goldstein, A. S. Synthetic Biomaterials for Regenerative Medicine Applications. In *Regenerative Medicine Applications in Organ Transplantation*; Elsevier, 2014; pp 81–99. https://doi.org/10.1016/B978-0-12-398523-1.00007-0.

(90) Bustin, S. A.; Benes, V.; Garson, J. A.; Hellemans, J.; Huggett, J.; Kubista, M.; Mueller, R.; Nolan, T.; Pfaffl, M. W.; Shipley, G. L.; Vandesompele, J.; Wittwer, C. T. The MIQE Guidelines: Minimum Information for Publication of Quantitative Real-Time PCR Experiments. *Clinical Chemistry* **2009**, *55* (4), 611–622. https://doi.org/10.1373/clinchem.2008.112797.

(91) Hellemans, J.; Mortier, G.; De Paepe, A.; Speleman, F.; Vandesompele, J. QBase Relative Quantification Framework and Software for Management and Automated Analysis of Real-Time Quantitative PCR Data. *Genome Biol* **2007**, *8* (2), R19. https://doi.org/10.1186/gb-2007-8-2-r19.

(92) Suchorska, W. M.; Lach, M. S.; Richter, M.; Kaczmarczyk, J.; Trzeciak, T. Bioimaging: An Useful Tool to Monitor Differentiation of Human Embryonic Stem Cells into Chondrocytes. *Ann Biomed Eng* **2016**, *44* (5), 1845–1859. https://doi.org/10.1007/s10439-015-1443-z.

(93) de Winter, J. C. F. Using the Student's t-Test with Extremely Small Sample Sizes. https://doi.org/10.7275/E4R6-DJ05.

(94) Liu, X.; Chen, W.; Zhang, C.; Thein-Han, W.; Hu, K.; Reynolds, M. A.; Bao, C.; Wang, P.; Zhao, L.; Xu, H. H. K. Co-Seeding Human Endothelial Cells with Human-Induced Pluripotent Stem Cell-Derived Mesenchymal Stem Cells on Calcium Phosphate Scaffold Enhances Osteogenesis and Vascularization in Rats. *Tissue Engineering Part A* **2017**, *23* (11–12), 546–555. https://doi.org/10.1089/ten.tea.2016.0485.

(95) Plotnikov, E. Y.; Khryapenkova, T. G.; Vasileva, A. K.; Marey, M. V.; Galkina, S. I.; Isaev, N. K.; Sheval, E. V.; Polyakov, V. Y.; Sukhikh, G. T.; Zorov, D. B. Cell-to-Cell Cross-Talk between Mesenchymal Stem Cells and Cardiomyocytes in Co-Culture. *Journal of Cellular and Molecular Medicine* **2008**, *12* (5a), 1622–1631. https://doi.org/10.1111/j.1582-4934.2007.00205.x.

(96) Asfour, H. A.; Allouh, M. Z.; Said, R. S. Myogenic Regulatory Factors: The Orchestrators of Myogenesis after 30 Years of Discovery. *Exp Biol Med (Maywood)* **2018**, *243* (2), 118–128. https://doi.org/10.1177/1535370217749494.

(97) Gang, E. J.; Bosnakovski, D.; Simsek, T.; To, K.; Perlingeiro, R. C. R. Pax3 Activation Promotes the Differentiation of Mesenchymal Stem Cells toward the Myogenic Lineage. *Experimental Cell Research* **2008**, *314* (8), 1721–1733. https://doi.org/10.1016/j.yexcr.2008.02.016.

(98) Kozlowska, U.; Krawczenko, A.; Futoma, K.; Jurek, T.; Rorat, M.; Patrzalek, D.; Klimczak, A. Similarities and Differences between Mesenchymal Stem/Progenitor Cells Derived from Various Human Tissues. *WJSC* **2019**, *11* (6), 347–374. https://doi.org/10.4252/wjsc.v11.i6.347.

(99) Zhao, Q.; Yang, S. T.; Wang, J. J.; Zhou, J.; Xing, S. S.; Shen, C. C.; Wang, X. X.; Yue, Y. X.; Song, J.; Chen, M.; Wei, Y. Y.; Zhou, Q. P.; Dai, T.; Song, Y. H. TNF Alpha Inhibits Myogenic Differentiation of C2C12 Cells through NF-KB Activation and Impairment of IGF-1 Signaling Pathway. *Biochemical and Biophysical Research Communications* **2015**, *458* (4), 790–795. https://doi.org/10.1016/j.bbrc.2015.02.026.

(100) Li, Y.-P. TNF-α Is a Mitogen in Skeletal Muscle. *American Journal of Physiology-Cell Physiology* **2003**, *285* (2), C370–C376. https://doi.org/10.1152/ajpcell.00453.2002.

(101) Chen, S.-E.; Jin, B.; Li, Y.-P. TNF-α Regulates Myogenesis and Muscle Regeneration by Activating P38 MAPK. *American Journal of Physiology-Cell Physiology* **2007**, *292* (5), C1660–C1671. https://doi.org/10.1152/ajpcell.00486.2006.

(102) Grabiec, K.; Tokarska, J.; Milewska, M.; Błaszczyk, M.; Gajewska, M.; Grzelkowska-Kowalczyk, K. Interleukin-1β Stimulates Early Myogenesis of Mouse

C2C12 Myoblasts: The Impact on Myogenic Regulatory Factors, Extracellular Matrix Components, IGF Binding Proteins and Protein Kinases. *Polish Journal of Veterinary Sciences* **2013**, *16* (2), 255–264. https://doi.org/10.2478/pjvs-2013-0036.

(103) Deng, B.; Wehling-Henricks, M.; Villalta, S. A.; Wang, Y.; Tidball, J. G. IL-10 Triggers Changes in Macrophage Phenotype That Promote Muscle Growth and Regeneration. *The Journal of Immunology* **2012**, *189* (7), 3669–3680. https://doi.org/10.4049/jimmunol.1103180.

(104) Chang, Y.-H.; Tsai, J.-N.; Chen, T.-L.; Ho, K.-T.; Cheng, H.-Y.; Hsiao, C.-W.; Shiau, M.-Y. Interleukin-4 Promotes Myogenesis and Boosts Myocyte Insulin Efficacy. *Mediators of Inflammation* **2019**, *2019*, 1–14. https://doi.org/10.1155/2019/4182015.

(105) Grasman, J. M.; Zayas, M. J.; Page, R. L.; Pins, G. D. Biomimetic Scaffolds for Regeneration of Volumetric Muscle Loss in Skeletal Muscle Injuries. *Acta Biomaterialia* **2015**, *25*, 2–15. https://doi.org/10.1016/j.actbio.2015.07.038.

(106) Cao, Y.; Liu, J.; Zhong, R.; Yu, Q.; Wang, H. Surface Modification of PBT Nonwoven Fabrics Used for Blood Filtration and Their Blood Compatibility Study. *Artificial Cells, Blood Substitutes, and Biotechnology* **2012**, *40* (5), 317–325. https://doi.org/10.3109/10731199.2012.657206.

(107) M. Fomovsky. Leukocyte Purification (EPO 2 602 315 A1).

(108) Kim, E. J.; Yeo, G.-D.; Pai, C.-M.; Kang, I.-K. Preparation of Surface-Modified Poly(Butylene Terephthalate) Nonwovens and Their Application as Leukocyte Removal Filters. *J. Biomed. Mater. Res.* **2009**, *90B* (2), 849–856. https://doi.org/10.1002/jbm.b.31354.

(109) Longo, U. G.; Loppini, M.; Berton, A.; Spiezia, F.; Maffulli, N.; Denaro, V. Tissue Engineered Strategies for Skeletal Muscle Injury. *Stem Cells International* **2012**, *2012*, 1–9. https://doi.org/10.1155/2012/175038.

(110) Geijo-Barrientos, E.; Pastore-Olmedo, C.; De Mingo, P.; Blanquer, M.; Gómez Espuch, J.; Iniesta, F.; Iniesta, N. G.; García-Hernández, A.; Martín-Estefanía, C.; Barrios, L.; Moraleda, J. M.; Martínez, S. Intramuscular Injection of Bone Marrow Stem Cells in Amyotrophic Lateral Sclerosis Patients: A Randomized Clinical Trial. *Front. Neurosci.* **2020**, *14*, 195. https://doi.org/10.3389/fnins.2020.00195.

(111) Winkler, T.; von Roth, P.; Matziolis, G.; Mehta, M.; Perka, C.; Duda, G. N. Dose–Response Relationship of Mesenchymal Stem Cell Transplantation and Functional Regeneration After Severe Skeletal Muscle Injury in Rats. *Tissue Engineering Part A* **2009**, *15* (3), 487–492.

https://doi.org/10.1089/ten.tea.2007.0426.

(112) Matziolis, G.; Winkler, T.; Schaser, K.; Wiemann, M.; Krocker, D.; Tuischer, J.; Perka, C.; Duda, G. N. Autologous Bone Marrow-Derived Cells Enhance Muscle Strength Following Skeletal Muscle Crush Injury in Rats. *Tissue Engineering* **2006**, *12* (2), 361–367. https://doi.org/10.1089/ten.2006.12.361.

(113) Moriya, J.; Minamino, T.; Tateno, K.; Shimizu, N.; Kuwabara, Y.; Sato, Y.; Saito, Y.; Komuro, I. Long-Term Outcome of Therapeutic Neovascularization Using Peripheral Blood Mononuclear Cells for Limb Ischemia. *Circ: Cardiovascular Interventions* **2009**, *2* (3), 245–254. https://doi.org/10.1161/CIRCINTERVENTIONS.108.799361.

(114) Huang, P. P.; Yang, X. F.; Li, S. Z.; Wen, J. C.; Zhang, Y.; Han, Z. C. Randomised Comparison of G-CSF-Mobilized Peripheral Blood Mononuclear Cells versus Bone Marrow-Mononuclear Cells for the Treatment of Patients with Lower Limb Arteriosclerosis Obliterans. *Thromb Haemost* **2007**, *98* (12), 1335–1342. https://doi.org/10.1160/TH07-02-0137.

(115) Nevskaya, T.; Ananieva, L.; Bykovskaia, S.; Eremin, I.; Karandashov, E.; Khrennikov, J.; Mach, E.; Zaprjagaeva, M.; Guseva, N.; Nassonov, E. Autologous Progenitor Cell Implantation as a Novel Therapeutic Intervention for Ischaemic Digits in Systemic Sclerosis. *Rheumatology* **2008**, *48* (1), 61–64. https://doi.org/10.1093/rheumatology/ken407.

(116) Havlíček, K.; Svobodová, L.; Bakalova, T.; Lederer, T. Influence of Electrospinning Methods on Characteristics of Polyvinyl Butyral and Polyurethane Nanofibres Essential for Biological Applications. *Materials & Design* **2020**, *194*, 108898. https://doi.org/10.1016/j.matdes.2020.108898.

(117) Longo, R.; Catauro, M.; Sorrentino, A.; Guadagno, L. Thermal and Mechanical Characterization of Complex Electrospun Systems Based on Polycaprolactone and Gelatin. *J Therm Anal Calorim* **2022**, *147* (9), 5391–5399. https://doi.org/10.1007/s10973-022-11225-7.

(118) Pereira, A. P. dos S.; Silva, M. H. P. da; Lima Júnior, É. P.; Paula, A. dos S.; Tommasini, F. J. Processing and Characterization of PET Composites Reinforced With Geopolymer Concrete Waste. *Mat. Res.* **2017**, *20* (suppl 2), 411–420. https://doi.org/10.1590/1980-5373-mr-2017-0734.

(119) Tsochatzis, E. D.; Lopes, J. A.; Holland, M. V.; Reniero, F.; Emons, H.; Guillou, C. Isolation, Characterization and Structural Elucidation of Polybutylene Terephthalate Cyclic Oligomers and Purity Assessment Using a 1H QNMR Method. *Polymers* **2019**, *11* (3), 464. https://doi.org/10.3390/polym11030464.

(120) Ma, M.; Niu, L.; Ma, J.; Ma, J.; Jiao, T. Fabrication and Thermal Degradation Kinetics of PBT/BEO/Nano-Sb2O3 Composites. *Journal of Nanomaterials* **2020**, *2020*, 1–10. https://doi.org/10.1155/2020/6641702.

(121) Konishi, T.; Miyamoto, Y. Smectic Structure and Glass Transition in Poly(Butylene Terephthalate). *Polym J* **2010**, *42* (4), 349–353. https://doi.org/10.1038/pj.2010.5.

(122) Dechet, M. A.; Gómez Bonilla, J. S.; Grünewald, M.; Popp, K.; Rudloff, J.; Lang, M.; Schmidt, J. A Novel, Precipitated Polybutylene Terephthalate Feedstock Material for Powder Bed Fusion of Polymers (PBF): Material Development and Initial PBF Processability. *Materials & Design* **2021**, *197*, 109265. https://doi.org/10.1016/j.matdes.2020.109265.

(123) Gago-Lopez, N.; Awaji, O.; Zhang, Y.; Ko, C.; Nsair, A.; Liem, D.; Stempien-Otero, A.; MacLellan, W. R. THY-1 Receptor Expression Differentiates Cardiosphere-Derived Cells with Divergent Cardiogenic Differentiation Potential. *Stem Cell Reports* **2014**, *2* (5), 576–591. https://doi.org/10.1016/j.stemcr.2014.03.003.

(124) Relaix, F.; Montarras, D.; Zaffran, S.; Gayraud-Morel, B.; Rocancourt, D.; Tajbakhsh, S.; Mansouri, A.; Cumano, A.; Buckingham, M. Pax3 and Pax7 Have Distinct and Overlapping Functions in Adult Muscle Progenitor Cells. *Journal of Cell Biology* **2006**, *172* (1), 91–102. https://doi.org/10.1083/jcb.200508044.

(125) Spaltro, G.; Straino, S.; Gambini, E.; Bassetti, B.; Persico, L.; Zoli, S.; Zanobini, M.; Capogrossi, M. C.; Spirito, R.; Quarti, C.; Pompilio, G. Characterization of the Pall Celeris System as a Point-of-Care Device for Therapeutic Angiogenesis. *Cytotherapy* **2015**, *17* (9), 1302–1313. https://doi.org/10.1016/j.jcyt.2015.04.006.

(126) Liu, D.; Black, B. L.; Derynck, R. TGF-β Inhibits Muscle Differentiation through Functional Repression of Myogenic Transcription Factors by Smad3. *Genes Dev.* **2001**, *15* (22), 2950–2966. https://doi.org/10.1101/gad.925901.

(127) Ge, X.; McFarlane, C.; Vajjala, A.; Lokireddy, S.; Ng, Z. H.; Tan, C. K.; Tan, N. S.; Wahli, W.; Sharma, M.; Kambadur, R. Smad3 Signaling Is Required for Satellite Cell Function and Myogenic Differentiation of Myoblasts. *Cell Res* **2011**, *21* (11), 1591–1604. https://doi.org/10.1038/cr.2011.72.

(128) Osses, N.; Brandan, E. ECM Is Required for Skeletal Muscle Differentiation Independently of Muscle Regulatory Factor Expression. *American Journal of Physiology-Cell Physiology* **2002**, *282* (2), C383–C394. https://doi.org/10.1152/ajpcell.00322.2001.

(129) Garcia, S. M.; Tamaki, S.; Xu, X.; Pomerantz, J. H. Human Satellite Cell Isolation and Xenotransplantation. In *Skeletal Muscle Development*; Ryall, J. G., Ed.; Methods in Molecular Biology; Springer New York: New York, NY, 2017; Vol. 1668, pp 105–123. https://doi.org/10.1007/978-1-4939-7283-8_8.

(130) Montarras, D.; Morgan, J.; Collins, C.; Relaix, F.; Zaffran, S.; Cumano, A.; Partridge, T.; Buckingham, M. Direct Isolation of Satellite Cells for Skeletal Muscle Regeneration. *Science* **2005**, *309* (5743), 2064–2067. https://doi.org/10.1126/science.1114758.

(131) Kuang, S.; Kuroda, K.; Le Grand, F.; Rudnicki, M. A. Asymmetric Self-Renewal and Commitment of Satellite Stem Cells in Muscle. *Cell* **2007**, *129* (5), 999–1010. https://doi.org/10.1016/j.cell.2007.03.044.

(132) Charville, G. W.; Cheung, T. H.; Yoo, B.; Santos, P. J.; Lee, G. K.; Shrager, J. B.; Rando, T. A. Ex Vivo Expansion and In Vivo Self-Renewal of Human Muscle Stem Cells. *Stem Cell Reports* **2015**, *5* (4), 621–632. https://doi.org/10.1016/j.stemcr.2015.08.004.

(133) Ciardulli, M. C.; Lovecchio, J.; Scala, P.; Lamparelli, E. P.; Dale, T. P.; Giudice, V.; Giordano, E.; Selleri, C.; Forsyth, N. R.; Maffulli, N.; Della Porta, G. 3D Biomimetic Scaffold for Growth Factor Controlled Delivery: An In-Vitro Study of Tenogenic Events on Wharton's Jelly Mesenchymal Stem Cells. *Pharmaceutics* **2021**, *13* (9), 1448. https://doi.org/10.3390/pharmaceutics13091448.

(134) Shi, Y.; Wang, Y.; Li, Q.; Liu, K.; Hou, J.; Shao, C.; Wang, Y. Immunoregulatory Mechanisms of Mesenchymal Stem and Stromal Cells in Inflammatory Diseases. *Nat Rev Nephrol* **2018**, *14* (8), 493–507. https://doi.org/10.1038/s41581-018-0023-5.

(135) Vater, C.; Kasten, P.; Stiehler, M. Culture Media for the Differentiation of Mesenchymal Stromal Cells. *Acta Biomaterialia* **2011**, *7* (2), 463–477. https://doi.org/10.1016/j.actbio.2010.07.037.

(136) Villalta, S. A.; Rinaldi, C.; Deng, B.; Liu, G.; Fedor, B.; Tidball, J. G. Interleukin-10 Reduces the Pathology of Mdx Muscular Dystrophy by Deactivating M1 Macrophages and Modulating Macrophage Phenotype. *Human Molecular Genetics* **2011**, *20* (4), 790–805. https://doi.org/10.1093/hmg/ddq523.

(137) Ergene, E.; Sezlev Bilecen, D.; Kaya, B.; Yilgor Huri, P.; Hasirci, V. 3D Cellular Alignment and Biomimetic Mechanical Stimulation Enhance Human Adipose-Derived Stem Cell Myogenesis. *Biomed. Mater.* **2020**, *15* (5), 055017. https://doi.org/10.1088/1748-605X/ab95e2.

(138) Manzo, P.; Scala, P.; Giudice, V.; Gorrese, M.; Bertolini, A.; Morini, D.;

D'Alto, F.; Pepe, R.; Pedicini, A.; Izzo, B.; Verdesca, F.; Langella, M.; Serio, B.; Della Porta, G.; Selleri, C. C-Kit M541L Variant Is Related to Ineffective Hemopoiesis Predisposing to Clonal Evolution in 3D in Vitro Biomimetic Co-Culture Model of Bone Marrow Niche. *Heliyon* **2022**, *8* (12), e11998. https://doi.org/10.1016/j.heliyon.2022.e11998.

(139) Govoni, M.; Berardi, A. C.; Muscari, C.; Campardelli, R.; Bonafè, F.; Guarnieri, C.; Reverchon, E.; Giordano, E.; Maffulli, N.; Della Porta, G. <sup/> An Engineered Multiphase Three-Dimensional Microenvironment to Ensure the Controlled Delivery of Cyclic Strain and Human Growth Differentiation Factor 5 for the Tenogenic Commitment of Human Bone Marrow Mesenchymal Stem Cells. *Tissue Engineering Part A* **2017**, *23* (15–16), 811–822. https://doi.org/10.1089/ten.tea.2016.0407.

(140) Huang, Y.-C.; Dennis, R. G.; Larkin, L.; Baar, K. Rapid Formation of Functional Muscle in Vitro Using Fibrin Gels. *Journal of Applied Physiology* **2005**, *98* (2), 706–713. https://doi.org/10.1152/japplphysiol.00273.2004.

(141) Engel, N.; Fechner, C.; Voges, A.; Ott, R.; Stenzel, J.; Siewert, S.; Bergner, C.; Khaimov, V.; Liese, J.; Schmitz, K.-P.; Krause, B. J.; Frerich, B. An Optimized 3D-Printed Perfusion Bioreactor for Homogeneous Cell Seeding in Bone Substitute Scaffolds for Future Chairside Applications. *Sci Rep* **2021**, *11* (1), 22228. https://doi.org/10.1038/s41598-021-01516-8.

(142) Grayson, W. L.; Marolt, D.; Bhumiratana, S.; Fröhlich, M.; Guo, X. E.; Vunjak-Novakovic, G. Optimizing the Medium Perfusion Rate in Bone Tissue Engineering Bioreactors. *Biotechnol. Bioeng.* **2011**, *108* (5), 1159–1170. https://doi.org/10.1002/bit.23024.

(143) Birru, B.; Mekala, N. K.; Parcha, S. R. Improved Osteogenic Differentiation of Umbilical Cord Blood MSCs Using Custom Made Perfusion Bioreactor. *Biomedical Journal* **2018**, *41* (5), 290–297. https://doi.org/10.1016/j.bj.2018.07.002.

(144) Della Porta, G.; Del Gaudio, P.; De Cicco, F.; Aquino, R. P.; Reverchon, E. Supercritical Drying of Alginate Beads for the Development of Aerogel Biomaterials: Optimization of Process Parameters and Exchange Solvents. *Ind. Eng. Chem. Res.* **2013**, *52* (34), 12003–12009. https://doi.org/10.1021/ie401335c.

(145) Zhang, H.; Shao, B.; Zhuge, Q.; Wang, P.; Zheng, C.; Huang, W.; Yang, C.; Wang, B.; Su, D.-M.; Jin, K. Cross-Talk between Human Neural Stem/Progenitor Cells and Peripheral Blood Mononuclear Cells in an Allogeneic Co-Culture Model. *PLoS ONE* **2015**, *10* (2), e0117432. https://doi.org/10.1371/journal.pone.0117432.

(146) Sturlan, S.; Sachet, M.; Baumann, S.; Kuznetsova, I.; Spittler, A.; Bergmann, M. Influenza A Virus Induces an Immediate Cytotoxic Activity in All

Major Subsets of Peripheral Blood Mononuclear Cells. *PLoS ONE* **2009**, *4* (1), e4122. https://doi.org/10.1371/journal.pone.0004122.

(147) Tsai, W. L.; Vian, L.; Giudice, V.; Kieltyka, J.; Liu, C.; Fonseca, V.; Gazaniga, N.; Gao, S.; Kajigaya, S.; Young, N. S.; Biancotto, A.; Gadina, M. High Throughput PSTAT Signaling Profiling by Fluorescent Cell Barcoding and Computational Analysis. *Journal of Immunological Methods* **2020**, *477*, 112667. https://doi.org/10.1016/j.jim.2019.112667.

(148) Porta, G. D.; Nguyen, B.-N. B.; Campardelli, R.; Reverchon, E.; Fisher, J. P. Synergistic Effect of Sustained Release of Growth Factors and Dynamic Culture on Osteoblastic Differentiation of Mesenchymal Stem Cells: Sustained Growth Factor Release for Osteoblastic Differentiation. *J. Biomed. Mater. Res.* **2015**, *103* (6), 2161–2171. https://doi.org/10.1002/jbm.a.35354.

(149) Longo, U. G.; Loppini, M.; Berton, A.; Spiezia, F.; Maffulli, N.; Denaro, V. Tissue Engineered Strategies for Skeletal Muscle Injury. *Stem Cells International* **2012**, *2012*, 1–9. https://doi.org/10.1155/2012/175038.

(150) Lovecchio, J.; Pannella, M.; Giardino, L.; Calzà, L.; Giordano, E. A Dynamic Culture Platform Enhances the Efficiency of the 3D HUVEC-based Tube Formation Assay. *Biotechnology and Bioengineering* **2020**, *117* (3), 789–797. https://doi.org/10.1002/bit.27227.

(151) Chiu, C. L.; Hecht, V.; Duong, H.; Wu, B.; Tawil, B. Permeability of Three-Dimensional Fibrin Constructs Corresponds to Fibrinogen and Thrombin Concentrations. *BioResearch Open Access* **2012**, *1* (1), 34–40. https://doi.org/10.1089/biores.2012.0211.

(152) Thomson, K. S.; Korte, F. S.; Giachelli, C. M.; Ratner, B. D.; Regnier, M.; Scatena, M. Prevascularized Microtemplated Fibrin Scaffolds for Cardiac Tissue Engineering Applications. *Tissue Engineering Part A* **2013**, *19* (7–8), 967–977. https://doi.org/10.1089/ten.tea.2012.0286.

(153) Mühleder, S.; Pill, K.; Schaupper, M.; Labuda, K.; Priglinger, E.; Hofbauer, P.; Charwat, V.; Marx, U.; Redl, H.; Holnthoner, W. The Role of Fibrinolysis Inhibition in Engineered Vascular Networks Derived from Endothelial Cells and Adipose-Derived Stem Cells. *Stem Cell Res Ther* **2018**, *9* (1), 35. https://doi.org/10.1186/s13287-017-0764-2.

(154) Sun, W.; Tiemessen, D. M.; Sloff, M.; Lammers, R. J.; de Mulder, E. L. W.; Hilborn, J.; Gupta, B.; Feitz, W. F. J.; Daamen, W. F.; van Kuppevelt, T. H.; Geutjes, P. J.; Oosterwijk, E. Improving the Cell Distribution in Collagen-Coated Poly-Caprolactone Knittings. *Tissue Engineering Part C: Methods* **2012**, *18* (10), 731–739. https://doi.org/10.1089/ten.tec.2011.0593.

(155) Ahmed, T. A. E.; Ringuette, R.; Wallace, V. A.; Griffith, M. Autologous Fibrin Glue as an Encapsulating Scaffold for Delivery of Retinal Progenitor Cells. *Front. Bioeng. Biotechnol.* **2015**, *2*. https://doi.org/10.3389/fbioe.2014.00085.

(156) Jensen, T.; Kierulf, P.; Sandset, P.; Klingenberg, O.; Joø, G.; Godal, H.; Skjønsberg, O. Fibrinogen and Fibrin Induce Synthesis of Proinflammatory Cytokines from Isolated Peripheral Blood Mononuclear Cells. *Thromb Haemost* **2007**, *97* (05), 822–829. https://doi.org/10.1160/TH07-01-0039.

(157) khodayari S. Inflammatory Microenvironment of Acute Myocardial Infarction Prevents Regeneration of Heart with Stem Cells Therapy. *Cell Physiol Biochem* **2019**, *53* (5), 887–909. https://doi.org/10.33594/000000180.